NOTICE

The quality of this microform is heavily dependent upon the quality of the original thesis submitted for microfilming. Every effort has been made to ensure the highest quality of reproduction possible.

If pages are missing, contact the university which granted the degree.

Some pages may have indistinct print especially if the original pages were typed with a poor typewriter ribbon or if the university sent us an inferior photocopy.

Previously copyrighted materials (journal articles, published tests, etc.) are not filmed.

Reproduction in full or in part of this microform is governed by the Canadian Copyright Act, R.S.C. 1970, c. C-30.

AVIS

La qualité de cette microforme dépend grandement de la qualité de la thèse soumise au microfilmage. Nous avons tout fait pour assurer une qualité supérieure de reproduction.

S'il manque des pages, veuillez communiquer avec l'université qui a conféré le grade.

La qualité d'impression de certaines pages peut laisser à désirer, surtout si les pages originales ont été dactylographiées à l'aide d'un ruban usé ou si l'université nous a fait parvenir une photocopie de qualité inférieure.

Les documents qui font déjà l'objet d'un droit d'auteur (articles de revue, tests publiés, etc.) ne sont pas microfilmés.

La reproduction, même partielle, de cette microforme est soumise à la Loi canadienne sur le droit d'auteur, SRC 1970, c. C-30.

Canada

Behavior of Composite Slab-on-Girder and Box Girder Bridges at Inelastic and Ultimate Limit States

By

Noureddine Benichou

A thesis
presented to the University of Ottawa
in partial fulfillment of the
requirements for the degree of
Master of Applied Science
in
Civil Engineering

DEPARTMENT OF CIVIL ENGINEERING
UNIVERSITY OF OTTAWA
OTTAWA, ONTARIO, MAY 1988

ISBN 0-315-46710-X

UNIVERSITÉ D'OTTAWA
UNIVERSITY OF OTTAWA

Contents

Acknowledgements

I wish to express my deep appreciations and grateful thanks to Dr. Mo. Cheung for his guidance, advice, understanding and encouragement during the course of this study.

I would also like to thank my mother, my wife, and my whole family for their continued support, as I pursued yet another degree. In addition great Mercy to my father who was all the time in my mind giving me courage and patience.

To my teacher Rhoda Diebel who spent her precious time correcting my English structure and to the numerous friends and colleagues, who helped and extended moral support during each phase of this project, I express my appreciation.

Abstract

In the field of bridge design, current practice is to use elastic methods of analysis to determine the distribution of force effects, while the capacities are set equal to the ultimate resistances of the various components which imply inelastic behavior. In addition, the capacity of the structure is normally limited to that load at which the first section reaches its capacity based on these elastic strength calculations. A reserve of capacity between first yield and complete collapse will usually exist. In a highly redundant structure such as composite slab-on-girder or box girder bridges, the magnitude of that reserve capacity could be significant.

An extensive analytical investigation was undertaken to study the load distribution characteristics of simply supported and continuous composite concrete slab on compact steel girder or box girder bridges at all stages of loading. The existence of some critical stages prior to the collapse was noticed. The changing patterns of moment distribution were monitored, and the potential reserve capacities identified.

The analytical tool employed was the non-linear finite element method. Because compact sections were used, only material non-linearities were dealt with.

List of Figures

List of Tables

Notations

x, y, z	Rectangular co-ordinate system.
u, v, w	Displacements of the nodes in x, y, and z direction respectively.
$AMLF_{mcf}$	Minimum adjusted multiple load factor at failure.
$AMLF_{mpf}$	Minimum adjusted multiple load factor at first plastic hinge.
A_g	Area of the steel girder or box girder.
A_w	Area of the web of the steel girder or box girder.
A'_s	Area of the reinforcing steel in the slab.
b	Half bridge width.
b_e	Effective total width of the concrete slab.
B	Actual width of the slab overhang.
B_e	Effective width of the slab overhang.
$[B]$	Strain-displacement matrix.
C_f	Correction factor used to adjust the D value.
$\{d\}$	Vector of nodal displacements.
$\{d\}^e$	Vector of nodal displacements in the element.
$\{\Delta d\}_i$	Vector of incremental displacements.
D	Transverse load distribution factor.
D_d	Design elastic load distribution factor.
D_f	Distribution factor.
D_x	Flexural rigidity in the x direction.
D_y	Flexural rigidity in the y direction.
D_{xy}	Longitudinal torsional rigidity.
D_{yx}	Transverse torsional rigidity.
D_1	Coupling longitudinal rigidity.

D_2	Coupling transverse rigidity.
$[D]$	Constitutive matrix.
DLA	Dynamic load allowance.
E	Elastic modulus.
E_T	Strain hardening modulus.
f'_c	Compressive strength of concrete.
f'_t	Tensile strength of concrete.
f_y	Yield stress of the reinforcement.
F	Plastic flow.
F_y	Yield force.
$\{F\}$	Vector of nodal forces.
$\{F\}_b$	Vector of nodal forces due to body forces.
$\{F\}_s$	Vector of nodal forces due to surface tractions.
$\{F\}_\varepsilon$	Vector of nodal forces due to initial strains.
$\{F\}_\sigma$	Vector of nodal forces due to initial stresses.
$\{\Delta F\}_i$	Vector of incremental loads.
h	Clear depth between flanges.
H	Hardening function.
K	Factor function of the bridge type in AASHTO ($K = S/D_f$).
$[k]$	Structural stiffness matrix.
L	Span length.
M	Longitudinal moment at a section.
M_{AASHTO}	Max. moment in a girder due to truck loading as given by AASHTO.
M_g	Moment resisted by one girder or box girder.
M_1	Total moment at the first plastic hinge.

M_n	Total moment at the n^{th} plastic hinge.
M_{ph}	Simple plastic hogging moment of a section.
M_{ps}	Simple plastic sagging moment of a section.
M_x	Moment at a cross section with respect to x.
$M_{x,max}$.	Maximum moment at a cross section with respect to x.
M_y	Yield moment at a section.
n	Number of lanes loaded.
N	No. of trucks / No. of traffics lanes.
NL	Number of traffic lanes.
$[N]$	Shape function matrix.
P_f	Probability of failure.
R	Ultimate resistance.
$\bar{R}$	Mean resistance.
R_d	Design resistance.
$\{R\}$	Vector of applied forces.
$\%R$	Percent longitudinal redistribution.
s_{ij}	Deviotoric stress.
S	Girder or box girder spacing.
SR	Strength reserve.
U	Service load.
$\bar{U}$	Mean load.
t	Thickness of the flanges.
U_d	Service resistance.
w	Web thickness.
W_e	Design lane width.

Y	Margin of safety.
α	Torsional parameter.
β	Characterizing parameter taking into account the torsion.
β_s	Safety index defining the probability of failure.
δ_{ij}	Kronecker delta.
$\{\delta\}$	Displacement field ($\{\delta\} = [N]\{d\}^e$).
ϵ_y	Yield strain.
$\{\epsilon\}$	Vector of strains.
$\{\bar{\epsilon}\}$	Vector of initial strains.
$\{\epsilon_0\}$	Vector of in-plane strains.
$\{\Delta\epsilon\}_i$	Vector of incremental strains.
$\{\chi\}$	Vector of curvature due to bending.
λ_1	Multiple load factor at first plastic hinge.
λ_n	Multiple load factor at n^{th} plastic hinge.
μ	Parameter specified in the OHBDC.
ν	Poisson's ratio.
Ψ	Longitudinal redistribution factor.
σ_R	Ultimate stress.
σ_U	Service stress.
σ_y	Yield stress.
$\{\sigma\}$	Vector of stresses.
$\{\bar{\sigma}\}$	Vector of initial stresses.
θ	Flexural parameter.

Chapter 1

INTRODUCTION

1.1 General

Most of the present highway systems require improvement and expansion which involve the rehabilitation of existing bridges and the construction of new ones. This is in part due to the deterioration of old bridges, the use of heavy trucks, and an increase in traffic volume.

Highway bridges are constructed of steel, reinforced concrete or prestressed concrete, or mixed concrete and steel. The latter type is referred to as composite bridges. The choice of different materials and structural systems in a bridge superstructure is governed by many criteria, including economic and structural requirements. Among the many types of structural systems, the slab-on-girder and box girder bridges are most suitable for short and medium spans. Composite bridges of these types are the easiest and fastest

to construct and to maintain. This is one reason for their popularity. Most of these bridges have been built over the past forty years. Their design was based on lighter truck loads and elastic analysis. Today, however, because of the growing demand for higher permissible loads for construction and overload vehicles, these bridges cannot meet current requests of the traffic loads. Regulatory authorities, such as the Ministry of Transportation of Ontario (MTO), are anxious to develop analytical procedures that would enable them to evaluate the actual strength of such bridges. In other words, they would like to know their exact load distribution characteristics over the entire loading range up to failure.

Existing highway bridge codes, such as the Ontario Highway Bridge Design Code (OHBDC), the American Association of State Highway and Transportation Officials (AASHTO) bridge code, or the Canadian Standards Association (CSA) bridge code provide different methods for the prediction of the ultimate load capacity. This is achieved by multiplying the longitudinal and transverse moments and shears obtained by elastic analysis by certain factors. Such simplifications are generally adequate for design purposes; however, the evaluation of live load capacities at ultimate state utilizing elastic load distribution capacities is neither realistic nor logical to predict the limit state or post-elastic response of the structure. In fact, the longitudinal and transverse distributions of vehicle load at ultimate state is significantly different from the distribution at serviceability limit state. Therefore, in order to assess realistically the load carrying capacity of existing bridges, studies are needed to determine the distribution of loads beyond the elastic range. In conducting such studies, it is important that the effect of different parameters at advanced stages of loading be consid-

ered. However, in the present thesis, only material and geometry properties of the different parts of the bridge superstructure and the types of loading and bridge are considered.

In a composite slab-on-girder bridge and box girder bridge, the main components are the reinforced concrete slab and the steel girders or box girders. In addition, any realistic analysis must also consider the interaction between these components. Although in some cases stiffeners and diaphragms may also be present, for the purpose of this study, these will not be considered. Studies [13,30] have showed that their effect on the load distribution is not significant in most of the cases.

1.2 Objective

The purpose of the work described herein is to determine how at inelastic and ultimate limit states, vehicle loads are distributed by the slab to the girders in composite slab-on-girder and box girder bridges. Specifically, the following items are examined:

- The exploration of certain aspects of the non-elastic behavior and their effects on the ultimate response.
- The magnitude and distribution of moments in each member at post-elastic state.
- The variation of load distribution characteristics with increased loading.

- Determination of the potential strength reserve of the analyzed bridges.
- Comparison of the load distribution characteristics obtained from this study with those of the OHBDC.

The load distribution factors reported in this thesis are based on the OHBDC truck specified in reference [28].

1.3 Scope

The study was confined to the analysis of straight simply supported and continuous bridges. The analysis will deal primarily with slab-on-girder and box girder bridge types. These structures will be loaded under different loading configurations up to failure.

Of the four bridges which have been analyzed the continuous slab-on-girder bridge is a scale model, while the other structures are prototype existing bridges. More details on the geometry and loading conditions of these structures are presented in the following chapters.

The development of the analysis was conducted using a finite element computer program called 'ADINA' (Automatic Dynamic Incremental Non-linear Analysis) [1] to predict the behavior of the bridges in the elastic and post-elastic ranges. Since the analytical procedure utilized herein is the non-linear finite element method, the results of the analysis are subjected to the same limitations as the finite element procedure used.

The analyses are limited to material non-linearities, therefore large deformation and buckling are not considered. However, in selecting the girder or box girder size, only compact sections have been used, which means that failure due to yielding will precede buckling of the steel girders. Furthermore, the reinforced concrete slab increases the buckling load of the girders which again implies that yielding will be the dominant mode of failure.

It is the author's belief that the analytical model adopted here provides very accurate results. This will be demonstrated in later chapters of this thesis.

1.4 Previous Research

Since the beginning of this century, analytical and experimental studies have been conducted to investigate the behavior of composite structures in buildings and bridges. These studies have primarily focussed on the general behavior and strength of such structures under different loading conditions and have been generally limited to single beams, either simply or continuously supported.

As stated earlier, the main concern of the current study is to determine load distribution in slab-on-girder and box girder bridges at inelastic and ultimate states. Therefore, the following paragraphs will briefly review some of the previous work related to this topic. Some work related to load distribution in concrete and steel bridges will also be cited. The reason is that the load distribution characteristics of composite bridges are known

to be similar to those of concrete and steel bridges at elastic stages.

Newmark [29] developed the analytical procedure for determining longitudinal and transverse shears and moments for both composite and non-composite bridges. This procedure is similar to the moment distribution method developed by Hardy Cross [16]. Newmark, however, carried out extensive parametric studies on different types of bridges. The results of his work were summarized in a series of tables that contained the fixed-end moments, distribution factors, and the carry-over factors for both non-composite and composite slab-on-girder bridges. His major finding was that the load distribution factor in such bridges is only a function of the girder spacing. In this fashion, he recommended that the distribution factor D_f be related to the girder spacing S as follows;

$$D_f = \frac{S}{K} \tag{1.1}$$

Where K is a constant equal to 1.676m. It is worthwhile to mention that the current AASHTO code uses this formula for girder spacing up to 1.829m to determine the design moment for each girder in composite bridges.

In the early sixties, the advent of computers helped bridge analysts to use refined numerical techniques to study load distribution problems. They analyzed and evaluated different responses due to various loading conditions. For example, Heins and Looney [17] wrote a computer program which incorporated the so-called slope-deflection method of analysis. This method was used to determine the actual bridge strain and deflection. They modelled the bridge as a continuous orthotropic plate resting on flexible supports (bridge girders) which is an improvement over the procedure introduced by Newmark [29]. They recommended that this method be used for analyzing

bridges whose girders have torsional stiffness of some significance such as box girder bridges.

Mattock and Johnston [27] evaluated lateral load distribution characteristics of two simply supported box girder model bridges. One was a two-box bridge and the other a three-box bridge. The problem was analyzed using both analytical (folded plate theory) and experimental methods to complement one another. The results obtained indicate that a satisfactory lateral distribution of loads is obtained without the use of transverse diaphragms within the span. This lateral distribution of loads is better than that assumed in the AASHTO specifications [3] for steel and concrete composite bridges.

The introduction of the limit state design philosophy motivated some investigators to use limit state analysis for evaluating the response of bridges to overloads. Percy [32] and Shaw [37] developed long hand methods to balance the moments in a grid framework at ultimate load, similar to the Hardy Cross method of elastic moment distribution [16]. Percy included torsional stiffness while Shaw neglected it. The resulting distribution of force effects is in equilibrium with the applied loads. However, these methods provide only distribution of moments at ultimate limit state (ULS), but no information regarding the sequence of plastic hinge formation.

However, Walsh [40] reported on a limit analysis of grid frameworks including torsional effects which did trace the sequence of hinge formation. He concluded that the effects of shear on hinge formation was negligible.

Lash and Najaraja [23] performed physical tests on multi-girder bridges.

They reported on the testing to failure of twelve scale model slab-on-girder bridges which had concrete longitudinal girders. These bridges were two-lane simply supported structures and included internal diaphragms. They concluded that test loads generally exceeded the theoretical values at failure. Longitudinal yield lines along the torsionally stiff girders were typical and less likely to occur in steel bridges due to lower torsional stiffness.

Lowe and Flint [24] reported on two scale model composite bridges loaded to failure under sealed AASHTO loading. Both were single span skewed structures. One was a narrow bridge with two longitudinal girders, while the other was a wide bridge with eight equally girders spaced. The two-girder model was loaded by a single vehicle positioned to maximize the longitudinal bending moment. It failed with a mechanism consisting of a single transverse yield line parallel to the supports. The eight-girder model was loaded also by one vehicle positioned between two outer girders. This suggests a rather poor transverse distribution of the load. However, a more uniform distribution of load would occur under multiple lane loading.

Heins and Kerzweil [18] performed an analytical study of different failure mechanisms in slab-on-girder bridges. They considered local failures of the slab due to yield line mechanism within an area bounded by longitudinal girders, support lines and free edges, and global collapse mechanisms consisting of hinge lines which involved all girders at sections of maximum moments. It was concluded that the design of the slab would generally be governed by serviceability requirements, not the ultimate limit state, and that global failure mechanisms would be the most likely to occur.

Heins and Kuo [19] performed an analytical study of single span multi-

girder composite bridges to determine the transverse distribution of live load applicable at ultimate limit state, which they defined as the formation of the first sagging hinge in accordance with AASHTO provisions. The authors believed that live load distribution factors based on elastic behavior may be too conservative, and that a more uniform distribution of load results from the yielding. A finite difference technique was used to analyze the composite bridges at inelastic and ultimate limit states for various girder spacing and aspect ratios. It was noted that a more uniform distribution of load occurred as the first hinge formed. The authors thus proposed a method to calculate the appropriate distribution factors at ULS.

Bakht et al [4,5,7] introduced a simplified method of analysis for load distribution in slab-on-girder and box girder bridges and this method forms the basis of the OHBDC recommendations. The method was derived using concepts from the orthotropic plate theory and the grillage analogy. They conducted an extensive parametric study and concluded that load distribution in slab-on-girder bridges is characterized by two parameters, a flexural parameter θ and a torsional parameter α which are functions of the geometric and material properties of the bridge. In the case of box girder bridges, an additional characterizing parameter β, which is related to the torsional rigidity of the bridge, is introduced in the analysis. Although this method is also based on linear elastic theory, it gives substantially more accurate results than the AASHTO recommendations [3]. In the following chapters, this method will be discussed in detail.

Shanmugan and Evans [36] reported on the use of a grillage analysis program to study the non-linear and ultimate behavior of cellular structures

under bending loads. These structures were analyzed under incremental increasing load until failure. At each increment, the grillage member proprieties were recalculated to account for the effective width reduction on the compression flanges resulting from progressive buckling. It was concluded that small load increments would minimize the resultant error and the failure of a member was due to yielding of an extreme fibre rather than the fully plastic behavior of the section. In addition, the use of square grids, simply supported and uniformly loaded at all nodal points, has induced a uniform distribution of the stresses in several members and rapid occurrence of failure after the first yield.

Wegmuller [41] investigated the same post-yielding behavior of simply supported, single span composite bridges using a finite element model which sub-divided the slab and girders into layered elements. Under incremental loading, an iterative procedure was used for convergence. An improvement in the transverse distribution of longitudinal bending moments in a range immediately after the post-cracking behavior was noted.

Improved transverse distribution of load in the post-elastic range was also the purpose of scale model bridge tests performed by Bozler and Colville [9]. A two span and a three span models were included, both with three longitudinal girders throughout. Loading consisted of a single concentrated point load over the middle girder at the center of one span, the middle span in the three span model. Loading was increased until yielding had occurred in both sagging and hogging regions. Based on measured strains, the transverse distribution of sagging moments at the loaded section was more uniform than at elastic load levels. Moments were also being redis-

tributed longitudinally, but apparently only along the loaded center girder. Progressing towards a collapse mechanism, transverse redistribution may have occurred at the hogging sections.

Kennedy and Grace [22] performed tests on two continuous composite model bridges to investigate the load distribution characteristics. Both bridges were two equal spans and had five longitudinal girders. It was concluded that the presence of steel I-beam diaphragms, when rigidly connected to longitudinal girders, enhances significantly the transverse distribution. The transverse cracking of the concrete deck at the intermediate support does not influence significantly the transverse distribution nor the deflections.

A numerical method of analysis was developed to trace the non-linear response of multi-cell reinforced concrete box girder bridges under stepwise increasing static loads by Seible and Scordelis [35]. The non-linearities considered were material non-linearities such as cracking of concrete and yielding of the reinforcement due to flexure, shear and torsion. Both analytical (using grillage method) and experimental methods were performed to compare the results. It was found that the proposed model can be used in limit state design for new bridge structures as well as for the prediction of overload capacities and possible failure modes of existing structures, which were originally designed by using the Working Stress Design (WSD) method. Furthermore, it has been shown that deterioration of the bridge structure under increasing eccentric overloads can cause substantial force redistributions in the longitudinal and transverse directions of the reinforced concrete structure.

The results of another experimental test to determine the load distribution factors at ULS were reported by Cheung, Ng and Gardner [13]. A scale model of single span simply supported slab-on-girder bridge was loaded with scaled OHBD vehicles in one or two of the three lanes until failure. There were six longitudinal girders with compact rolled sections, with the interior ones most heavily loaded, which resulted in the transverse distribution becoming more peaked. Subsequently, moments were redistributed transversely and the distribution improved. The nature of failure was obviously not due to the formation of collapse mechanisms, otherwise the transverse distribution of moments would have been more uniform.

Tharmabala [39] reported on the recent development of a computer method for the non-linear analysis of grids. The analysis was performed on a single span simply supported composite bridge. Failure was based on excessively large deflections under small load increments. No limits were placed on the rotation at the hinge locations, and complete transverse distribution of moments was achieved with a uniform distribution resulting across the sagging hinge line.

1.5 Outlines of the Thesis

Since the problems studied in this thesis are related to the load distribution at ultimate, design philosophy and the code approach regarding the load distribution are reviewed in chapter two and three to provide some insight into idealized behavior of slab-on-girder and box girder bridges. In chapter four, the finite element method and the finite element program are

discussed in detail. Chapter five provides a full description of the structures studied. The results, parametric studies of load distribution factors and the discussion of these results are presented in chapter six. The last chapter provides a summary of the conclusions and recommendations .

Chapter 2

DESIGN PHILOSOPHIES

2.1 General

Since plastic design implies identification of all potential modes of failure and determination of acceptable levels of safety it is only applicable within the framework of a Limit States Design (LSD) philosophy. LSD, which includes the Strength Design or Load Factor Design, is becoming the principal design philosophy in North America. In the United States specifications for highway bridges [3] published by the American Association of State Highway and Transportation Officials (AASHTO) allows the use of either LSD or Working Stress Design (WSD, also known as Allowable Stress Design) in the design of both concrete and steel members.

The national bridge design code in Canada, the Canadian Standards Association's (CSA) Design of Highway Bridges [10], is similar to the AASHTO

code. The most recent edition (1978) includes the option of using WSD or LSD for the design of concrete members, but has not yet adopted the LSD option for the design of steel members. It is expected in a forthcoming edition.

The relatively new Ontario Highway Bridge Design Code (OHBDC) [28] published by the Ontario Ministry of Transportation and Communications (MTC) is based solely on the LSD philosophy. It does not consider the WSD methods as appropriate for the design or evaluation of highway bridges.

2.2 Working Stress Design

In the WSD method, force effects in a structure under specified loading are calculated using elastic methods of analysis. The individual members are designed so that the maximum stresses due to these force effects do not exceed an allowable fraction of the yield stress of the material. This allowable stress would normally vary with the type of force effect being resisted. The ratio of the yield stress to the allowable stress provides a factor of safety against failure under an overload while satisfactory performance under the specified service loads is ensured since the material is kept well within the elastic regime. However, the actual factor of safety against collapse will likely be much higher than this ratio since most structural elements possess a strength reserve between first yield and failure. The magnitude of this reserve will vary with the type of force effect being resisted, the proportion of the structural elements, the shape of the member, and the material properties. Not only can the true resistance vary

considerably from those determined by an allowable stress design, but also the actual loadings vary from the design loading. Specified loads are only estimates of the loads the structure may resist in its life. The actual loads vary with some probability distribution and may well exceed the specified loads. The aforementioned factor of safety is also intended to compensate for that possibility in WSD. It is apparent that this variability of resistances and loads results in a highly non-uniform level of safety among structures designed using WSD. Although an acceptable rate of failure suggests that the minimum levels of safety as provided by WSD are satisfactory, some structures are over-designed and hence, are uneconomical.

2.3 Limit States Design

The popularity of LSD over WSD is based on its more uniform level of safety and hence greater economy. Limit States Design is based on the principle that the structure must perform satisfactorily at different limit states. At the Serviceability Limit States (SLS) the structure must be able to support the anticipated service loads without excessive deformations, cracking, etc., or susceptibility to fatigue failure. The structure would normally behave elastically at these load levels. The Ultimate Limit States (ULS) ensures that the probability of failure is sufficiently low. This is achieved by applying load factors which are derived from the distributions of the loads such that the probability of exceeding the factored loads within a specified return period is acceptably low. Since different load types have different distributions, they will also have different load factors. The resistance of

the structural members at ULS is the maximum resistance that can be expected. Depending on the force effect being considered, the resistance will vary with the dimensions of the section, bracing, and boundary condition as well as material properties and mode of failure.

Regardless, the combination of load factors and performance factors is intended to provide satisfactory performance under service loads and an acceptably low probability of failure at ULS. It should be obvious that the probability of failure can never be reduced to zero, but economically feasible structures can be built with an acceptably low probability of failure. The level of safety in LSD structures is bound to be more uniform than in WSD structures.

2.4 Basic Procedures for Defining Safety

There are two basic methods of defining structural safety. They will be reviewed briefly in the following subsections. More details can be found in reference [25].

2.4.1 Factor of Safety

The factor of safety can be defined as

$$Factor\ of\ Safety = \frac{Ultimate\ Resistance}{Service\ Load} = \frac{R}{U} \qquad (2.1)$$

This implies that both of these quantities are well defined each with a unique value. However, the resistance, R, is affected by a number of variables

and is a variable itself as shown by the frequency diagram for R in figure (2.1). Similarly, the maximum load, U, that the structure will receive in its lifetime is also a variable. As a result, the definition of the factor of safety given in equation (2.1) lacks clarity. Two possible restatements of equation (2.1) are

$$Central\ Factor\ of\ Safety = \frac{Mean\ Resistance}{Mean\ Load} = \frac{\bar{R}}{\bar{U}} \qquad (2.2)$$

or,

$$Nominal\ Factor\ of\ Safety = \frac{Design\ Resistance}{Design\ Service\ Load} = \frac{R_d}{U_d} \qquad (2.3)$$

Where R_d is the capacity computed according to the design code and U_d is the design service load given in the design code. The intersection of the frequency diagrams for R and U, shown shaded in figure (2.1), suggests that there is a definite probability that failure will occur under some possible combination of strength and load. It should be noted, however, that this area is not equal to the probability of failure.

This method of defining safety has four drawbacks:

1. It does not adequately account for the variability of loadings and resistance. Two extreme cases are compared in figure (2.2). In figure (2.2a) the control of loading and resistance are both very good and there is relatively little probability of failure as evidenced by the small overlap of the curves. Figure (2.2b) corresponds to a case with poor control of loadings and resistance. Although the central factor of safety is the same for both cases, the probability of failure is much higher in the second case.

2. It does not adequately account for variations in loadings which increase at different rates or have different signs. The factor of safety assumes that all loadings will increase at approximately the same rate. This becomes serious in the case where a highly variable load such as wind, or earthquake causes forces opposite in sign to those resulting from relatively constant loads such as dead load. The stress due to an overload may be opposite in sign to those at service loads and the reinforcement provided for service load conditions may not be adequate to prevent failure.

3. There is no attempt to evaluate the ultimate load capacity. In working stress design it is assumed that the ratio between service load capacity and ultimate capacity is the same as the ratio between allowable stresses and material strengths. This relationship has not been checked adequately for the high strength materials currently used.

4. There is no rational method for estimating safety factors against failure and the type of failure.

2.4.2 Maximum Probability of Failure Method

If R, $\bar{R}$, and σ_R represent the distribution of strengths and U, $\bar{U}$, and σ_U represent the loads, any given structure will fail if $U > R$. Thus, the probability of failure is the probability that $U > R$ or,

$$P_f = P\left((R - U) < 0\right) \tag{2.4}$$

or alternatively,

$$P_f = P\left(\frac{R}{U} < 1.0\right) \tag{2.5}$$

or since $\log 1.0 = 0$,

$$P_f = P\left(\log \frac{R}{U} < 0\right) \tag{2.6}$$

If we know $\bar{R}$, σ_R, $\bar{U}$, and σ_U, we can define a new function $Y = R - U$ (figure (2.3)). The function Y represents the *margin of safety* for a given structure. The shaded area shown in figure (2.3) represents the probability of failure of a particular structure.

$$P_f \doteq P\left((R - U) < 0\right) = \textit{shaded area} \tag{2.7}$$

For normal distribution or other standard distributions this probability can be calculated or obtained from tables as a function of the type of distribution and the value of the safety index β_s. Most ULS codes calibrated safety index $\beta_s = 3.5$ allowing for a probability of failure $P_f = 1.3 \times 10^{-4}$.

This procedure is not generally used in this form because of the work involved in evaluating the probabilities of failure for every structure. However, it forms the basis for computing load and resistance factors and hence, indirectly it is of considerable importance to designers. The major problems in the use of probabilities of failure to define safety involve the choice of acceptable probabilities of failure and the need for statistical data on many aspects of loading and construction. On the other hand, this philosophy leads to rational method for estimating safety factors.

2.5 Inelastic Methods in Bridge Design

2.5.1 Resistance to Plastic Design

Although the LSD philosophy has gained acceptance, the use of plastic analysis is not widespread in bridge design outside of yield line theory for slabs. This has led to the inconsistency of using elastic analysis to predict the distribution of load effects in a structure while the capacities are based on ultimate resistances which imply inelastic behavior. The strength calculations based on an elastic analysis normally limit the capacity of the structure to the load at which the first section reaches its capacity. In an indeterminate structure, there is usually a strength reserve between the failure of the first section and the collapse of the structure. The magnitude of that strength will depend on the degree of redundancy and the loading configuration.

There are numerous reasons for the slow acceptance of plastic analysis among bridge designers. One is the perception that it will require more work. Although plastic analysis is generally simpler than elastic analysis, the latter would still be required to check SLS requirements. Another argument against carrying out additional plastic analysis is that any elastic analysis which yields an equilibrium set of forces results in a lower bound estimate of the plastic collapse. However, if the elastic bending moment distribution is significantly different from that at plastic collapse, the predicted collapse loads will be over-conservative. A plastic analysis is required if a better estimate of the plastic collapse loads is desired. However, many designers would prefer to use an elastic analysis knowing it is conservative.

2.5.2 AASHTO Inelastic Analysis Provisions

It is often argued that any economy which may be realized by exploiting these strength reserves would not offset time and expense of the required plastic analysis. Some codes allow designers to include some of the benefits of plasticity without the inherent work of a plastic analysis by permitting a limited redistribution of the elastic bending moments. Within the LSD option, AASHTO allows a minimum of 10% reduction of the negative moments over supports, accompanied by an appropriate increase in the maximum positive moments for continuous steel beams with compact section [3]. AASHTO defines a compact section as one that is able to reach the simple plastic moment and rotate at near constant moment during redistribution. The simple plastic moments for a composite section are calculated using the assumed stress distribution shown in figure (2.4). A section is compact if the flanges and web do not exceed slenderness limits which ensure they can resist local buckling over some measure of plastic rotation. Other requirements to satisfy the compactness of the section are illustrated in table (2.1).

When the compactness requirements are satisfied, a 10% redistribution of elastic moments is allowed. This 10% is applicable at ULS and may still meet the AASHTO overload criterion, which represents the infrequent passage of heavy vehicles. This is a serviceability limit state with the criterion being that no objectionable permanent deformations occur. These are prevented by limiting the flange stress to 80% of the yield stress, σ_y, in non-composite sections under the redistributed moment, and 95% of σ_y in composite sections under the original moment distribution. However,

these limits effectively prevent any redistribution in either case. For the non-composite sections, the allowed redistribution of the elastic bending moments effectively increases the allowable flange stress to $0.89 * \sigma_y$ at a negative bending section under the elastic moments, and less than $0.80 * \sigma_y$ at the positive bending section.

2.5.3 Provisions for Inelastic Analysis in Canadian Codes

Since the CSA's "Design of Highway Bridges" [10] has not yet adopted the LSD option for steel bridges, there are no provisions for longitudinal redistribution of bending moment. Nor does the OHBDC [28] make any allowance for plastic redistribution. No non-linear analytical methods may be used except in special areas such as yield line theory for slabs. The OHBDC still classifies steel sections as compact or non-compact: a compact section being one that can reach the simple plastic moments but need not have adequate rotational capacity to allow for any redistribution. The compactness requirements are shown in table (2.1). Capacities are calculated using the fully plastic stress distribution of figure (2.4), but the effective slab widths are given by

$$\frac{B}{B_e} = 1 - \left(1 - \frac{L}{15B}\right)^3 \not> 1 \qquad (2.8)$$

Where B, B_e = Slab dimension as shown in figure (2.4),

L = Equivalent span length in positive or negative bending.

To further clarify the difference between an AASHTO compact section and an OHBDC compact section, reference is made to the CSA's "Steel Structure for Buildings-Limit States Design" [10]. Here a class 1 or plastic design section will reach the plastic moment and allow subsequent redistribution. A class 2 or compact section will reach the plastic moment but need not allow any redistribution. As seen in table (2.1), class 1 and class 2 sections correspond to the AASHTO and OHBDC compact sections respectively. Henceforth in this thesis, compact section will refer to a section suitable for plastic design.

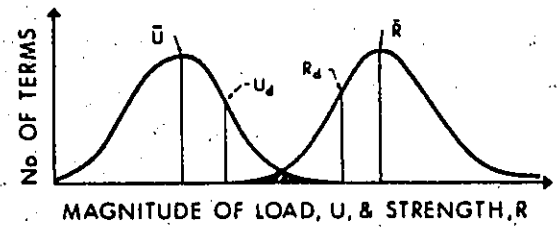

Figure 2.1: Variation of the Loads and Strengths of the Same Structures

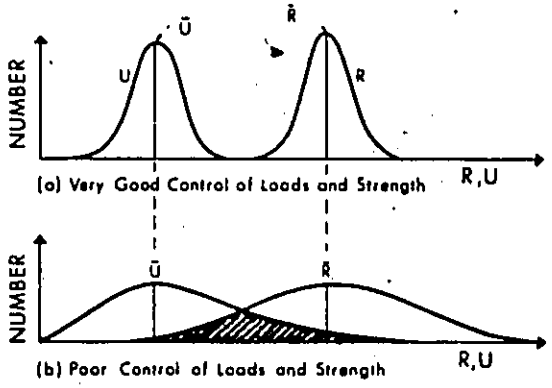

Figure 2.2: Effects of Dispersion of Loads and Strengths of Probability of Failure for Constant Central Factor of Safety

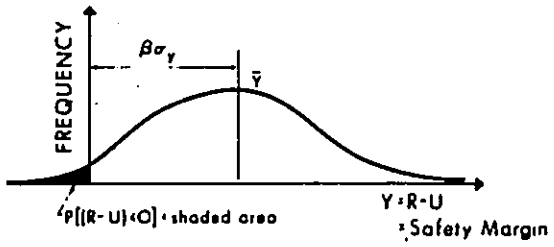

Figure 2.3: Definition of Probability of Failure and Safety Index β

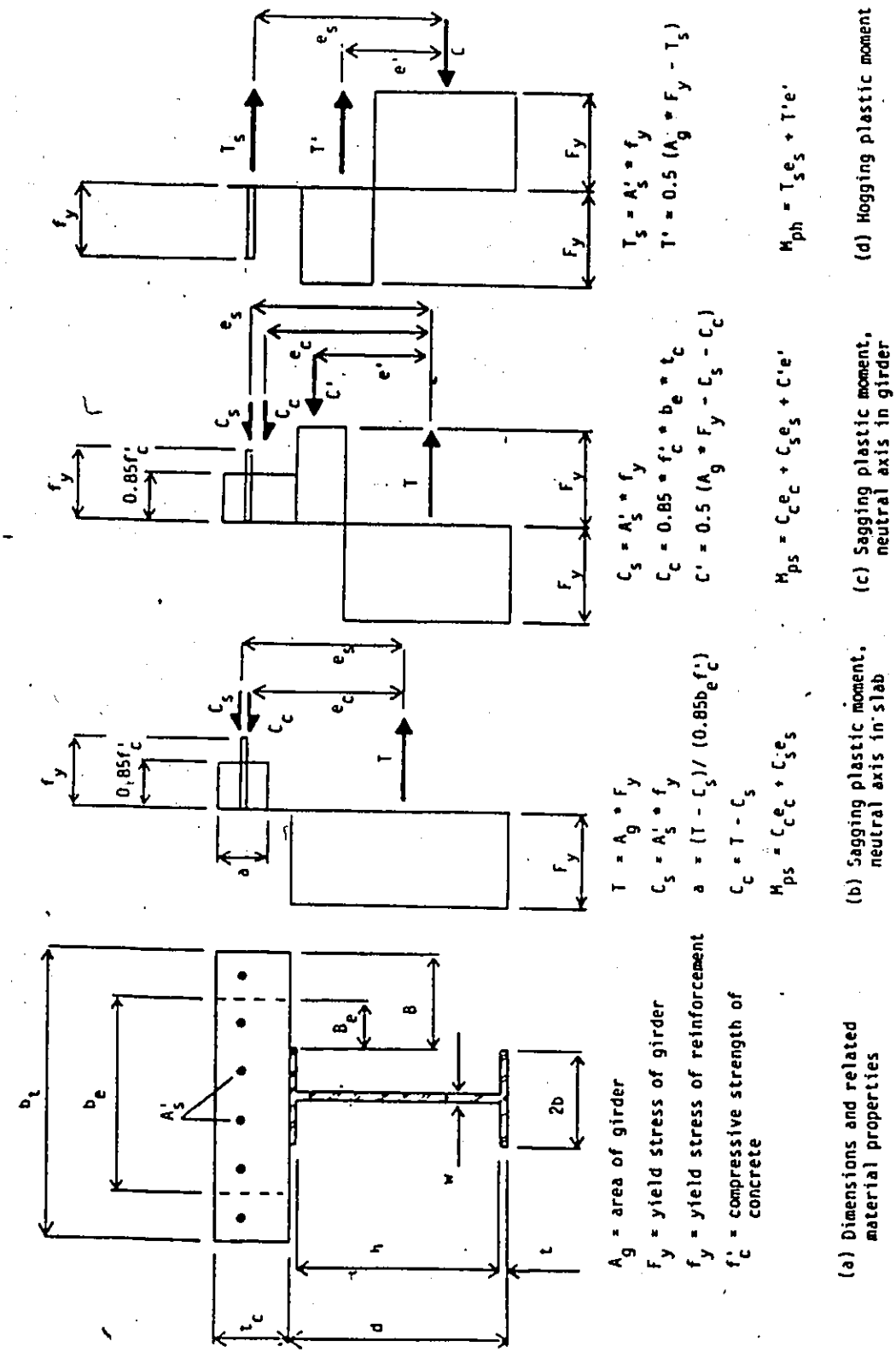

Figure 2.4: Composite Cross Section: Dimensions and Capacities Calculations

Table 2.1: Slenderness and Bracing Requirements ($M_1 < M_2$)

Slenderness or Lateral Bracing Requirement	AASHTO Compact Section	OHBDC Compact Section	CSA Class 1 (Plastic) Section	CSA Class 2 (Compact) Section
Flange Slenderness Requirement	$\frac{b}{t} \leq \frac{133}{\sqrt{F_y}}$	$\frac{b}{t} \leq \frac{170}{\sqrt{F_y}}$	$\frac{b}{t} \leq \frac{145}{\sqrt{F_y}}$	$\frac{b}{t} \leq \frac{170}{\sqrt{F_y}}$
Web Slenderness Requirement in Flexure	$\frac{d}{w} \leq \frac{1104}{\sqrt{F_y}}$	$\frac{d}{w} \leq \frac{1370}{\sqrt{F_y}}$	$\frac{h}{w} \leq \frac{1100}{\sqrt{F_y}}$	$\frac{h}{w} \leq \frac{1370}{\sqrt{F_y}}$
Maximum Unbraced Length for no Reduction in Simple Plastic Moment	$L_b \leq \frac{581 * r_y}{\sqrt{F_y}}$ for $M_1 > 0.7M_2$ $L_b \leq \frac{996 * r_y}{\sqrt{F_y}}$ for $M_1 < 0.7M_2$	$L_b \leq \frac{550 * r_y}{\sqrt{F_y}}$ for $M_1 > 0.7M_2$ $L_b \leq \frac{980 * r_y}{\sqrt{F_y}}$ for $M_1 < 0.7M_2$	$L_b \leq \frac{550 * r_y}{\sqrt{F_y}}$ for $M_1 > 0.5M_2$ $L_b \leq \frac{980 * r_y}{\sqrt{F_y}}$ for $M_1 < 0.5M_2$	$L_b \leq \frac{550 * r_y}{\sqrt{F_y}}$ for $M_1 > 0.5M_2$ $L_b \leq \frac{980 * r_y}{\sqrt{F_y}}$ for $M_1 < 0.5M_2$

Chapter 3

LOAD DISTRIBUTION METHODS

3.1 General

Following the advent of the digital computer, and the subsequent development of analytical and numerical techniques based upon its use, the bridge designer has available today a number of powerful analytical and numerical refined methods of analysis such as the orthotropic plate theory, the grillage analogy, the finite difference method, the finite element method etc... The finite element method is considered the most powerful method of analysis. It has been, by and large, applied to the elastic and plastic analysis of composite bridges. Since the current study also employs this method, it will be fully explained in chapter four.

Most of bridge design codes use these simplified methods of analysis to determine the load distribution characteristics in which the D-type method forms the basis. A D-type method, which is usually developed by idealizing a bridge as an orthotropic plate, is based upon the premise that the distribution pattern of longitudinal moments across a transverse cross section is reasonably independent of the longitudinal position of the load.

The concept of the factor D can be explained with reference to figure (3.1), which shows the transverse distribution M_x at a cross section due to a vehicle on a slab-on-girder bridge idealized as an orthotropic plate.

The total live-load moment M_g that the second girder from the left should be required to sustain is equal to the area under the curve shown hatched in the figure (3.1). If the intensity of the maximum longitudinal moment is $M_{x,max.}$, and the girder spacing is S, then this area is approximately equal to

$$M_g = SM_{x,max.} \tag{3.1}$$

Assuming that the quantity $M_{x,max.}$ can be obtained by a factor D given by

$$D = \frac{M}{M_{x,max.}} \tag{3.2}$$

Where M is the moment due to one line of wheels at the section under consideration.

Substituting $M_{x,max.}$ from equation (3.1) into equation (3.2) gives

$$M_g = \frac{S}{D}M \tag{3.3}$$

Thus, if the value of D is known for a bridge, the maximum live-load moment in width S of the bridge can be obtained as a fraction S/D of the beam bending moment due to one line of wheels.

3.2 Codes Approach

The most important codes of practice for the analysis of composite and non-composite bridges in North America are:

1. Standard Specifications for Highway Bridges, American Association of State Highway and Transportation Officials, (AASHTO-77), 1977.
2. Ontario Highway Bridge Design Code (OHBDC), 1983.
3. Canadian Standards Association for Design of Highway Bridges (CAN3-S6-M78), 1978.

The codes specify two types of loading to be considered in design, the truck load and the lane load. The latter is not critical in load distribution; hence only truck load will be discussed. The codes have devised a truck model that is supposed to simulate the actual loading conditions. The configuration of this truck varies among the three codes. The loading configuration corresponding to these three codes is shown in figure (3.2). The recommended methods for the distribution of loads in the AASHTO-77 and CAN3-S6-M78 are identical, whereas the OHBD code's method is different.

3.2.1 The AASHTO Method of Analysis

The AASHTO specifications for highway bridges [3] permit a simplified method for obtaining longitudinal moments and shears due to live loads. According to this method, a longitudinal girder or box girder is isolated from the rest of the structure and treated as a one-dimensional beam. The fraction of the wheel load carried by each girder or box girder shall not be less than the distribution factor, D_f, which is a dimensionless number and is specified in terms of the girder or web spacing S,

$$D_f = \frac{S}{K} \tag{3.4}$$

Where K is a factor which has the unit of length and its value is a function of the bridge type.

It can be observed that according to equation (3.4) the only parameters that influence the load distribution in bridges are the girder or web spacing and the bridge type which is an extreme simplification. This over-simplification can give erroneous results for some cases. Values of K for various types of bridges are given in AASHTO specifications [3]. These values are based upon research reported in reference [3]. In the AASHTO method, the value of K depends only on the bridge type; however, it is intuitively obvious, and confirmed by accurate analysis, that the load distribution in a narrow and long bridge is different from that in a short and wide bridge of the same type. The AASHTO method is unable to allow for differences in pattern of load distribution arising from such factors as the aspect ratio of the bridge.

The AASHTO method which is based on the orthotropic plate theory, has two basic assumptions;

- For a given bridge, the transverse distribution pattern is the same for all load effects, i.e. deflections, moments and shear.
- The transverse distribution of load effects is independent of the longitudinal positions of loads and reference section.

3.2.2 OHBDC Simplified Method

Because of the inadequacy of the AASHTO method, the OHBDC was developed to provide a more refined method of analysis which accounts for the material and geometric characteristics of the bridge. The OHBDC requires that the load distribution characteristics resulting from different relative torsional and flexural rigidities in the longitudinal and transverse directions must be taken into consideration.

The Ontario code requires that for the ultimate limit state and serviceability limit state type II, as many lanes in a bridge must be loaded as will produce the maximum load effect. The method was developed for one, two, three, and four lane bridges for the various loaded lane conditions. It involves the calculation of two characteristic parameters, α and θ, where α is called the torsional parameter and θ the flexural parameter. These are given by

$$\alpha = \frac{D_{xy} + D_{yx} + D_1 + D_2}{2(D_x D_y)^{0.5}} \tag{3.5}$$

$$\theta = \frac{b}{L}\left(\frac{D_x}{D_y}\right)^{0.25} \tag{3.6}$$

Where b = Half width of the bridge,

L = Span length of the bridge,

D_x = Flexural rigidity in the x direction,

D_y = Flexural rigidity in the y direction,

D_{xy} = Longitudinal torsional rigidity,

D_{yx} = Transverse torsional rigidity,

D_1 = Coupling longitudinal rigidity,

D_2 = Coupling transverse rigidity.

The calculation of the live load longitudinal moments in both the internal and external portions of a bridge can be summarized in the following steps:

1. Obtain an initial value of D from the OHBDC, according to the number of design lanes and bridge type.

2. Calculate the initial load fraction S/D, where S is the girder spacing in slab-on-girder bridges and web spacing in box girder bridges.

3. Obtain the moment due to one-half of the OHBDC truck or lane loading.

4. Multiply the moment obtained by $S/D(1+DLA)$, where DLA is the dynamic load allowance as described in the OHBDC clause [2-4.3.2].

5. Calculate α and θ from the equations (3.5) and (3.6).

6. Calculate μ from

$$\mu = \frac{W_e - 3.3}{0.6} \leq 1$$

W_e=design lane width in meters.

7. From the OHBDC charts of clause [3-7.1.2.1], obtain the value of D and C_f for internal and external portions.

8. Obtain the final value of D_{design} using:

$$D_d = D\left(1 + \frac{\mu C_f}{100}\right)$$

9. Obtain the final value of the moments for external and internal portions by multiplying the moment obtained in step 3 by the term $S/D_d(1 + DLA)$, (D_d being found in step 8).

The parameters α and θ describing slab-on-girder bridges are not capable of characterizing box girder bridges due to the distortion or shear effect. In order to account for this effect, another parameter must be derived and is defined as follows

$$\beta = \pi\left(\frac{2b}{L}\right)\left(\frac{D_x}{D_{xy}}\right)^{0.5} \tag{3.7}$$

or,

$$\beta = \sqrt{2}\pi\frac{\theta}{\sqrt{\alpha}} \tag{3.8}$$

The calculation of moments for box girder bridges follows the same steps described above with the additional calculation of the parameter β from equation (3.7) after step 4 and the obtaining of D and C_f from other charts which are a function of the parameter β as shown in appendix A.

For the continuous bridges, different D_d values will apply for each region on positive and negative bending. The calculation of D_d values for the bridges analyzed in this study are included in appendix A.

It can be seen that the OHBDC is far more elaborate, although relatively simple to apply. As described by Bakht et al [4,12] the attractive feature

of this procedure is that it unifies the load distribution analysis of almost all types of bridges. What distinguishes the different bridge cross-section is the manner in which the various rigidities values are calculated. The remaining steps are identical.

3.3 Load Distribution Factors Based on Non-linear Analysis

Studies in this regard are scant and of limited scope. Heins et al [19,20] conducted studies using an elasto-perfectly plastic finite difference model as described earlier. Accordingly, they used two methods to evaluate the load distribution characteristics of slab-on-girder bridges.

Method 1: In this method the distribution factor is given by

$$D_f = \frac{2\left(Max.\frac{M}{M_y}\right)M_y}{N * M_{AASHTO}} \qquad (3.9)$$

Where M = Total longitudinal moment on a given section of the bridge,

M_y = Yielding moment of girder,

N = No. of trucks/No. of traffic lanes,

M_{AASHTO} = Maximum moment in a single girder due to truck loading as given by AASHTO code specifications.

Note that the first term in the numerator of equation (3.9) is the absolute

maximum of all the girders in the bridge. As can be seen, D_f is based on the fraction of the total moment carried by each girder.

Method 2: In this method the distribution factor is based on the fraction of a line of truck wheels, i.e.

$$D_f = \frac{\left(Max.\frac{M}{M_y}\right) * (No.\ of\ line\ wheels)}{\left(\sum \frac{M}{M_y}\right)} \tag{3.10}$$

or,

$$D_f = \frac{\left(Max.\frac{M}{M_y}\right) * (2 * NL)}{\left(\sum \frac{M}{M_y}\right)} \tag{3.11}$$

Where NL = Number of traffic lanes,

$\sum \frac{M}{M_y}$ = Sum of moment ratios for all girders across the bridge.

Using the above two methods, they obtained the $K = S/D_f$ values listed in tables (3.1) and (3.2) for the elastic analysis and ultimate limit states, respectively.

In table (3.1), it can be seen that the two methods give results that are fairly close. Secondly, we observe that the $K = 5.5$, as suggested by AASHTO, is generally conservative.

At the ultimate limit state, the results in table (3.2) show that again the two methods compare favorably. However, in this case the AASHTO values for K are conservative for all bridges considered. This suggests that the bridges can carry more load than anticipated by current AASHTO requirements.

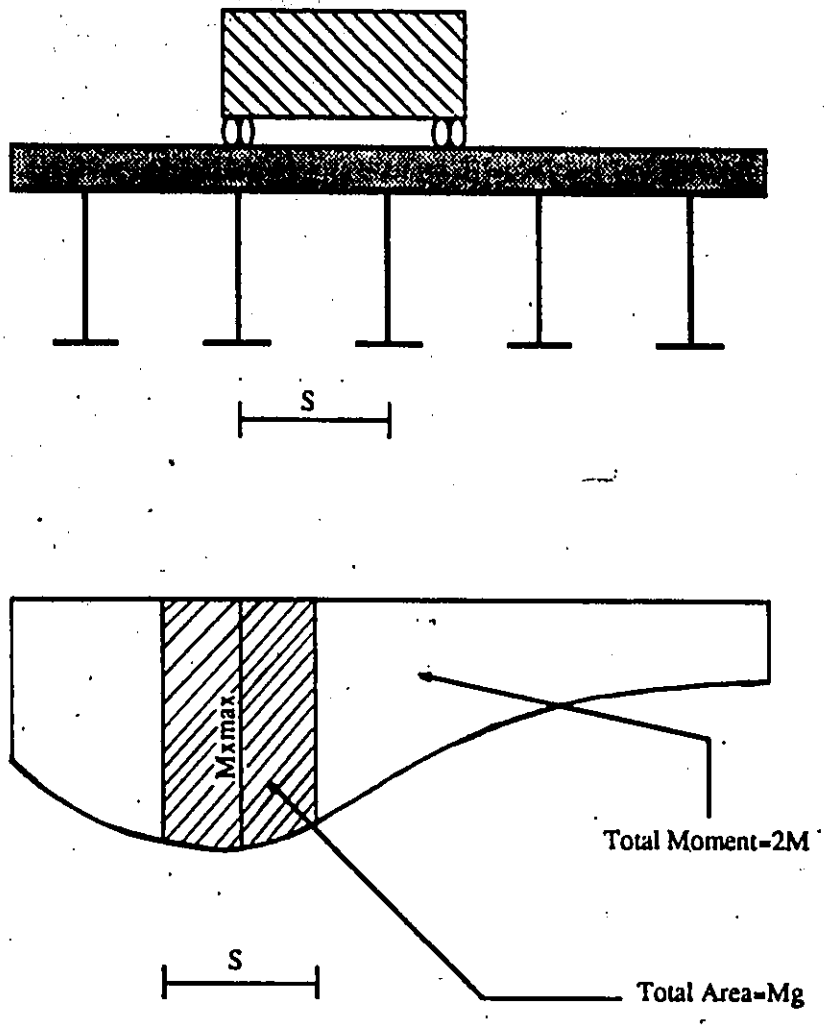

Figure 3.1: Transverse Distribution of the Longitudinal Moments

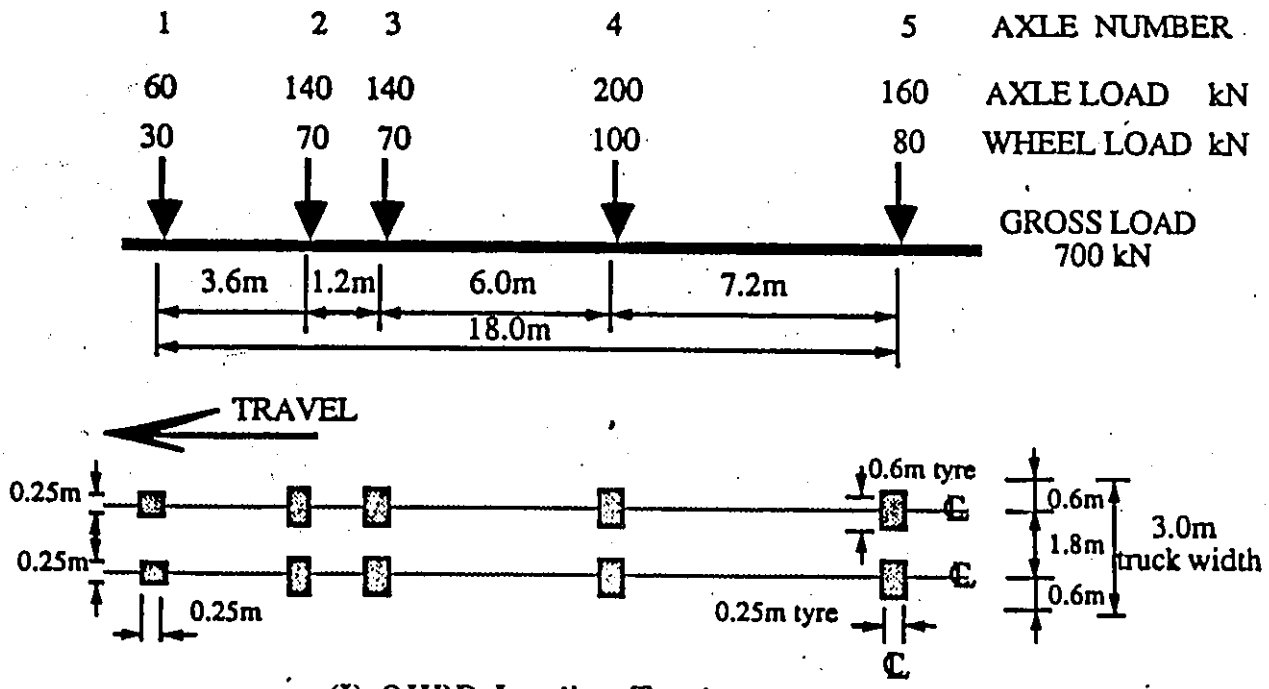

(I) OHBD Loading Truck

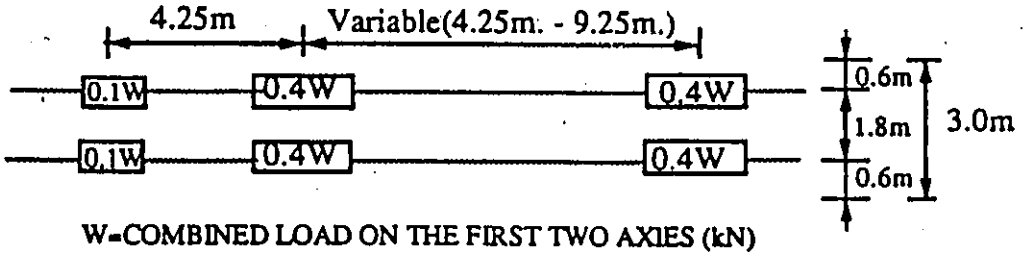

W=COMBINED LOAD ON THE FIRST TWO AXIES (kN)

(II) MS-77 Loading Truck

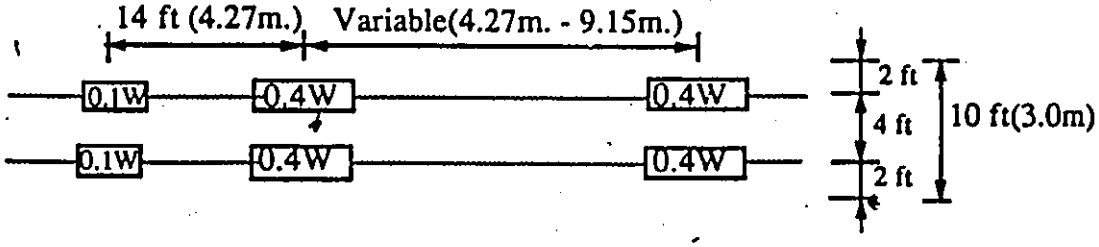

(III) HS AASHTO Loading Truck

Figure 3.2: Loading Configuration of the Three Codes

Table 3.1: Distribution Parameter (Elastic Load)

Span	Spacing	2-Lanes		3-Lanes		4-Lanes	
(Ft.)	(Ft.)	Method1	Method2	Method1	Method2	Method1	Method2
40	6.0	5.68	5.94	5.45	5.50	5.23	5.23
	7.0	6.03	5.92	5.23	5.29	5.30	5.22
	8.0	6.27	6.14	5.45	5.27	5.26	5.16
	9.0	6.51	6.42	5.42	5.33	5.31	5.16
50	6.0	5.82	5.87	5.25	5.19	5.12	4.97
	7.0	6.34	5.87	5.25	5.31	5.12	5.00
	8.0	6.35	6.50	5.34	5.36	5.07	5.15
	9.0	6.65	6.28	5.32	5.15	5.18	5.00
60	6.0	5.91	5.80	5.33	5.24	5.07	4.80
	7.0	6.11	6.17	5.20	5.35	5.10	4.93
	8.0	6.41	6.62	5.39	5.46	5.05	4.96
	9.0	6.65	6.89	5.75	5.05	5.20	4.90
70	6.0	6.27	5.74	5.40	5.16	5.03	4.65
	7.0	6.16	6.30	5.25	5.48	5.10	5.22
	8.0	6.45	6.65	5.41	5.48	5.01	4.91
	9.0	6.72	6.93	5.38	5.50	5.15	4.87
80	6.0	6.00	6.55	5.37	5.64	5.03	5.26
	7.0	6.23	6.51	5.40	5.69	5.04	4.67
	8.0	6.62	6.95	5.45	5.62	4.98	4.84
	9.0	6.95	7.32	5.48	5.70	5.18	4.77
90	6.0	6.03	6.63	5.41	5.79	4.98	4.52
	7.0	6.26	6.55	5.43	5.80	5.11	4.73
	8.0	6.74	7.08	5.51	5.71	5.01	4.87
	9.0	7.11	7.46	5.57	5.80	5.37	5.34
100	6.0	6.07	5.48	5.46	5.89	5.10	6.59
	7.0	6.28	6.57	5.45	5.83	5.17	5.40
	8.0	6.86	7.18	5.55	5.75	5.10	5.32
	9.0	–	–	–	–	–	–

Table 3.2: Distribution Parameter (Ultimate Load)

Span	Spacing	2-Lanes		3-Lanes		4-Lanes	
(Ft.)	(Ft.)	Method1	Method2	Method1	Method2	Method1	Method2
40	6.0	6.68	7.44	6.22	6.76	6.17	6.67
	7.0	7.03	6.79	6.37	6.98	6.02	6.01
	8.0	7.69	7.94	6.18	6.28	6.12	6.70
	9.0	7.98	8.26	6.35	6.71	5.76	5.71
50	6.0	7.35	7.44	6.34	6.83	6.45	6.68
	7.0	7.35	7.00	6.39	6.93	5.82	6.41
	8.0	7.63	7.99	6.58	6.63	6.36	6.72
	9.0	7.88	7.57	7.03	7.28	6.00	6.66
60	6.0	7.50	7.33	5.68	5.75	6.64	6.64
	7.0	7.09	7.00	6.40	6.92	6.13	6.95
	8.0	7.62	7.96	6.42	6.66	6.40	6.65
	9.0	8.33	8.91	6.75	6.52	6.15	6.72
70	6.0	7.43	6.75	6.95	6.84	5.90	6.07
	7.0	7.06	7.00	6.38	6.94	6.17	6.74
	8.0	7.83	7.95	6.42	6.64	6.20	6.35
	9.0	9.45	8.91	6.97	7.35	6.30	6.36
80	6.0	6.88	7.51	6.52	6.95	6.23	6.58
	7.0	6.94	7.00	6.77	6.98	6.81	6.92
	8.0	7.70	8.00	6.67	8.00	6.37	6.51
	9.0	8.83	8.99	7.09	7.46	6.65	6.70
90	6.0	6.92	7.52	6.29	6.98	6.71	6.61
	7.0	6.84	6.00	6.67	6.99	7.20	6.72
	8.0	7.66	8.00	6.48	6.66	6.55	6.72
	9.0	8.39	8.96	6.97	7.43	6.65	6.62
100	6.0	6.98	7.52	6.56	6.98	6.10	6.59
	7.0	6.75	7.00	6.38	6.95	6.20	6.71
	8.0	7.92	7.97	6.42	6.64	6.48	6.77
	9.0	–	–	–	–	–	–

Chapter 4

FINITE ELEMENT ANALYSIS

4.1 General

It was mentioned in the beginning of this thesis that the non-linear finite element technique will be used in the present study. This chapter will describe the finite element method and program and its development. A composite bridge consists of two main components, each with its distinct behavior: the reinforced concrete slab and the steel girders or box girders. The shear studs that connect the slab to the girders or box girders are not considered in this study. In the subsequent sections, the modelling of each of the two components will be described.

The finite element program utilized for the purpose of this current study is

called ADINA [1,2] (Automatic Dynamic Incremental Non-linear Analysis). More details on this program are given in the section 4.5.

4.2 Finite Element Method

4.2.1 General

The finite element method is the most versatile method of analysis available today. The concept of finite element stems from the idea of discretization and numerical approximations. The finite element method is a technique for analyzing complicated structures by rationally dividing the continuum of the prototype into a number of small elements. These elements are connected at discrete joints called nodes. A brief discussion of the method and the element types will be presented in the next sections.

4.2.2 Basic Equations of Finite Element

In order to establish a basis for the material models used, some basic equations of the finite element method will be presented. Using the principle of minimization of the total potential energy, the following equation of equilibrium can be written

$$[k]\{d\} = \{R\} + \{F\}_b + \{F\}_s + \{F\}_\varepsilon + \{F\}_\sigma \qquad (4.1)$$

Where [k] = Structure stiffness matrix,

$\{d\}$ = Vector of nodal displacements,

$\{R\}$ = Vector of applied nodal forces,

$\{F\}_b$ = Vector of nodal forces due to body forces,

$\{F\}_s$ = Vector of nodal forces due to surface tractions,

$\{F\}_\epsilon$ = Vector of nodal forces due to initial strains,

$\{F\}_\sigma$ = Vector of nodal forces due to initial stresses.

The displacement field $\{\delta\}$ inside an element can be related to the nodal displacement $\{d\}^e$ as

$$\{\delta\} = [N]\{d\}^e \tag{4.2}$$

Where $[N]$ is the shape functions matrix. Note that the superscript e is used to denote quantities at the element level. The strain $\{\epsilon\}$ and nodal displacements $\{d\}^e$ are related by the strain-displacement matrix $[B]$ as

$$\{\epsilon\} = [B]\{d\}^e \tag{4.3}$$

Using the constitutive matrix $[D]$, the element stresses are computed from the element strain as follows

$$\{\sigma\} = [D](\{\epsilon\} - \{\bar{\epsilon}\}) + \{\bar{\sigma}\} \tag{4.4}$$

Where $\{\bar{\epsilon}\}$= Vector of initial strains,

$\{\bar{\sigma}\}$= Vector of initial stresses.

By applying equations (4.2) to (4.4), elements of equation (4.1) can now be written in more detail as

$$[k] = \sum_e \int [B]^T [D][B] dV^e \tag{4.5}$$

$$\{F\}_b = \sum_e \int [N]^T \{g\} dV^e \tag{4.6}$$

$$\{F\}_s = \sum_e \int [N]^T \{p\} dS^e \tag{4.7}$$

$$\{F\}_\varepsilon = \sum_e \int [B]^T [D] \{\bar{\epsilon}\} dV^e \tag{4.8}$$

$$\{F\}_\sigma = \sum_e \int [B]^T \{\bar{\sigma}\} dV^e \tag{4.9}$$

In the above $\{g\}$ and $\{p\}$ are vectors of body forces and surface tractions, respectively.

4.2.3 Element Types

A structure can be modelled using one-, two- or three-dimensional elements or a combination of these elements.

One-Dimensional Elements

The one-dimensional (line) element connects two or more nodes which lie on a line. The first, shown in figure (4.1a) is a bar element which can take only axial tension or compression; in consequence, it has one degree of freedom at each node. The second one-dimensional element is the beam, shown in figure (4.1b), which has bending strength with respect to principal axes of bending as well as axial strength, and which consequently has six degrees of freedom per node.

Two-Dimensional Elements

A two-dimensional (plate) element connects three or more non-linear nodes. If the nodes are allowed to have displacements only in their own plane, the element is termed an extensional or membrane element. It has two degrees of freedom (u, v) at each node, as shown in figure (4.2a). This implies that the element has stiffness in its own plane only. Alternatively, the element may be used to simulate plate-bending (flexural) action by specifying three-degrees of freedom (w, θ_x, θ_y) at each node as shown in figure (4.2b). These two-dimensional elements are, for the most part, triangular or rectangular in shape.

Membrane actions and flexural actions can be combined to form a flat shell element, thus giving five degrees of freedom $(u, v, w, \theta_x, \theta_y)$ at each node of the element, as shown in figure (4.2c). Consistent with linear, small deformation theory, it is usually assumed that the in-plane deformation (u, v) and the bending deformations (w, θ_x, θ_y) are uncoupled [21].

It can be seen that the two-dimensional elements form a natural extension from the one-dimensional bar and beam elements. However, degrees of freedom at each node need not be restricted to those mentioned here. Additional degrees of freedom (curvature, twist, etc.) or additional nodes within the element or along its edges may be introduced to improve accuracy or, for various specialized applications. Some examples of these higher order elements are illustrated in figure (4.3).

When plate bending is to be used to form a shallow surface (i.e. an almost plane surface having a small curvature out of its own plane), the nodes will

possess six degrees of freedom (figure 4.4). If the curvature is slight, this will result in an ill-conditioned matrix and poor numerical accuracy, because of the omission of an in-plane bending capability. This disadvantage can be overcome by introducing special rotational constraints in the form of boundary elements. A better way still is to use shell elements which themselves have finite curvature and which have six degrees of freedom if they are available in the finite element system. This is important in the case of bridge decks having curvature out of its own plane which has to be modelled taking into account its true geometry. An important application of this case is an arch bridge with a slab deck.

Three-Dimensional Elements

Three-dimensional solid elements connect four or more nodes which are not in plane. They are rarely used to model bridge superstructures. The simplest ones are tetrahedral and hexahedral elements. They are shown in figure (4.5).

It should be noted that formulations for most of the two-dimensional plate or shell bending elements are based on the Kirshoff hypothesis for thin plates, which actually neglects cross-sectional shear distortion. This is analogous to the omission of shear distortion terms in calculating beam bending stiffness. In the cases where shear distortion effects are likely to be significant, such as voided slab and cellular structures, special attention should be paid to selecting the type of element, if a two-dimensional formulation of the finite element model is desired.

4.2.4 Quadrilateral Shell Elements

The shell element is a 4- to 32-node isoparametric element that can be employed to model thick and thin general shell structures. However, depending on the application, an appropriate number of nodes on the element must be employed.

The shell element can be used in the following analysis conditions:

- Linear analysis, in which case the displacements, rotations, and strains are infinitesimally small and the material is linear elastic.
- Materially-non-linear-only for which the displacements and strains are infinitesimally small, but the material behavior is non-linear.
- Total Lagrangian formulation for very large displacements and rotations but small strains, and the material behavior can be linear elastic or non-linear elasto-plastic.

The shell element is formulated treating the shell as a three dimensional continuum. The in-plane and bending actions are assumed to be coupled in the element. Figure (4.6) shows a typical polygonal flat element subject simultaneously to in-plane and bending actions. The strain $\{\epsilon\}$ at a general point within the element can be expressed as

$$\{\epsilon\} = \{\epsilon_0\} - z\{\chi\} \tag{4.10}$$

Where $\{\epsilon_0\}$ are the in-plane strains of the projection of the same point on the reference plane, $\{\chi\}$ is the vector of curvatures due to bending and z is the local z coordinate of the point under consideration. From basic theory,

$$\{\epsilon_0\} = [B]_p\{d\}_p \tag{4.11}$$

$$\{\chi\} = [B]_b\{d\}_b \tag{4.12}$$

Where the subscript p and b stand for in-plane and bending components. Equation (4.10) can be rewritten as

$$\{\epsilon\} = ([B]_p - z[B]_b)\begin{pmatrix} d_p \\ d_b \end{pmatrix} = [B]\{d\} \tag{4.13}$$

The stiffness of the element is given by

$$[k] = \int [B]^T[D][B]dV \tag{4.14}$$

Substituting for $[B]$ from equation (4.13) into equation (4.14), we obtain

$$[k] = \int \begin{bmatrix} [B]_p{}^T[D][B]_p & -z[B]_p{}^T[D][B]_b \\ -z[B]_b{}^T[D][B]_p & z^2[B]_b{}^T[D][B]_b \end{bmatrix} dV \tag{4.15}$$

or,

$$[k] = \begin{bmatrix} [k]_{pp} & [k]_{pb} \\ [k]_{bp} & [k]_{bb} \end{bmatrix} \tag{4.16}$$

The two diagonal terms are the stiffness of in-plane and bending actions, respectively. The off-diagonal terms are the coupling matrices.

The minimization of the total potential energy gives nodal forces due to displacements parameters d as

$$\{F\}^e = [k]^e\{d\}, \tag{4.17}$$

Where

$$\{F\}^e = \begin{Bmatrix} U_i \\ V_i \\ W_i \\ M_{xi} \\ M_{yi} \\ M_{zi} \end{Bmatrix} \quad and \quad \{d\}_i = \begin{Bmatrix} u_i \\ v_i \\ w_i \\ \theta_{xi} \\ \theta_{yi} \\ \theta_{zi} \end{Bmatrix}$$

For the purpose of this study, a nine-node shell element was used with five degrees of freedom at each node. This was considered to provide the best modelling of the structure and to be in accordance with the ADINA modelling recommendations [2].

4.2.5 Accuracy of the Method

The basic philosophy of the finite element method is piecewise approximation. An approximate solution is sought to a complicated problem by sub-dividing the region of interest. The solution within each element is defined by a relatively simple function. In the more commonly used displacement method of structural analysis, the assumed solution consists of a displacement function which is specified in terms of nodal coordinates, and which is sometimes referred to as the shape function. If the exact solution to the structural problem is defined as $\phi(x, y, z)$, then this idealization can be considered as a series of piecewise shape functions defined at each node point which can be interpolated over the element boundaries. Inherent in this approximation is the concept of convergence to the exact solution $\phi(x, y, z)$, i.e. that the greater the number of elements used to define a structural model, the better is the accuracy of the solution obtained from

the analysis. Unfortunately, this convergence is not always obtainable unless certain conditions are satisfied. It may be noted that the accuracy and the convergence to the exact solution depend not only on the number of elements, but also on the type of element.

4.3 Material Modelling

It is important to recognize what stress and strain measures are employed in the material model:

- In the preparation of the ADINA input data in which the material parameters are defined with respect to these stress and strain measures; and
- In the interpretation of the analysis results in which the type of stresses and strains output must be considered.

The materials involved in the present study are concrete and steel plates. In the following, the constitutive models used for each material will be described.

4.3.1 Linear Elastic Concrete Model

The linear elastic material models available in ADINA [1,2] are the isotropic linear elastic and the orthotropic linear elastic. In each case, it is assumed that the total stress is uniquely determined by the total strain. In the

present analysis, the two material constants used to define the constitutive relation in the material matrix C are:

- E= Young's modulus.
- ν= Poisson's ratio.

These constants are employed in infinitesimal displacement analyses and large displacement analyses. Hence the material matrices C are identically the same for all formulations.

4.3.2. Plastic Steel Modelling

A fundamental observation comparing elastic and inelastic analysis is that in elastic solutions the total stress can be evaluated from the total strain alone, whereas in an inelastic response calculation the total stress at time t depends on the stress and strain history.

The three plasticity models used in ADINA [1,2] are the von Mises model, the Drucker-Prager model, and the Ilyushin model. Since the von Mises is used in this thesis, its basic formulations will be summarized.

The von Mises model is based on

- The von Mises yield condition, which specifies the state of multi-axial stress corresponding to the start of plastic flow;
- An associated flow rule, which relates the plastic strain increments to

the current stresses and the stress increments subsequent to yielding, and

- A hardening rule, which specifies how the yield condition is modified during plastic flow.

The von Mises model yield surface is a cylinder in the principal stress space as shown in figure (4.7), and is given by

$$F = \frac{1}{2}s_{ij}s_{ij} - \frac{1}{3}(\sigma_y)^2 \tag{4.18}$$

$$s_{ij} = \sigma_{ij} - \frac{\sigma_{mm}}{3}\delta_{ij} \tag{4.19}$$

$$\sigma_{mm} = \sum_m \sigma_{mm} \tag{4.20}$$

$$\delta_{ij} = \begin{cases} 0 & \text{when } i \neq j \\ 1 & \text{when } i = j \end{cases} \tag{4.21}$$

In which s_{ij} = Deviatoric stress,

σ_y = Yield stress at time t,

δ_{ij} = Kronecker delta.

The hardening function H for work hardening can be obtained from simple tension as

$$H = \frac{2}{3}\left(\frac{E * E_T}{E - E_T}\right) \tag{4.22}$$

Where E_T is the strain-hardening modulus illustrated in figure (4.7). Note that the variable H is zero in perfect plasticity.

The von Mises models can be used for the following analysis conditions:

- Materially-non-linear-analysis for infinitesimally small displacements and strains.
- Total Lagrangian for large displacements and rotations but small strains.
- Updated Lagrangian formulation for large displacements and large strains for two- and three-dimensional solid elements (isotropic hardening).

4.4 Non-linear Analysis Method

It was stated earlier that an incremental-iterative procedure is applied to solve the system of non-linear equations. The non-linearity dealt with here is due to the non-linear stress-strain relationship of the materials (steel) involved. Specifically, the constitutive matrix $[D]$ is a function of the stress level, i.e.

$$[D] = f(\{\sigma\}) \tag{4.23}$$

Since stresses are dependent on the nodal displacements, it is obvious that the stiffness matrix, which contains $[D]$, is also a function of the nodal displacements. This makes equation (4.1) non-linear.

If we denote the total nodal force vector on the right-hand side of equation (4.1) by $\{F\}$, then it can be written as

$$[k]\{d\} = \{F\} \tag{4.24}$$

It should be observed that $[k]$ is a function of $\{d\}$. Since $[k]$ is not known *a priori*, the solution of equation (4.24) requires an iterative procedure. In implementing this procedure, the load is divided into a number of increments. After the application of a load increment i, for the first iteration the tangent stiffness evaluated at the end of the preceding load increment, $[k]_{i-1}$, is used to evaluate the incremental displacements $\{\Delta d\}_i$ as

$$[k]_{i-1}\{\Delta d\}_i = \{\Delta F\}_i \tag{4.25}$$

In Which $\{\Delta F\}_i$ is the vector of incremental load corresponding to the increment i.

Using $\{\Delta d\}_i$, the incremental strains $\{\Delta \epsilon\}_i$ are calculated according to equation (4.3). The incremental strains are added to the previous total strains to obtain the new total strains. These total strains are then used in conjunction with the available stress-strain relations to obtain the new total stresses.

The internal nodal forces corresponding to the total stresses are evaluated next, and then equilibrium is checked between the internal and external forces. If there are any residual forces, these are reversed in direction and applied as new nodal forces. This procedure is repeated until equilibrium is satisfied within prescribed limits. More details of non-linear analysis are given among others by Zienkiewicz [42] and Bathe [8]. Some of the most generally applicable methods available are described in detail in reference [31]. They will be listed below:

1. The method of direct iteration (or successive approximations);
2. The Newton-Raphson method;

3. The tangential stiffness method; and

4. The initial stiffness method.

4.5 Finite Element Program

The ADINA program used herein to carry out the inelastic analysis was developed at Massachusetts Institute of Technology (M.I.T.) by Bathe in 1983. It was then modified by the same person in 1984. The program was later implemented on the university of Ottawa AMDAHL computer. This program has the capability to trace the full non-linear behavior of any structure modelled as an assemblage of thin shell elements. This includes beams, plates, shells, folded plates, box girder etc. The finite element package provides the distribution of displacements and stresses across a section in the bridge. This distribution results from the discretization of the slab and the longitudinal members of the structure into longitudinal and transverse strips. The ratio in the formed element should not exceed four.

Input for the program consists of the structure geometry and the properties of the models representing the structure. Appendix B includes some of the input data used in the analysis.

As a first step in this thesis, it was thought appropriate to check the accuracy of the ADINA program. Two beams were considered for the verification. The first one is an I-beam and the second is a box-beam. The method of verification consisted of idealizing the two beams by finite element. De-

rive the displacements and stresses from the ADINA finite element analysis. Finally, compare the finite element results with those of the beam theory. Both beams were single span, simply supported. The cross-section, elevations, and finite element idealizations are shown in figures (4.8) and (4.9). The properties of the beams were assumed and are tabulated in table (4.1).

Table (4.2) shows values of displacements, stresses, and percent error for both theoretical and numerical analyses. Since the error is less than 6%, ADINA program can be considered as an accurate program that fits well with the beam theory. The errors would be smaller if the idealizations were finer.

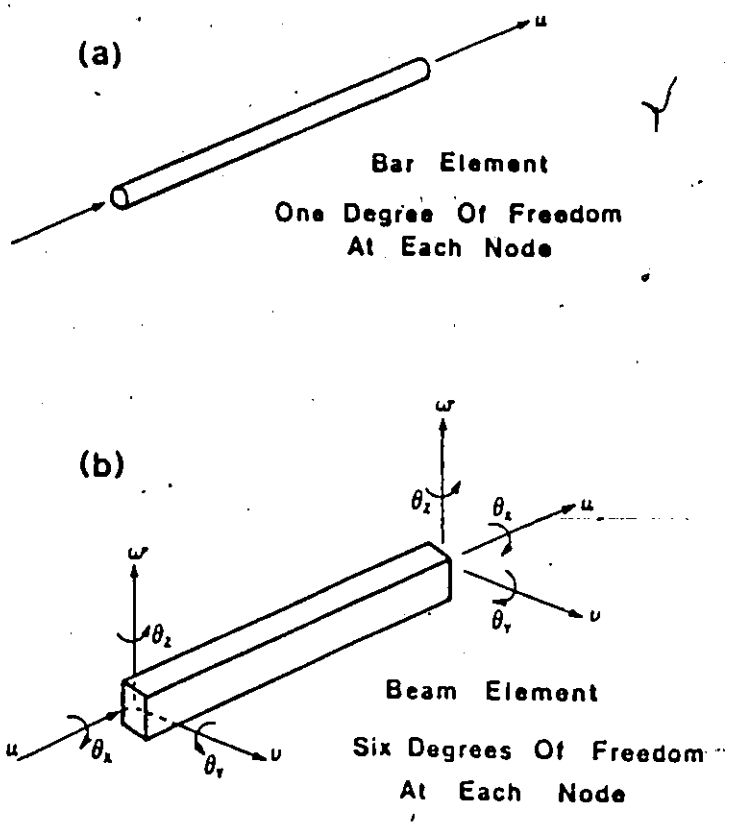

Figure 4.1: One-Dimensional Elements

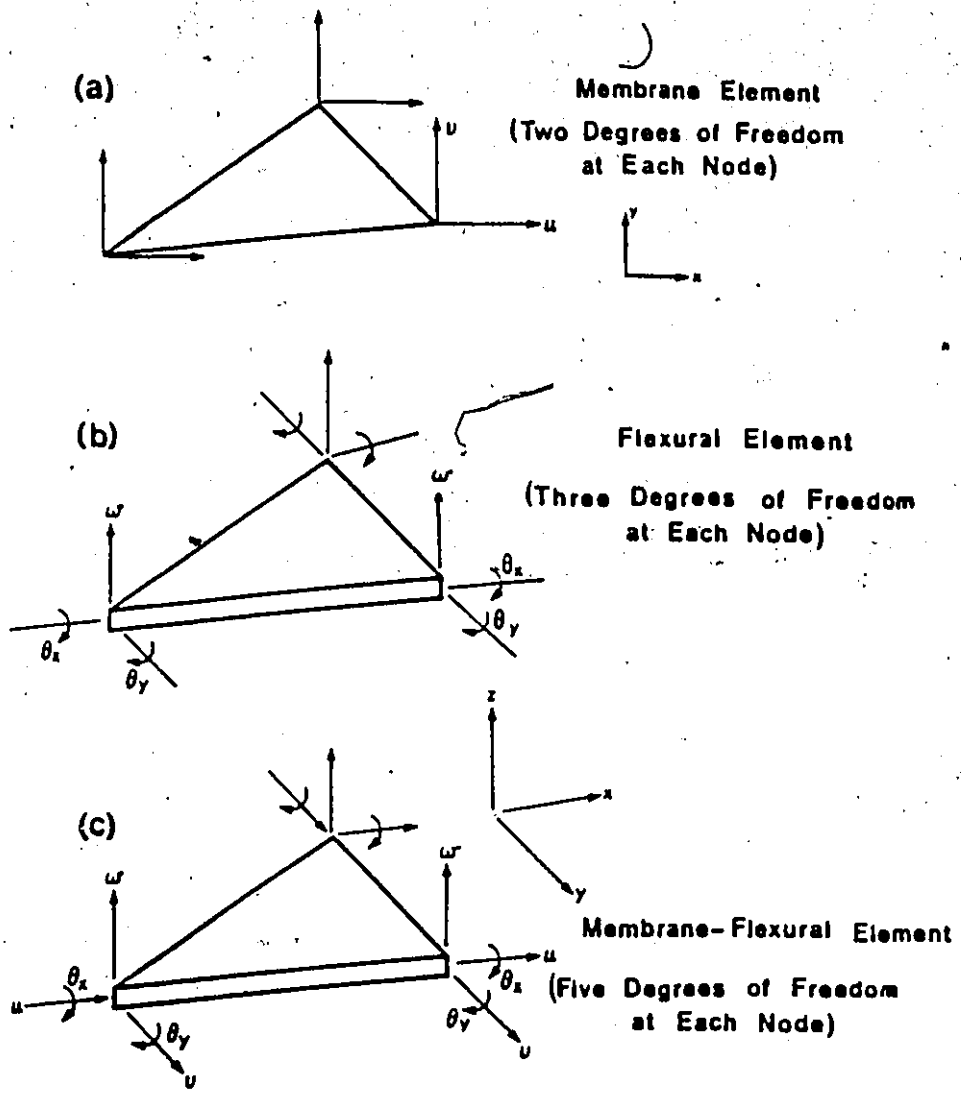

Figure 4.2: Two-Dimensional Elements (Typical Triangular Elements)

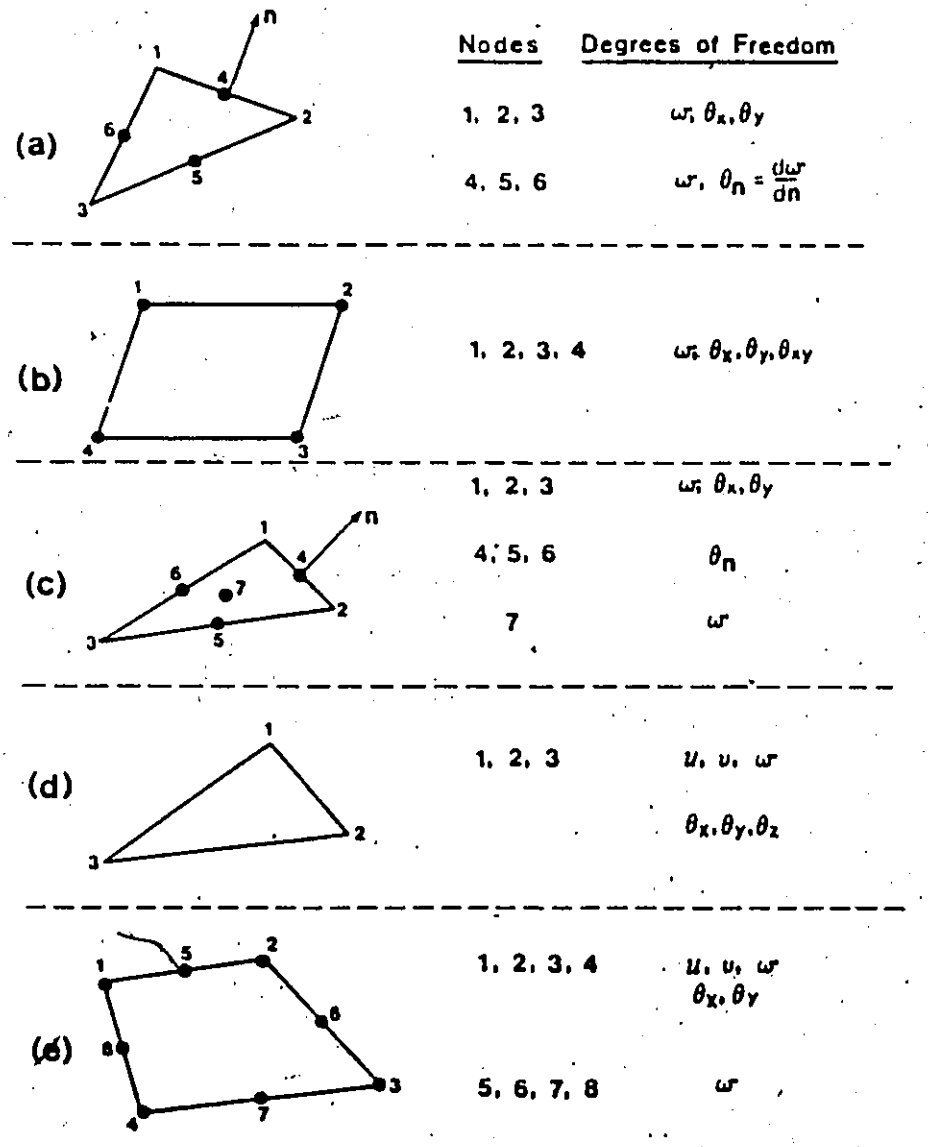

Figure 4.3: Some Examples of Higher Flexural Elements

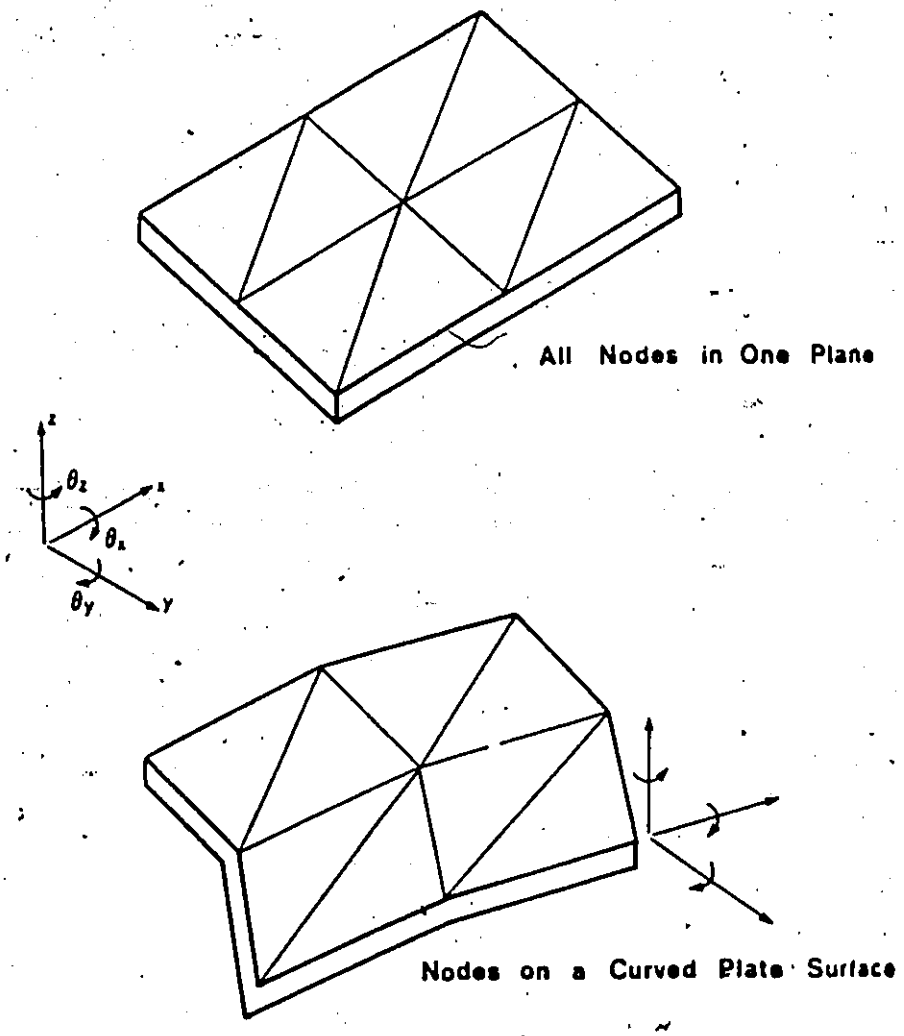

Figure 4.4: Shallow Shell Surface Using Flat Plat Elements

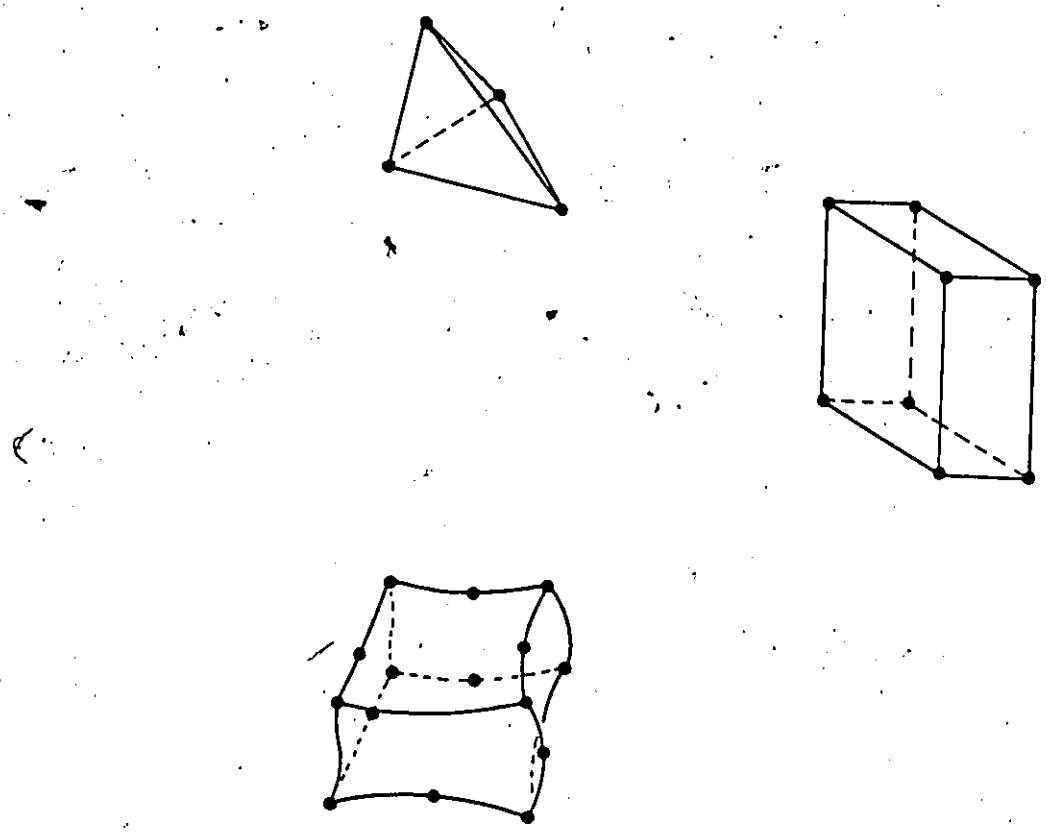

Figure 4.5: Three-Dimensional Elements

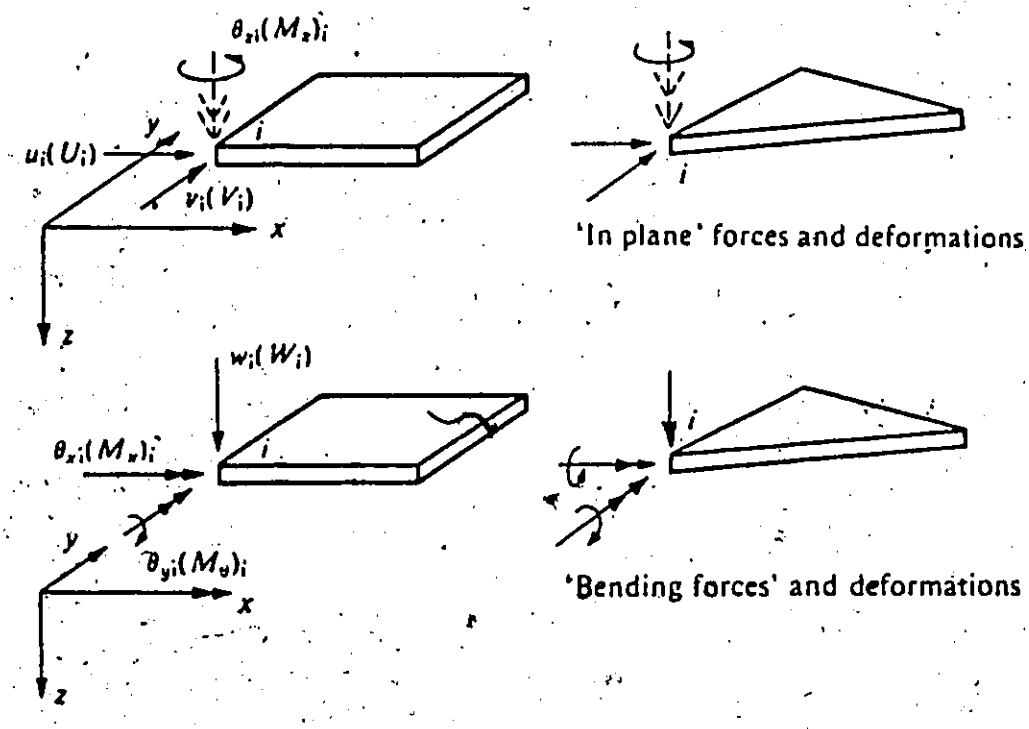

Figure 4.6: A Flat Element Subject to In-plane and Bending Actions

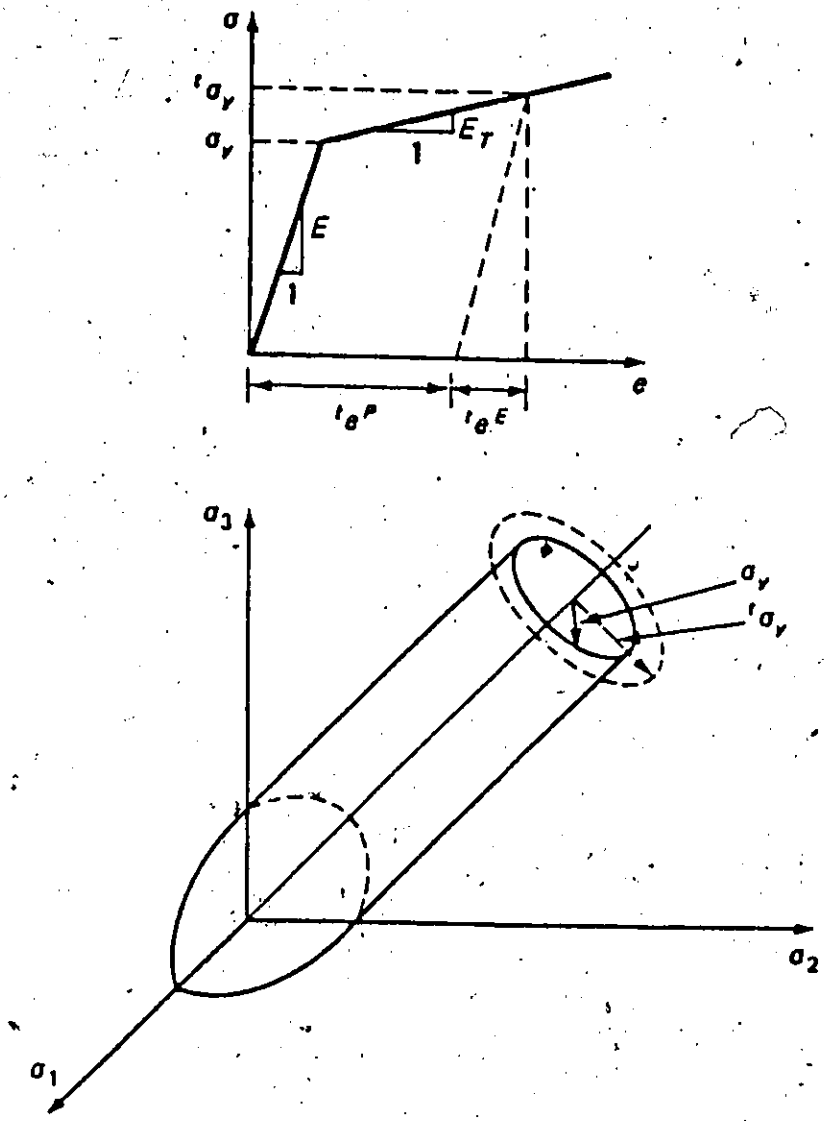

Figure 4.7: Von Mises Yield Condition

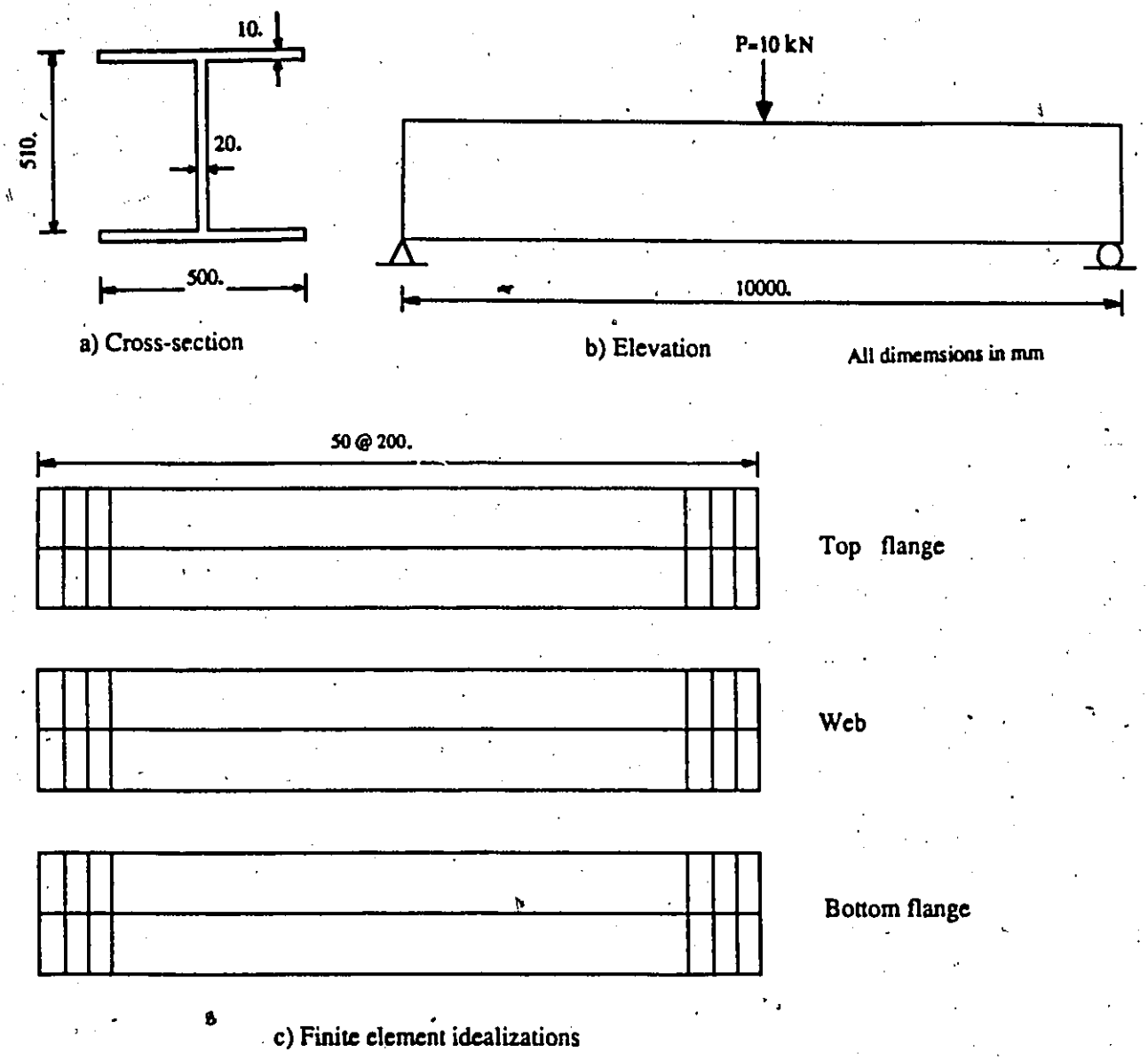

Figure 4.8: Cross Section, Elevation, and Finite Element Idealizations of the I-beam

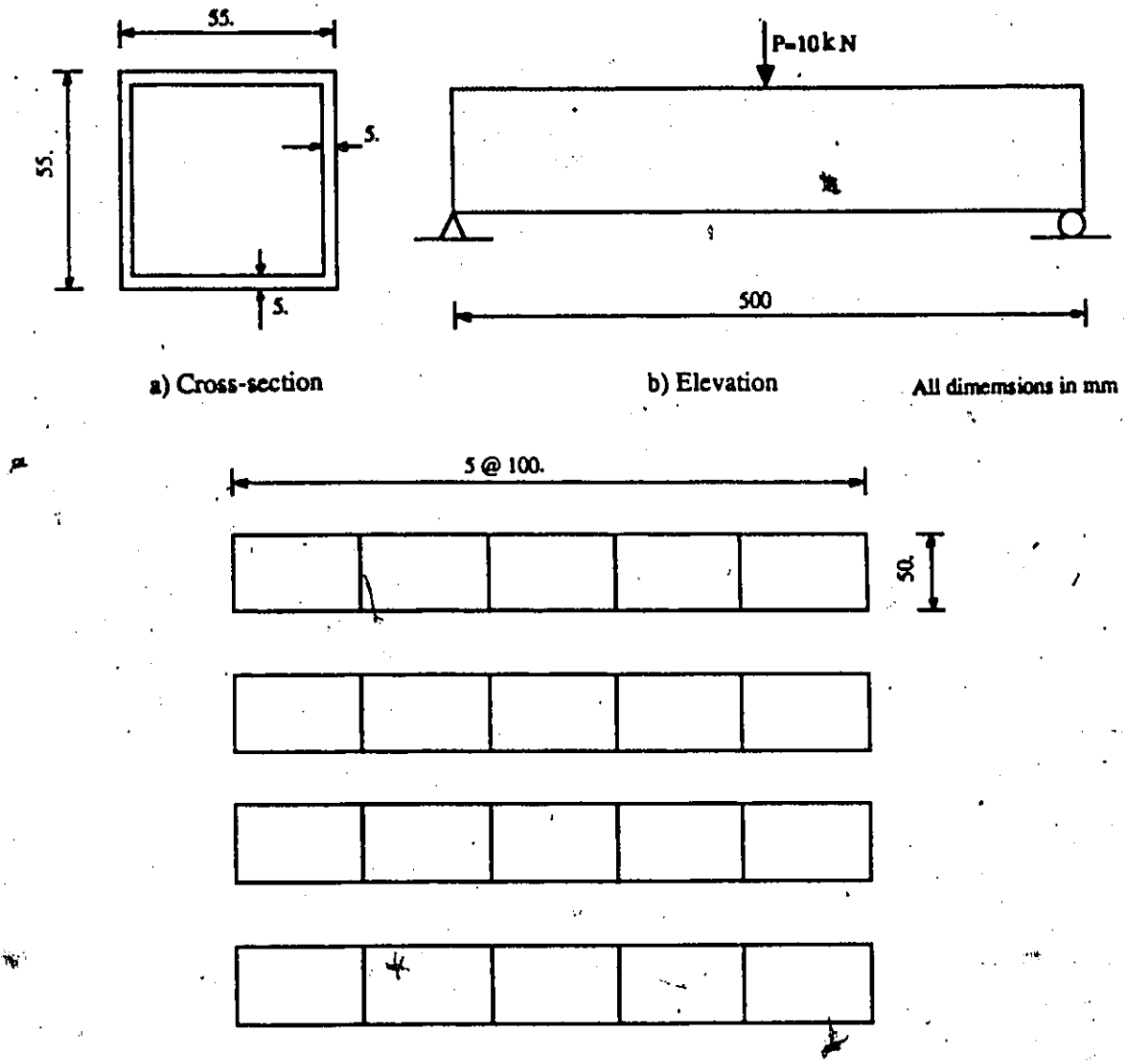

Figure 4.9: Cross Section, Elevation, and Finite Element Idealizations of the Box-beam

Table 4.1: Material Properties of the Two Beams

Material Constant	I-beam	Box-beam
E	10^7	1.00
ν	0.00	0.15
σ_y	300.00	300.00

Table 4.2: Comparison Between ADINA and Beam Theory

	ADINA		Beam Theory		Error	
	I-beam	Box-beam	I-beam	Box-beam	I-beam	Box-beam
Maximum Deflection	$2.57 * 10^{-5}$	58.770	$2.53 * 10^{-5}$	61.880	1.57%	5.00%
Maximum Stress	$7.48 * 10^{-3}$	0.086	$7.61 * 10^{-3}$	0.082	1.75%	5.80%

Chapter 5

DESCRIPTION OF THE ANALYSIS

5.1 General

Two types of bridges have been selected to illustrate the post-elastic analysis process. The first type is a slab-on-girder bridge and the second type is a box girder bridge. Before providing a full description of these structures (see sections 5.8-5.9), some factors in common for these two types of bridges will be discussed in sections 5.2 to 5.7.

5.2 Modelling of the Structures

A kinematic plastic analysis usually assumes a rigid perfectly plastic material represented by the stress-strain diagram of figure (5.1). However, as decided in section 4.5, the method used in this analysis assumes a linear elastic behavior of the concrete and a linearly elastic-perfectly plastic behavior of the steel as shown in figure (5.2). An elastic behavior of the concrete was assumed for the following reasons:

- The interest of investigating the behavior of the steel rather than the behavior of the concrete.
- The lack of input data to model the concrete according to the ADINA program.
- The time-consuming execution if the concrete was modelled as recommended in ADINA.
- Assumed elastic behavior of the concrete deck, will not have significant effects on the behavior of steel girders or box girders at ultimate.

5.3 Interface Slip and Residual Stresses

The proposed procedure does not include any allowance for interface slip between the concrete deck slab and the steel beams or residual stresses in the steel. Several studies [11,32] concluded that both would have a

significant effect on the post-elastic deflections, but neither were critical in determining the ultimate loads.

5.4 Formation of Plastic Hinges

A plastic hinge was assumed to form when the bending moment in a member exceeded the simple plastic moments determined using the rectangular stress distribution in figure (2.4), or the flexural capacity of the slab in transverse bending.

The torsional stiffness, if significant, such as in the case of box girder bridges, can lead to an interaction between flexure and torsion. This interaction although not significant sometimes, may influence the formation of plastic hinges by decreasing the flexural capacity of the member. However, this occurred only rarely. Indeed, various studies [15,26,33,34] concluded that neither the torsion nor the shear dominate the plastic behavior of a member, but their presence should always be taken into account in addition to flexure, especially in box girder bridge types.

In the study, hinges in both longitudinal and transverse directions were considered in order to detect the failure of the structure. A hinge in the transverse member represents a longitudinal yield line in the member, and would form when the transverse bending moment reached the transverse flexural capacity of the slab under a proportional increase of load. The first hinge formed across the bridge was under the loads or at the support where the maximum bending moment occurs. The collapse mechanism

would form when all members develop a plastic hinge in their longitudinal yield line. Sometimes, the slab can develop a strength greater than its flexural capacity, which leads to a total failure of the structure. This is caused mainly by arch action, membrane forces, and strain hardening of the steel.

5.5 Failure Criteria

It has been established that a bridge like any other structure can fail due to a variety of reasons:

- The largest possible failure load would be associated with a plastic collapse mechanism. This occurs when enough hinges form to render the structure or a portion of it unstable. At the point of collapse, all the hinges are free to rotate while still resisting their simple plastic moments.

- High vertical shear could also cause a failure prior to the formation of a collapse mechanism, or could cause a reduction in the flexural capacity at hogging hinges over interior supports for continuous structures. This failure can be avoided by thickening the steel web, which will influence the redistribution of moments but only in small amounts. Another alternative, is the consideration of the composite section, i.e. there will be a reduction of shear effect due to the presence of shear connectors. However, this was not expected to be critical in this study.

- Excessive deflections are also used as a measure of failure. Rather than associate failure with a specific limit on the maximum deflections, a sudden increase in deflections after the formation of plastic hinges was used as a guideline. This would imply a significant decrease in the overall stiffness of the structure, after which deflections would increase rapidly and the small deformation assumption necessary for an elastic analysis would no longer be valid.

5.6 Location of Plastic Hinges

The program output can give the location of the nodes that yielded. The stresses shown on the output are of two kinds, elastic and plastic. At the first stage of loading, all the stresses are elastic and are well below the yield stress σ_y. The increase of the load induces an increase in the stresses leading to plastic stresses. The first hinge is formed when a section of a structural member yields. Obviously, this section will be at the location where the maximum moment occurs. After the formation of the first hinge the load was further increased until failure occurred. At each stage of loading, the force effects, deflections and reactions represent the distribution of the loads in the bridge. The formation of the collapse mechanism would occur when all the stresses of each girder or box girder at the maximum moment position, reach their ultimate capacity. This stage varies according to the load position. After this stage the bridge cannot take any more load and the distribution characteristics of the moments will become constant.

5.7 Determination of the Maximum Moment Position

To design a beam, girder or any other structure supporting moving loads, the designer must be able to determine where these loads cause maximum shear and moment in the structure. Obviously, the critical position (i.e. maximum) will be found from the influence lines. If however, the structure is to support a series of concentrated loads of varying magnitude, such as groups of trucks or train wheels, the problem is not as simple. The influence line will, of course, indicate the approximate positions for placing the loads. It is reasonable to assume that the heaviest loads should be grouped in the vicinity of the largest ordinates of the influence lines diagram. The procedure for finding the exact critical positions of the loads is substantially a trial-and-error method for which the influence line will provide a good estimate. In the study, the determination of the moment in a bridge was accomplished by modelling this bridge as a beam. The rules to detect the maximum moment are as follows:

- In simply supported beams: A general rule for absolute maximum moment in a beam loaded with a moving series of concentrated loads will occur at the load nearest to the center of gravity of the loads on the beam when the center of gravity is at the same distance on one side of the centerline of the beam as the load nearest the center of gravity of the loads is on the other side.
- In continuous beams: In this case, there is no general rule, but the maximum moment is determined by trials. The series of concentrated

loads are positioned on one side and then moved to the left or right such that they increase the value of the moment relative to the previous moment. This procedure is carried out until there will be a decrease in the moment. The maximum moment is at the position of the load just before the decrease. In this study, a computer program was used to determine the maximum moment position.

5.8 Slab-on-Girder Bridges

To achieve the objective of the analytical procedure, the non-linear analyses were carried out for two bridges. A simply supported bridge prototype and a scale continuous bridge model. More details on the geometry, idealizations and loading configurations are described in the following subsections.

5.8.1 Bridge Geometries

The simply supported bridge prototype is a three-lane bridge, 13.72 meters wide and 18.29 meters long. The span length of 18.29 meters means that this bridge belongs to the medium span bridge category. It consists of six $W_{690X265}$ compact steel girders of a standard rolled section spaced at 2.36 meters. The six girders were roller supported at one end and hinged at the other end. The concrete slab has a total thickness of 190.0 mm. The general layout of the bridge is given in figure (5.3). It shows the cross-section and the elevation of the bridge.

The scale continuous bridge model is a three-lane bridge. It is symmetrical

with three continuous spans with the end spans measuring 4.856 meters and the center span measuring 6.474 meters. The deck slab is 65.5 mm thick with a total width of 3.240 meters. The deck slab is supported by four W_{50X10} steel beams with a uniform spacing of 900.0 mm. The cross-section and elevation of the bridge are shown in figure (5.4).

The material properties of the concrete slab and the steel girders of the two bridges are given in table (5.1). In addition, the stress-strain relationship of the materials are shown in figures (5.5).

The finite element idealizations for the two bridges are illustrated in figures (5.6) and (5.7). Two idealizations are shown for the continuous bridge model because two longitudinal positions of the load were considered. Note that since the loads are applied symmetrically only half of the bridges were modelled.

5.8.2 Bridge Loading

The load consisted of the OHBDC truck shown in figure (3.2). This axle load configuration was developed to model the force effect that would be caused by types of heavy vehicles observed on Ontario highways during an extensive survey in 1967, rather than to be visually representative of a specific type truck.

The loads were positioned on the structures at the longitudinal positions shown in figures (5.8) and (5.9) to maximize the positive or negative bending moments. One longitudinal position for the simply supported bridge

and two longitudinal positions for the continuous bridge were considered. Only those axle loads which contribute to the critical effect in question are included. The loading scheme described in figures (5.8) and (5.9) is intended to simulate the OHBD code truck of figure (3.2) in a modified form. The modified truck combines the two $140kN$ axle loads into a single $280kN$ load. Furthermore, the $60kN$ load was eliminated to create a minimum number of loading points. The other loads were then increased by 13% in order to produce the same maximum moment as was produced with the original loading. This readjustment of the load increased the maximum value of the shear by 3% for the simply supported bridge and 5% for the continuous bridge. The development of this simplification is shown in figures (5.10) and (5.11).

The transverse positions of the loads are also shown in figures (5.8) and (5.9). For both bridges only three loaded lanes were considered. This configuration will always govern in the slab-on-girder bridge type. In a post-elastic analysis, the transverse redistribution that can occur will depend on the transverse positions of the loads. Obviously, a multitude of combinations of transverse positioning could be considered. However, to keep the time and expense of this analysis within reason, only one transverse position of the trucks was included. This was at the center of the lane for the interior trucks and at a distance of one meter from the curb to the outmost axle of the truck for the vehicles in the exterior lanes. As can be seen in figures (5.8) and (5.9), the load was applied in a symmetrical fashion over the centerline of the bridge and in small increments up to failure.

5.9 Box Girder Bridges

Two bridges were considered to test the elasto-plastic design process. The first is a simply supported bridge and the second is a continuous bridge. Both are composite bridge prototypes. Their geometries and idealizations are described in section 5.9.1 and the various loading configurations in section 5.9.2.

5.9.1 Bridge Geometries

The simply supported bridge prototype is a two-lane bridge. It has two steel boxes positioned at equal spacing of 2.44 meters. The slab is 203.2 mm thick. The bridge is 45.72 meters long and 9.45 meters wide. Thus, it is included in the medium and narrow bridge category.

The three-lane continuous bridge prototype is a symmetrical two-span bridge. Two spans of 54.00 meters each are sufficient to consider redistribution from a sagging region to a hogging region and vice versa. The span length of 54.00 meters is representative of medium span bridges. The deck slab is 230.0 mm thick with a total width of 13.40 meters. The three box girders supporting the concrete slab are of standard rolled sections and positioned at a uniform spacing of 2.28 meters. Dimensions and other relevant data of the two bridges are shown in the cross sections and elevations in figures (5.12) and (5.13).

The concrete and steel material properties of the two bridges are tabulated in table (5.2). The stress-strain relationship of the materials used are also

illustrated in figure (5.14).

The bridges were analyzed using the finite element meshes in figures (5.15) and (5.16). Two idealizations are considered for the continuous bridge corresponding to two longitudinal loading positions, in which the symmetry was exploited.

Note that for all finite element discretizations described before, a 9-node shell element was used to model the structures.

5.9.2 Bridge Loading

Again, the OHBD code truck was used to load the bridges. The OHBD vehicles were positioned longitudinally to create the most critical effect in the positive and negative sections. Two loading configurations were considered for both bridges. This includes one and two lanes loaded for the simply supported bridge and two longitudinal positions for the continuous bridge. Only one transverse position of the wheel axles was adopted as described in section 5.8.1. Details of the longitudinal and transverse loading conditions are shown in figures (5.17) and (5.18). As illustrated in figures (5.17) and (5.18), the symmetry of the applied load was exploited to reduce the large volume of data and computer execution time otherwise demanded.

In this type of bridge, only one simplification of the load was utilized. It is the combination of the two $140kN$ loads into one single load for the simply supported bridge.

5.10 Approximations

In order to facilitate the finite element idealizations, it was believed appropriate to include the top flanges in the thickness of the concrete deck slab. This approximation was performed by converting the steel top plates into concrete. The application of the reactions instead of the actual load was another approximation to simplify the finite element mesh. It also permits the transmission of the loads directly to the longitudinal steel members so that the yielding of the steel will occur prior to the crushing of the concrete.

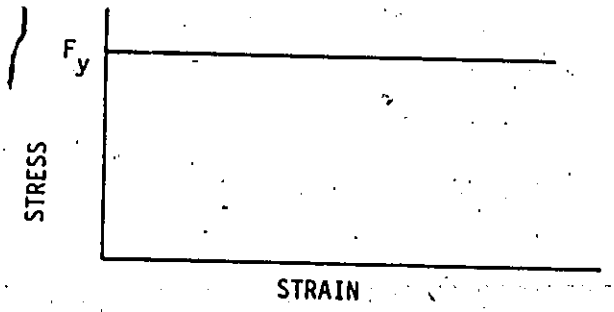

Figure 5.1: Rigid-Perfectly Plastic Material Behavior

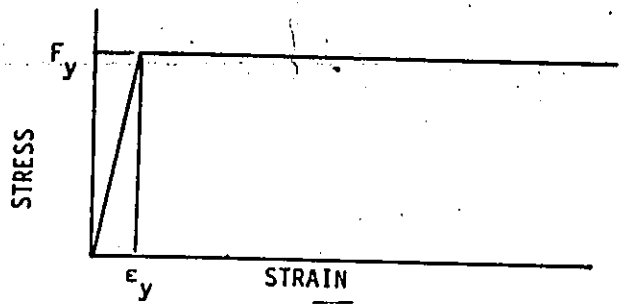

Figure 5.2: Linearly Elastic-Perfectly Plastic Steel Behavior

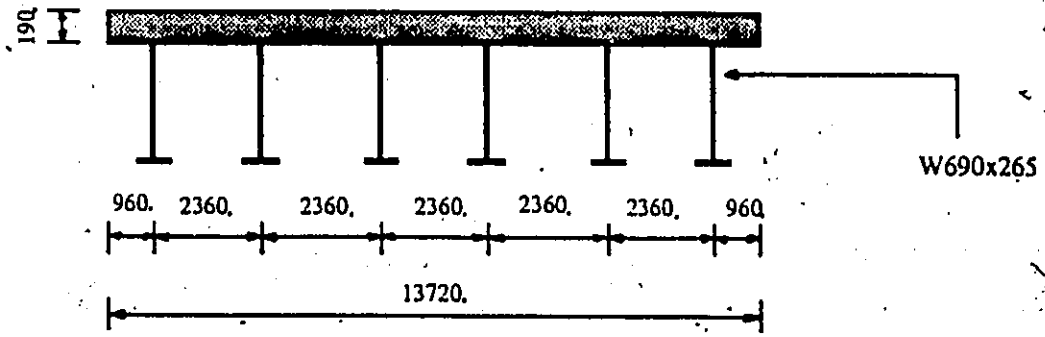

a) Cross section

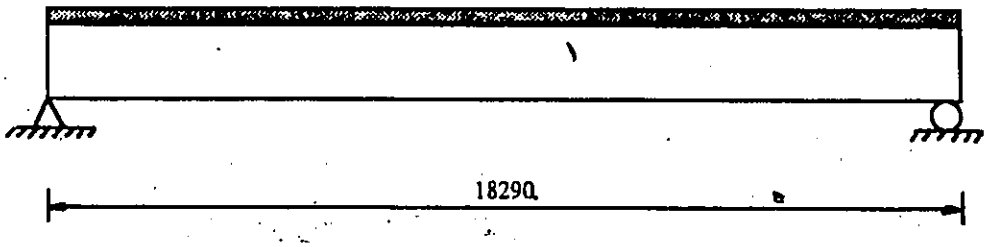

b) Elevation

Figure 5.3: Cross Section and Elevation of the S.S. Slab-on-Girder Bridge

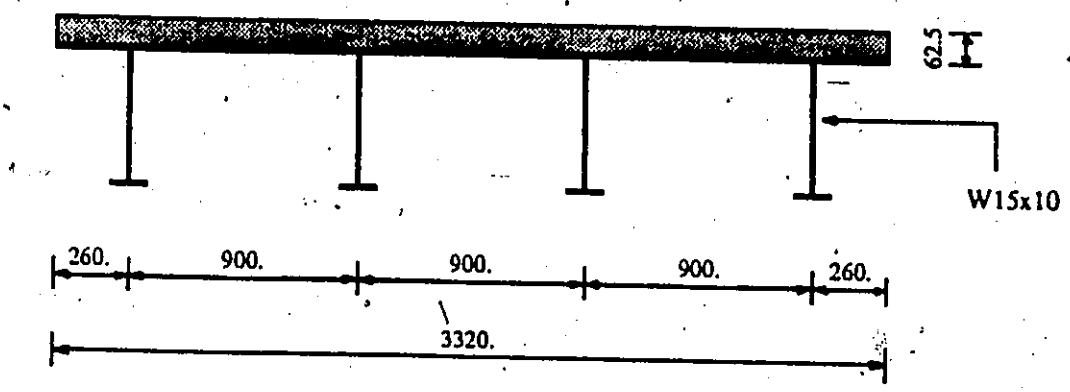

a) Cross section

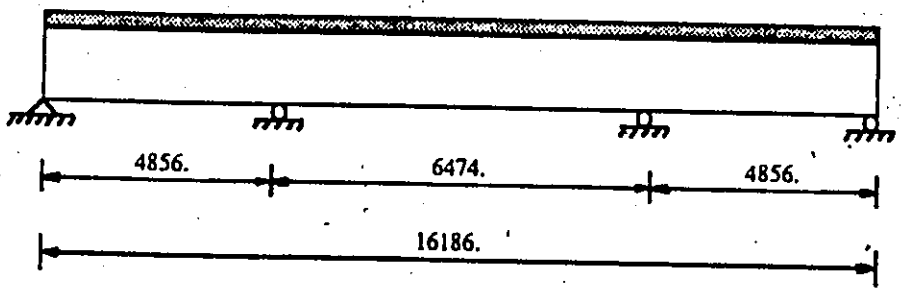

b) Elevation

Figure 5.4: Cross Section and Elevation of the Cont. Slab-on-Girder Bridge

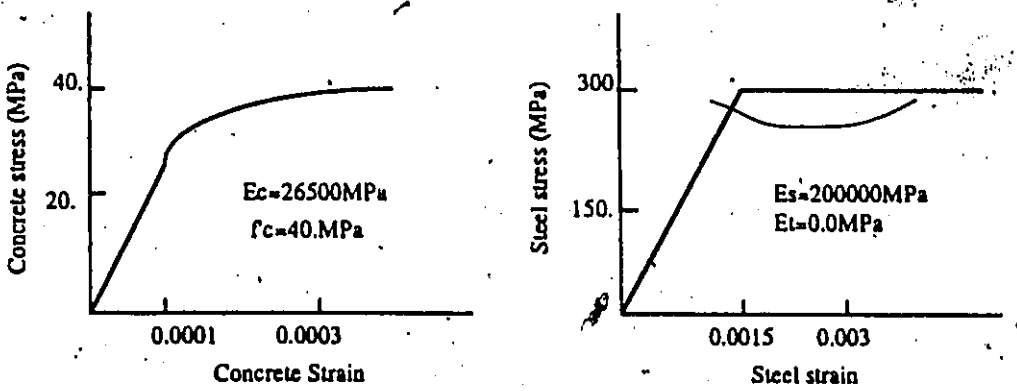

Simply supported slab-on-girder bridge

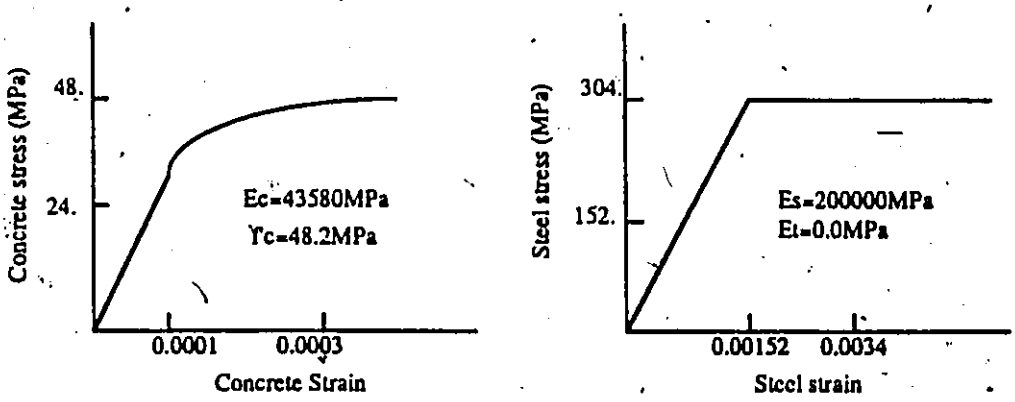

Continuous slab-on-girder bridge

Figure 5.5: Stress-Strain relationship of the Slab-on-Girder Bridges

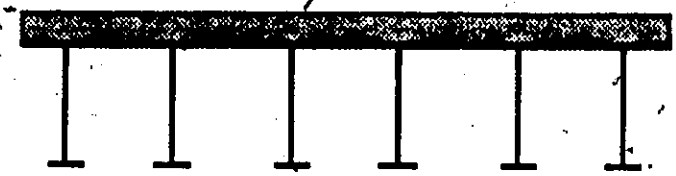

All dimemsions in mm

Section A-A

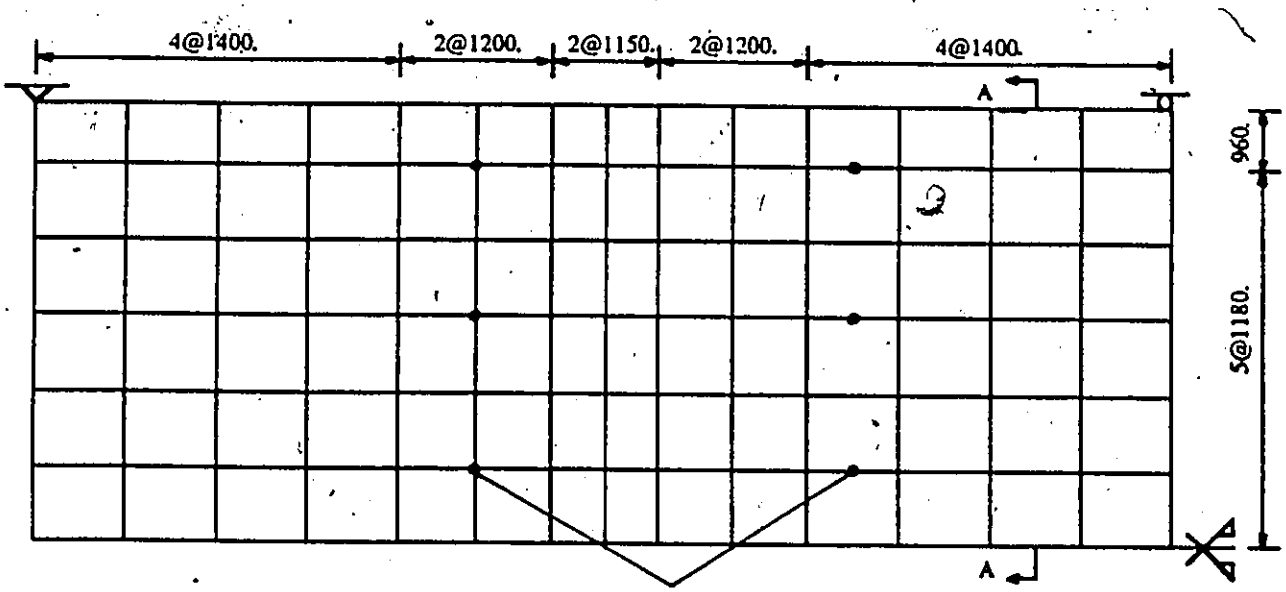

a) Slab idealization

Point loads

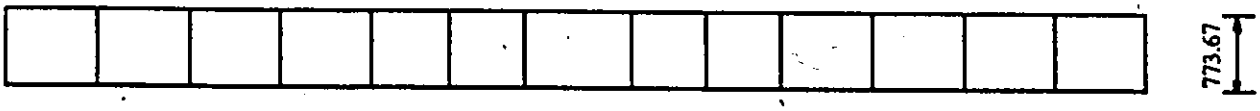

b) Web idealization

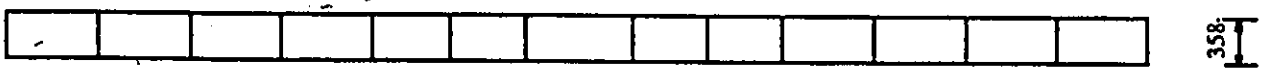

c) Flange idealization

Figure 5.6: Finite Element Idealization of the S.S. Slab-on-Girder Bridge

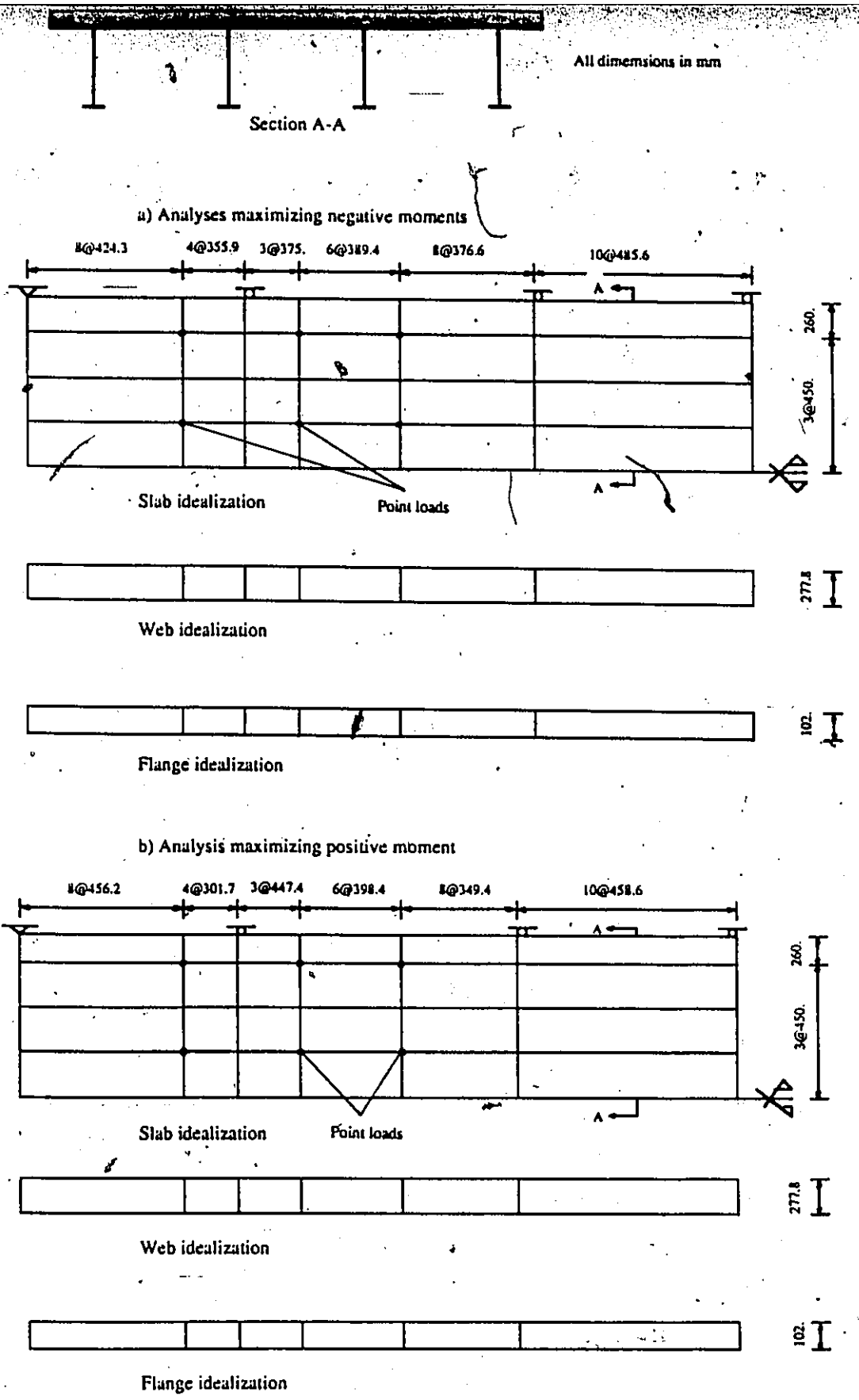

Figure 5.7: Finite Element Idealization of the Cont. Slab-on-Girder Bridge

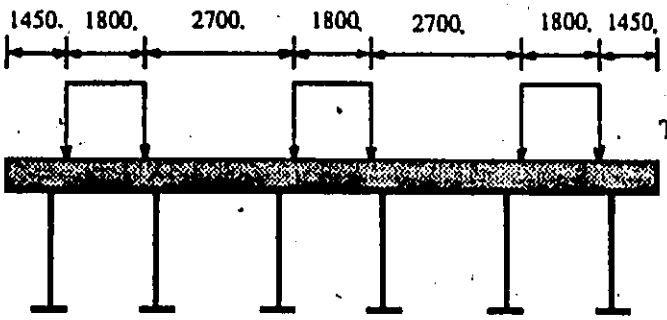

a) Transverse position of OHBD vehicles

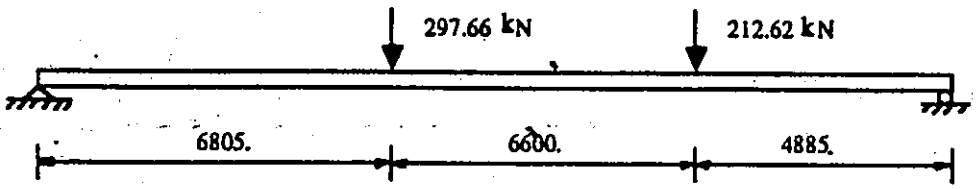

b) Longitudinal position of the loads

Figure 5.8: Load Position in the S.S. Slab-on-Girder Bridge

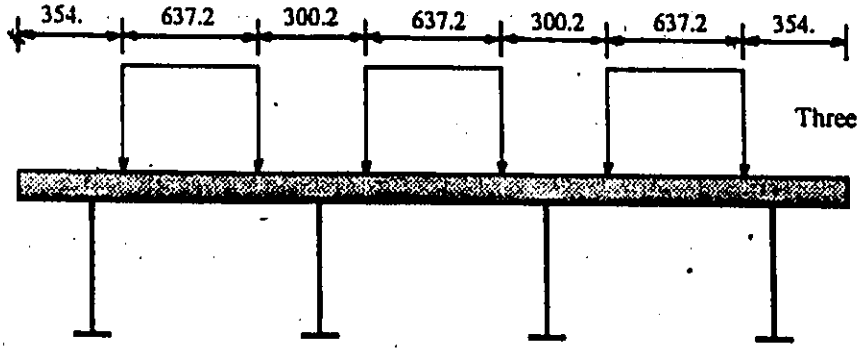

a) Transverse position of the OHBD vehicles

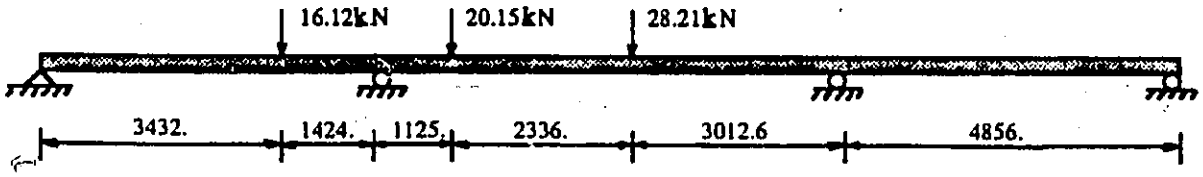

b) Longitudinal position to maximize negative moments

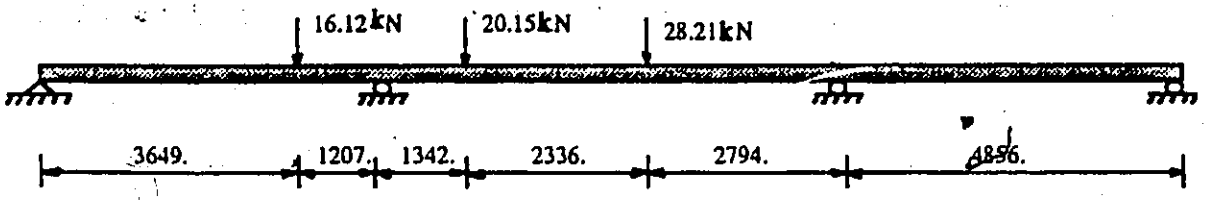

c) Longitudinal position to maximize positive moments

Figure 5.9: Load Position in the Cont. Slab-on-Girder Bridge

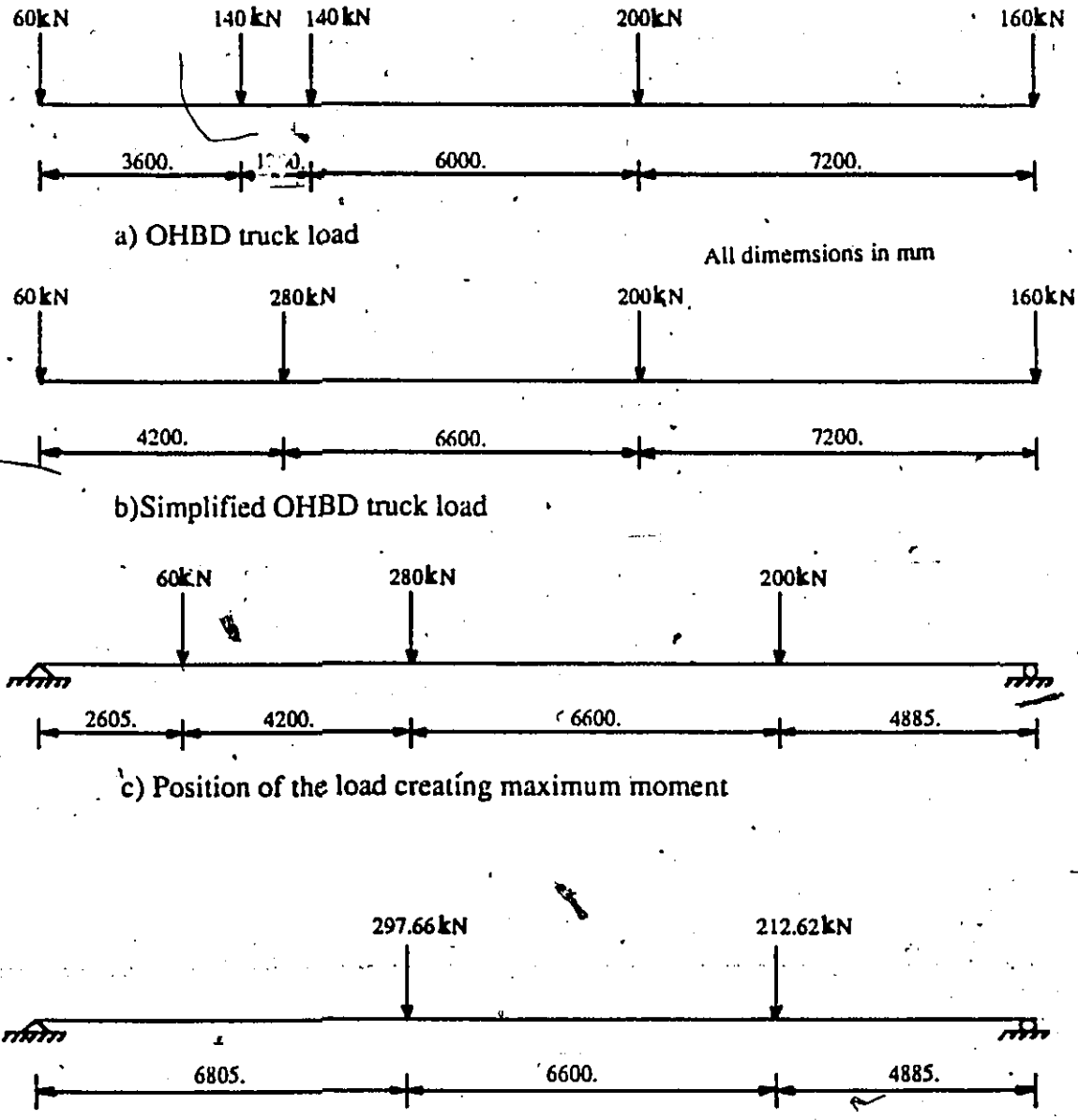

Figure 5.10: Simplification of the Load in the S.S. Slab-on-Girder Bridge

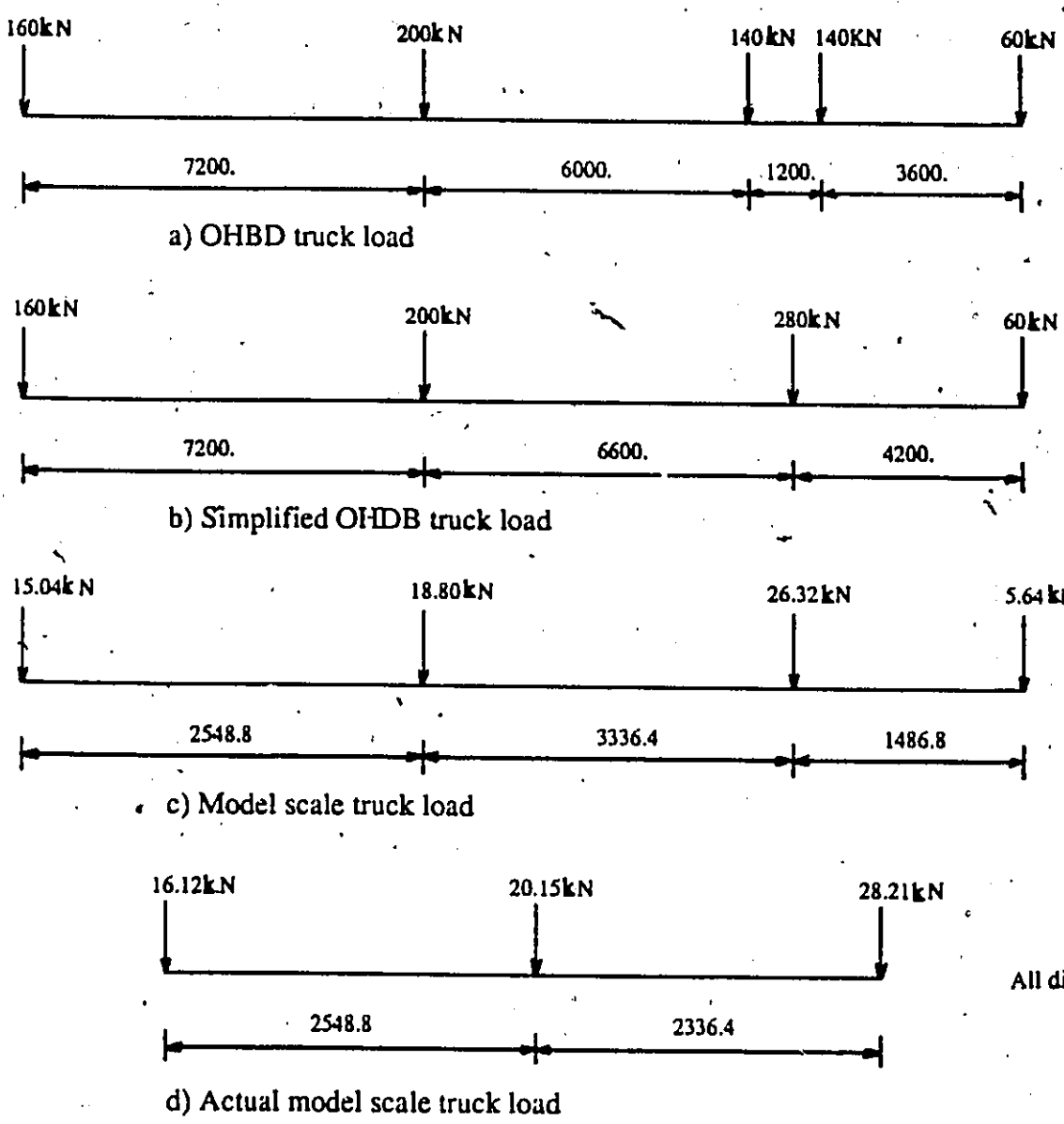

Figure 5.11: Simplification of the Load in the Cont. Slab-on-Girder Bridge

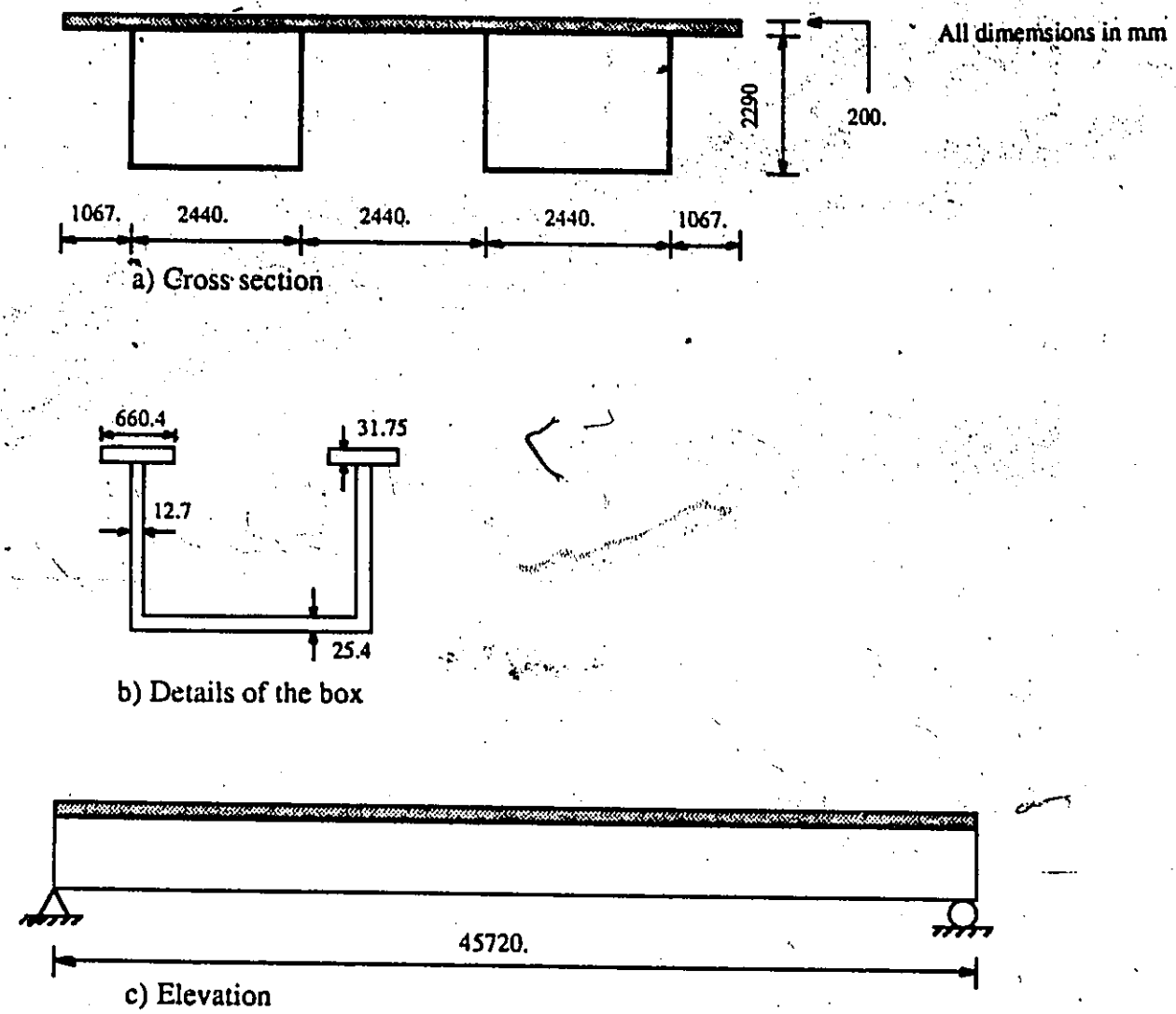

Figure 5.12: Cross Section and Elevation of the S.S. Box Girder Bridge

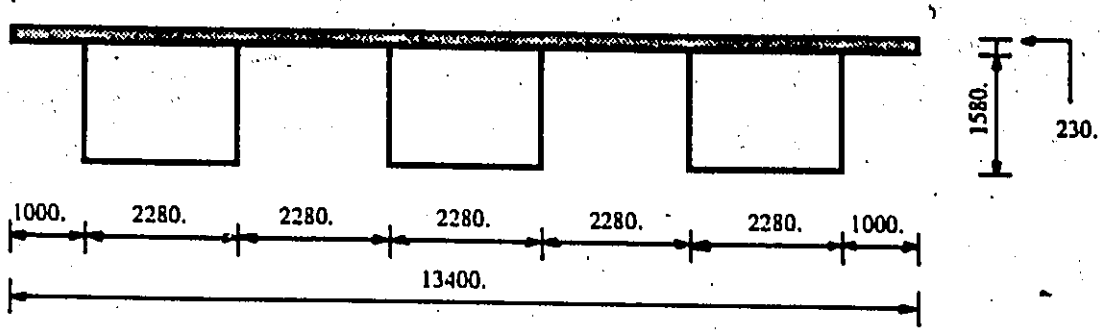

a) Cross section

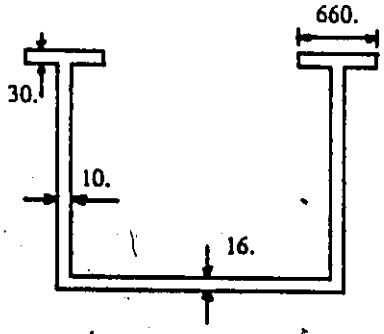

b) Details of the box

All dimensions in mm

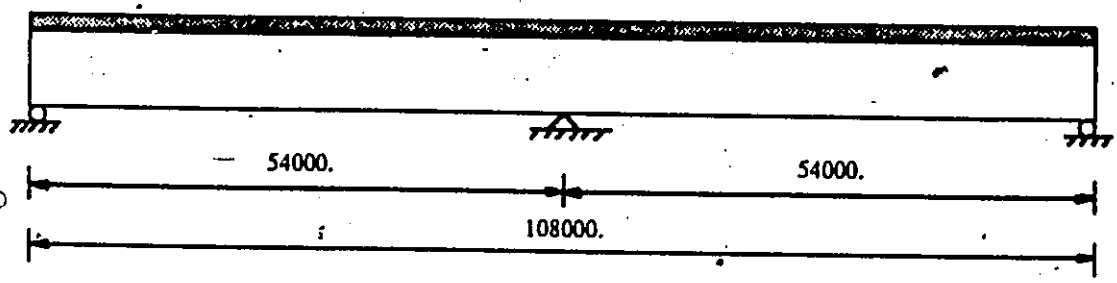

c) Elevation

Figure 5.13: Cross Section and Elevation of the Cont. Box Girder Bridge

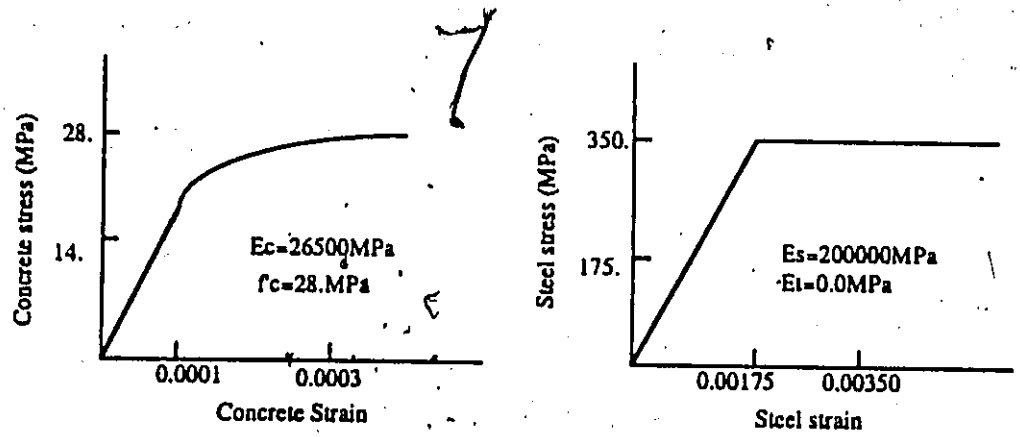

Simply supported box girder bridge

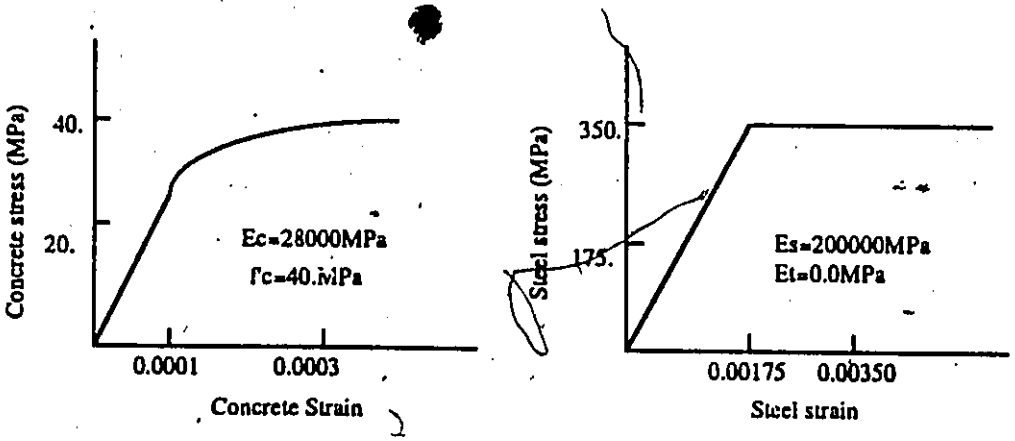

Continuous box girder bridge

Figure 5.14: Stress-Strain relationship of the Box Girder Bridges

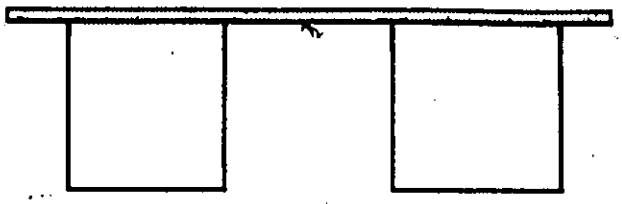

All dimensions in mm

Section A-A

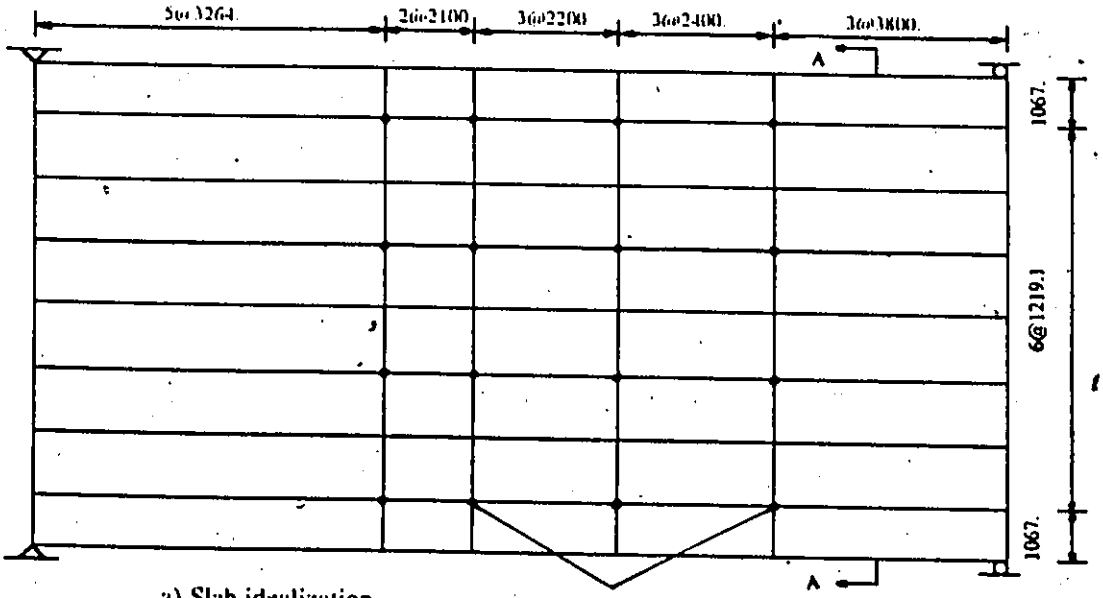

a) Slab idealization

Point loads

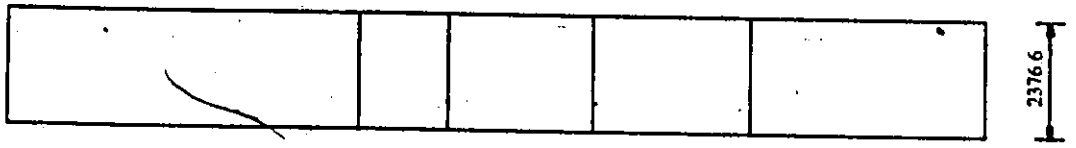

b) Web idealization

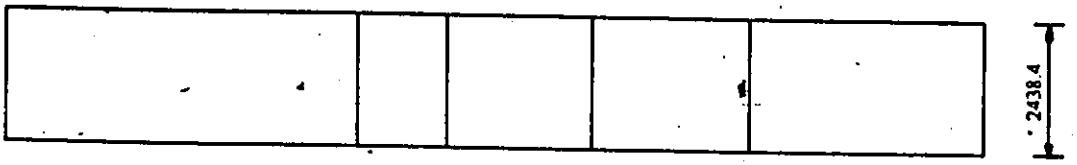

c) Flange idealization

Figure 5.15:- Finite Element Idealization of the S.S. Box Girder Bridge

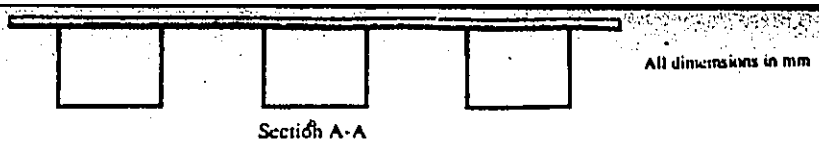

a) Analysis maximizing negative moment

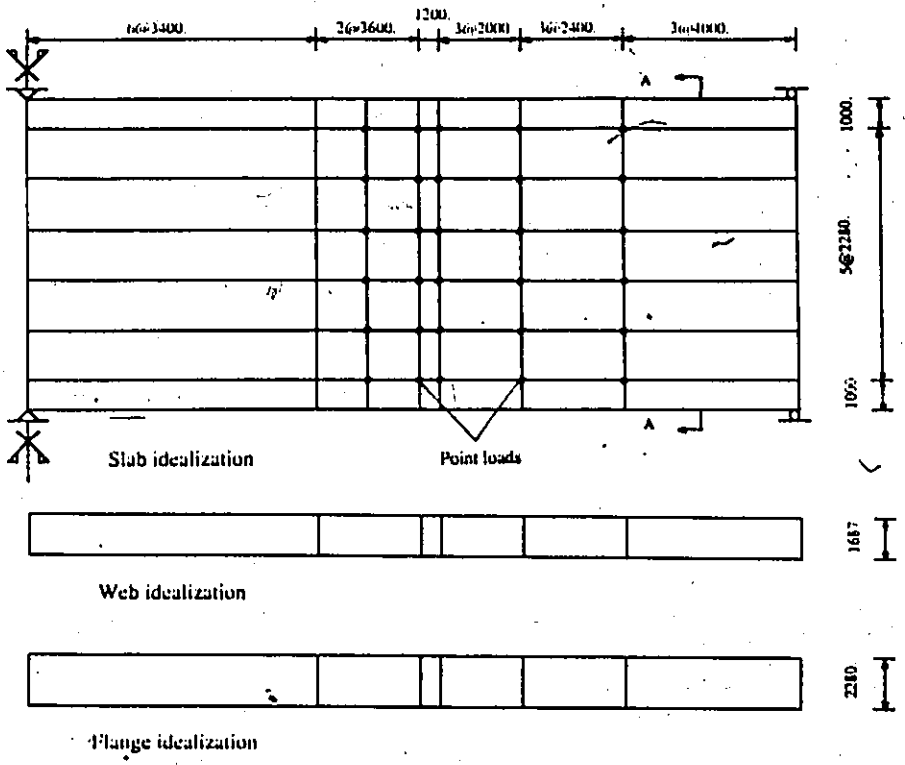

b) Analysis maximizing positive moment

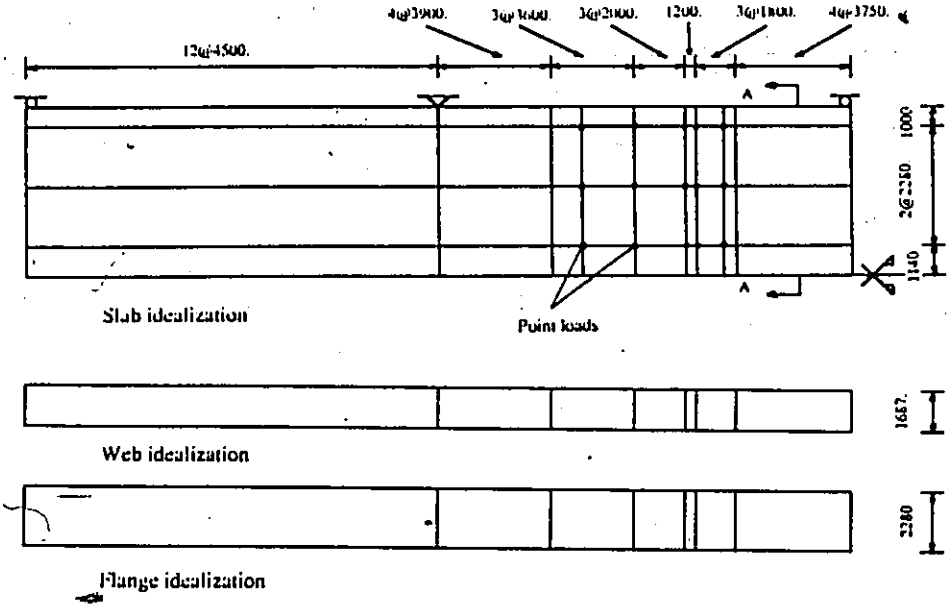

Figure 5.16: Finite Element Idealization of the Cont. Box Girder Bridge

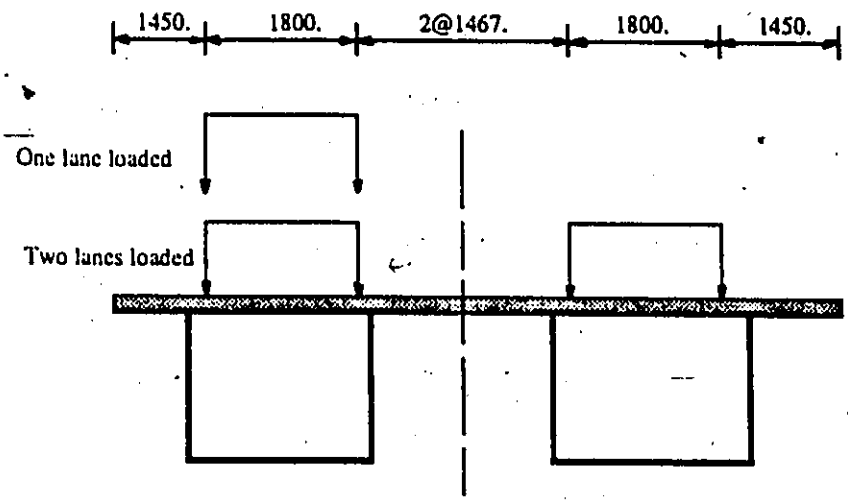

All dimensions in mm

a) Transverse position of the OHBD vehicles

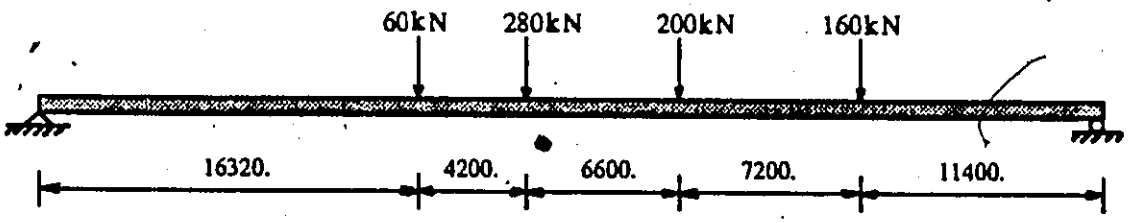

b) Longitudinal position of the loads

Figure 5.17: Load Position in the S.S. Box Girder Bridge

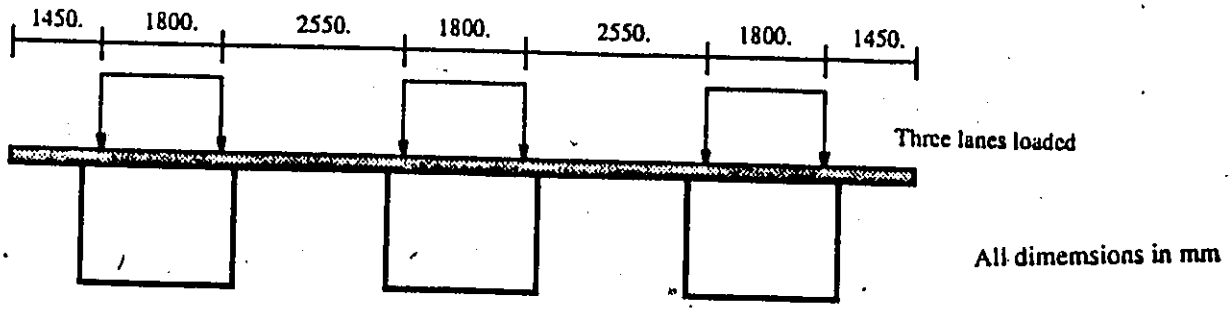

a) Transverse position of the OHBD vehicles

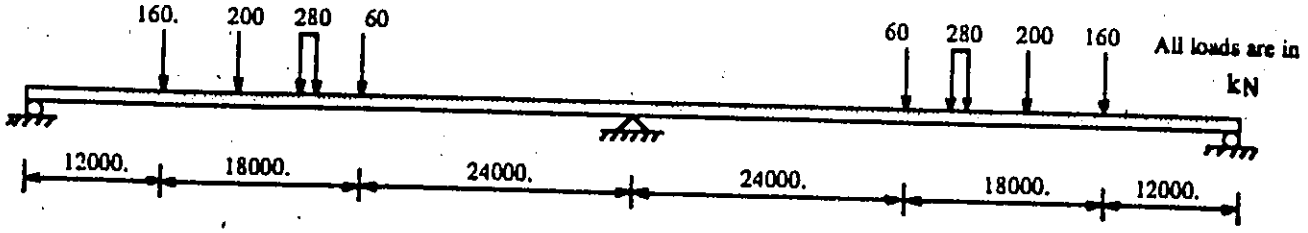

b) Longitudinal position to maximize negative moments

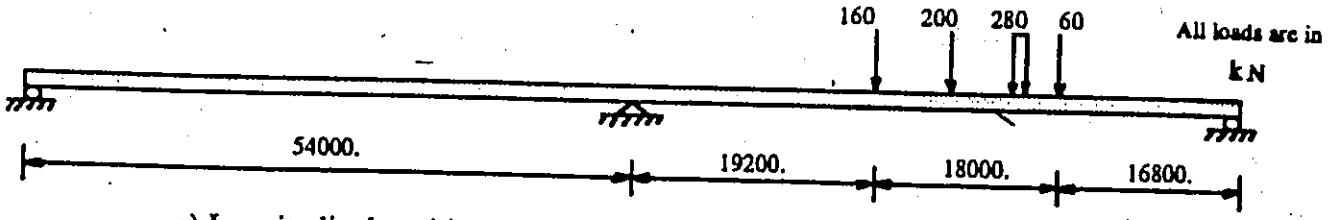

c) Longitudinal position to maximize positive moments

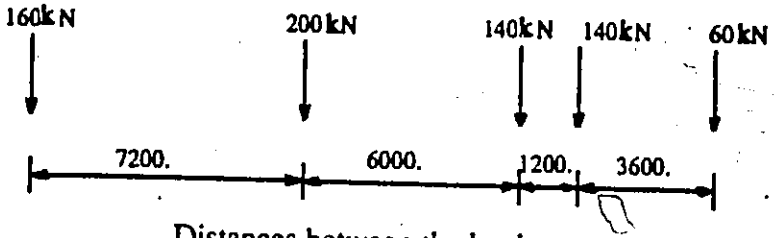

Distances between the loads

Figure 5.18: Load Position in the Cont. Box Girder Bridge

Table 5.1: Material Properties of the Slab-on-Girder Bridges

Material constant	S.S. Slab-on-Girder		Cont. Slab-on-Girder	
	Concrete	Steel	Concrete	Steel
$f'_c\ (MPa)$	40.0	–	48.2	–
$f'_t\ (MPa)$	3.5	–	4.0	–
$\sigma_y\ (MPa)$	–	300.0	–	304.0
ϵ_y	0.0005	0.0015	0.0005	0.00152
$E\ (MPa)$	26500.	200000.	43580.	200000.
ν	0.15	0.30	0.15	0.30

Table 5.2: Material Properties of the Box Girder Bridges

Material constant	S.S. Box Girder		Cont. Box Girder	
	Concrete	Steel	Concrete	Steel
$f'_c\ (MPa)$	28.0	–	40.0	–
$f'_t\ (MPa)$	5.0	–	4.5	–
$\sigma_y\ (MPa)$	–	350.0	–	350.0
ϵ_y	0.0005	0.00175	0.0005	0.00175
$E\ (MPa)$	26500.	200000.	28000.	200000.
ν	0.15	0.30	0.15	0.30

Chapter 6

RESULTS AND DISCUSSION

6.1 General

It has been generally recognized by many investigators, Bakht and Jaeger [6,7] , Heins and Kuo [19], and Cheung et al [13], that some of the main parameters that influence the load distribution in composite bridges are:

1. Bridge width;
2. Girder or box girder spacing;
3. Truck position;
4. Number of lanes loaded;
5. Bridge type; and
6. Number of girders or box girders.

In this study, the effect of some parameters on the distribution of load over the complete loading range up to failure will be considered. In selecting the range of parameters, the OHBD code was used as a guide. To show the extend to which the bridges studied here are representative of actual bridges, let us consider the $\alpha - \theta$ plane in figure (6.1). Bakht et al [4,7] studied many existing bridges and established that the $\alpha - \theta$ values within the shaded regions characterize the overwhelming majority.

6.2 Presentation of the Results

The finite element program outputs for each loading step stresses at Gauss points, strains, curvatures, moments, and deflections at nodal points. The plethora of information it provides is indeed overwhelming. We will limit ourselves, however, to some of the quantities: basically, the load-deflection curves, the load-rotation curves and the transverse and longitudinal moment distribution of the girders and box girders.

The variation of the above quantities under increasing load will be plotted for the critical sections. The load-deflection and load-rotation curves are useful as they illustrate the elastic limit, the onset of inelasticity and yield, and the occurrence of failure. They also give the ultimate capacity of the bridge and their shape is indicative of the stability.

The moment diagrams in their raw form give some indication of the load distribution at various levels of loading at different sections along the bridge. They also identify the critical section and the critical girder or box girder.

However, from a load distribution point of view the raw diagrams are not useful as the D diagrams to be discussed below. For this reason, in this chapter the moment in each girder or box girder will be tabulated only.

To assess properly the load distribution and to relate the findings of this study to the provisions of the code, we shall plot the distribution parameter D for the girders or box girders. It may be recalled from Chapter Three that the D-type distribution forms the basis of both the OHBD and the AASHTO codes. It must be mentioned that the D values in the code are based upon the most critical loading case for any beam. In this study we obtain the D values for individual loading cases. Therefore, the comparison with the code should be for the most critical positions of the loading cases studied.

Finally, to relate the applied loads to the design load, all loads are expressed in terms of the number of OHBD trucks. In other words, the actual loads are normalized with respect to the wheel loads suggested by the OHBD code. Hence, when the load is shown to be one truck, it does not imply that only one truck is placed on the bridge. There could be any number of trucks but the wheel load in each will correspond to the wheel loads of the code's truck.

The results of seven separate analyses are presented in this chapter. They are listed below and labeled so that they can easily be identified in the following discussions.

1. SSSGB-3P : The three lane loaded simply supported slab-on-girder bridge with maximum positive moment.

2. CSGB-3N : The three lane loaded continuous slab-on-girder bridge with maximum negative moment.

3. CSGB-3P : The three lane loaded continuous slab-on-girder bridge with maximum positive moment.

4. SSBGB-2P : The two lane loaded simply supported box girder bridge with maximum positive moment.

5. SSBGB-1P : The one lane loaded simply supported box girder bridge with maximum positive moment.

6. CBGB-3N : The three lane loaded continuous box girder bridge with maximum negative moment.

7. CBGB-3P : The three lane loaded continuous box girder bridge with maximum positive moment.

6.3 Load vs Deflection

In figures (6.2) to (6.8), the maximum deflections are plotted against the load for the seven analyses. In the case of loading symmetry, half of the bridge was loaded. These figures are intended to depict the deflections of the structure at the various load stages and assess the declining stiffness of the structure as it becomes plastic.

It can be seen in figures (6.2) to (6.8) that the behavior was essentially elastic up to a load corresponding to approximately the formation of the first plastic hinge in the bridge. This elastic limit varies in each structure.

Above this load, deflection commenced to increase more rapidly with increase in load as yielding spread across the bottom plates of girders or box girders. After a certain stage, the deflection increased very rapidly, because the girders or box girder plates were at that point yielding across their entire width. At the formation of enough plastic hinges, the deformations of the bridge became so great that it caused a sharp declining in the stiffness. This has led to an instability failure of the structure.

6.4 Deflection vs Transverse Position

The maximum deflections for each girder or box girder are plotted against the transverse position of the girder or box girder at different load stages as depicted in figures (6.9) to (6.15). The deflected shape through a transverse section is bending more and more while the load is increased. When all the lanes of the bridge are loaded, the interior girder exhibits a more critical deflection. This deflection increases rapidly in comparison with the deflection of the exterior girder when yielding spreads. However, the deflection in the exterior girder or box-girder can be more critical when a reduced number of lanes is loaded which is the case of SSBGB-1P shown in figure (6.13).

6.5 Load vs Rotations

The maximum rotations at the supports are plotted against load in figures (6.16) to (6.25). These rotations are provided directly from the ADINA output. As with the deflections, they are intended to indicate the declining stiffness of the structure. It can be noted that the rotations vary linearly with the load up to a stage at which the bridge starts yielding which leads to an increase of the rotations and a decrease in the stiffness. In addition, the rotations at outside supports are almost the same for the simply supported bridges and continuous bridges with maximum negative bending moment. This is due to the occurrence of the maximum deflection at mid-span for the simply supported bridges and the perfect symmetry in the continuous. In the case of continuous bridges with maximum positive moment, the support of the loaded span develops more rotations and the declining of the stiffness of the structure is more critical. The values of the rotations at the internal supports for continuous bridges fall between the values of the external supports.

6.6 Critical Stages

The plastic collapse mechanism is not the only mode of failure in a non-linear elasto-plastic analysis. Rapid increase in the deflection or rotation leading to a significant decline of the stiffness is another type of failure even though the structure may still be stable. In most load-deflection or load-rotation graphs, it can be seen that this type of failure occurs in al-

most every case. However, in the cases where all the lanes are loaded, the collapse failure might be reached after that point. For the case where a reduced number of lanes are loaded, it was not possible to reach the collapse mechanism. There are other stages in the post-elastic loading that may also be critical with respect to the behavioral changes. The formation of the first hinge at the first stage of post-elasticity would be one. According to OHBDC specifications, this would represent the capacity of the bridge at ULS for the specific loading configuration. None of the bridges studied exhibited such behavior.

In summary, there are three stages in the elasto-plastic loading where the behavior of the structure may become critical. The three stages are defined as follows:

- Formation of the first hinge;
- Significant reduction in the overall stiffness of the structure due to a rapid increase of the deformations and rotations; and
- Collapse mechanism when enough hinges are formed at the ultimate load.

These critical stages need not occur in sequence, nor are they mutually exclusive. In the case of the analyzed bridges, only stage two and three were noticed in sequence or mutually exclusive. Further information about the failure modes is illustrated in the following section.

6.7 Failure Modes

In all the cases where all lanes were loaded, it was possible to continue the analysis until the formation of a distinct plastic collapse mechanism. At least one positive or one negative plastic hinge, depending on the bridge and the loading, formed in each one of the longitudinal girders or box girders in one span, rendering that span unstable. The formation of each mechanism can be seen in the load-deflection curves as a sharp declining in the structural stiffness appears. The last hinge, for each bridge, formed at a level where the mid-span section or the support section or any other section had entirely yielded. At each time, it was noted that the section that yielded completely is exactly at a position where the bending moment was maximum either positive or negative.

The non-linear analysis showed that in addition to the plastic hinge formation in the longitudinal girders or box girders, plastic mechanisms in the direction of transverse bending were also evident, especially in the vicinity of the load of maximum moment. When an excess of hinges occurs in both critical and non critical positions (case of SSBGB-1P), and two hinges form in adjacent members either sides of a transverse member, (however only one really exists at that location), the collapse mechanisms were over-complete. This is caused by a concentration of the torsional stiffness of the slab in the transverse member leading to a discontinuity of the longitudinal bending moment and then to a hinge separation. This separation may be due to the need of torsional stiff diaphragms not used in this study.

In the case where a reduced number of lanes in the bridge were loaded,

(case of SSBGB-1P), it was possible to continue loading until the collapse mechanism formed. However, a rapid increase in the deflections accompanied by a significant decrease in the stiffness after a certain stage of loading could invalidate the assumption of small deformations implicit in the elastic analysis and lead to a divergence in the results.

6.8 Multiple Load Factors

The multiples of the proportional live load at each load stage are summarized in table (6.1). For those cases where all the lanes are loaded, an adjusted load multiple is also given in brackets. This includes the effect of a modification factor to account for the reduced probability of the presence of multiple heavy vehicles, and is provided so that the results for a reduced number of lanes and all the lanes loaded can be compared. In the OHBDC, it is specified that a bridge with three lanes accounts for a factor of 0.9 when two lanes are loaded and a factor of 0.8 when all the lanes are loaded. In the case of a two lane bridge, the factor is 0.9 when both lanes are loaded.

The adjusted multiple load factors are also presented graphically in figure (6.26) from which certain observations are readily made. First, for a given longitudinal positioning of the vehicles the multiple load factors for all lanes loaded are less in magnitude than those when a reduced number of lanes are loaded. This indicates that all lanes loaded will always govern the plastic as well as elastic design and fewer lanes loaded need only be accounted for in elastic analysis for serviceability requirements. Second, the multiple

load factors for continuous bridges when the maximum positive moment is maximized (CSGB-3P and CBGB-3P), are less than those factors when the negative moment is maximized (CSGB-3N and CBGB-3N). In all cases the positive moment governed.

6.9 Strength Reserve

The strength reserve is defined as the strength that a member can take or overtake after its first yielding [26], i.e. it is the amount of energy absorbed between the formation of the first plastic hinge (elastic failure) and the plastic collapse of the structure. This energy is computed at figure (6.26) as the ratio of the minimum plastic collapse multiple load factor and the minimum elastic failure multiple load. The multiple load factor need not necessarily be for the same load position. In a mathematical form, the strength reserve is

$$SR = \frac{AMLF_{mpf}}{AMLF_{mef}} \tag{6.1}$$

Where SR = Strength reserve,

$AMLF_{mpf}$ = Minimum adjusted multiple load at failure,

$AMLF_{mef}$ = Minimum adjusted multiple load at first hinge.

The values of the strength reserve for each bridge analyzed are shown in table (6.2).

6.10 Longitudinal Redistribution

The longitudinal distribution of live load bending moments for the continuous bridges at different load stages are shown schematically in figures (6.27) to (6.30). These longitudinal distribution factors represent the fraction of the total live load moment summed up over each of the longitudinal girders or box girders. Also shown in these figures, is the redistribution factor Ψ for each critical stage, given by

$$\Psi = \left(\frac{M_n}{M_1}\right) * \left(\frac{\lambda_1}{\lambda_n}\right) \tag{6.2}$$

Where M_1 = Total moment at the first stage (first plastic hinge),
M_n = Total moment at the n^{th} stage (n^{th} plastic hinge),
λ_1 = Multiple load factor at first stage,
λ_n = Multiple load factor at n^{th} stage.

Thus the load redistribution factor Ψ is the ratio of the elasto-plastic moment to the elastic moment at an equivalent multiple load factor.

From the above equation, it is evident that at the formation of the first plastic hinge, the redistribution is elastic and the factor Ψ is equal to one. The percent redistribution from the negative section to the positive one or vice versa is given by

$$\%R = 100(1 - \Psi) \tag{6.3}$$

A value of Ψ greater than one (i.e. $\%R < 0$) indicates a redistribution of load from some other region (positive or negative) to the maximum moment

region. The values of percent load redistribution are shown graphically in figure (6.31). They show an amount of about 10% redistribution for the cases of CBGB-3P, CBGB-3N, and CSGB-3N. An amount of about 19% is noted in the case of CSGB-3P. The values of Ψ and percent redistribution are also tabulated in tables (6.3) to (6.6).

6.11 Transverse Redistribution

Figures (6.32) to (6.38) show the transverse redistribution of live load longitudinal bending moment at different load stages. The transverse distribution can be considered in two different ways: the ratio of the live load moment in each girder or box girder to the total live load moment across the section or load distribution factor D. In this study, the load distribution factor D was considered, and plotted against the transverse position of the girder or box girder. This value of D, which has the unit of length, is used to calculate the fraction of the load effects due to one wheel line of the design vehicle to be carried by one girder or box girder. From the finite element results, the value of D can be calculated as follows:

$$D = \left(\frac{S}{2n}\right) * \left(\frac{M}{M_g}\right) \tag{6.4}$$

Where S = Girder spacing,

n = Number of lanes loaded,

M = Total live load bending moment at a section,

M_g = Live load bending moment for a specific girder or box girder.

Some conclusions can be easily drawn from the above formula. First, the larger the value of D of a girder or a box girder, the less moment that girder or box girder will carry. Second, those cases where all lanes are loaded always govern the distribution because of the presence of the parameter n in the denominator. In addition, when all lanes are loaded, the D values for the interior girder are always less than those for the exterior until the first plastic hinge is formed. It follows that at the elastic range, the moment is mostly taken by the interior girders. After the formation of the first plastic hinge, the value of D started to increase for the interior girders and decrease for the exterior ones, allowing for a more equal value of D across a section, resulting in a more uniform transverse distribution of the bending moment. The decrease in D for the exterior girders was faster compared to the increase in the interior girders due probably to a concentration of moments at the considered section and also the early realization of the ultimate flexural capacity of the interior girders. After the establishment of the plastic collapse mechanism, the D value was nearly equal for all girders. At that stage, the live load flexural capacities of the girders or box girders are reached.

In the case of SSBGB-2P (see figure (6.35)), the distribution factor D did not change during all the load stages and showed mostly a uniform behavior. The unchanged value of D is probably due to the narrow form of the bridge. In addition, the plastic hinges in the two steel boxes were formed simultaneously. This had made the ratio of the total moment across a section to the moment in the girder remaining constant for all the loading stages up to failure.

The analysis of transverse distribution was also carried out for the SSBGB-1P as shown on figure (6.36). This analysis was intended to determine the effects of the number of lanes loaded, as well as the effect of torsion in box girder bridges. It is clear from the figure that the moment is mostly taken by the box girder where the truck is positioned. The other box girder resists only a small bending moment up to the formation of the first plastic hinge. After that stage, the transverse distribution starts improving. However, this distribution was not perfectly uniform even at failure of the bridge. The failure observed in this case was due to a rapid increase in the deflections and a sharp decline in the stiffness. The transverse distribution would have been uniform if the plastic collapse mechanism was reached.

The values of the transverse load distribution factors are tabulated in tables (6.7) to (6.13). The D values for the exterior and interior girders in the case of box girder bridges, are very close compared with the values of slab-on-girder bridges. This is probably due to the fact that box girder structures are more rigid than others and can develop a significant torsional effect. The comparison of the SSBGB-2P and CBGB-3N or CBGB-3P shows a higher D value for the simply supported bridge than for the continuous bridge. No comparison was carried out for the continuous bridges because the continuous slab-on-girder bridge was a scale model.

The design distribution factors, D_d, of the studied bridge prototypes, calculated in accordance with the simplified methods of analysis of the OHBDC [28] which were referred to in section 3.2.2, are included in appendix A. These values represent an elastic distribution of loads and apply therefore only to the elastic stage prior to the formation of the first plastic hinge.

They compare well to a degree with the values of D calculated from the finite element analysis. However D was determined for the most critical transverse positions of each of the design vehicles for each bridge type. This implies that the transverse positions used in the elasto-plastic finite element analysis were not critical.

6.12 Factors Affecting the Distribution

A series of studies [12,14,30,34] were exploited to ascertain the influence of some parameters on the transverse and longitudinal redistribution of longitudinal moments. The findings of the studies are as follows:

6.12.1 Width of the Bridge

This is related to the box girder bridge. The two-lane simply supported bridge was a narrow bridge compared the three-lane continuous bridge. Predictably, the maximum intensity of the moment in a narrower bridge is always higher than the maximum moment in a wider bridge. This prediction confirms the findings in the analyzed box girder bridges.

6.12.2 Girder Spacing

Girder spacing, as it affects the rigidities of the structure, is adequately accounted for in the D value defined in equation (6.4). The manner in

which the results of finite element analysis should be interpreted for different girder spacing requires elaboration. However, from equation (6.4), the distribution factor D is directly related to the spacing. Further, an increase in the spacing leads to an increase in the distribution factor D. The increase in D leads itself to a reduction in the ultimate capacity and a non-uniformity of the distribution.

6.12.3 Position of the Vehicle

Longitudinal Position

The longitudinal position of the vehicle will affect the potential for longitudinal and transverse redistribution, and thereby determine the nature of the redistribution and the magnitude of the strength reserve. In the case of continuous bridges, the potential of longitudinal redistribution is the difference in the ratios of the live load flexural capacities to the elastic live load bending moment at the critical sections. Redistribution of 10% was noted from both positive and negative regions in the box girder bridge and 10% and 19% from negative and positive regions respectively, in the slab-on-girder bridge. These ratios of capacities show a small longitudinal redistribution taking place. Associated with this redistribution is a limited strength reserve which is added during the transverse redistribution. This strength reserve was in the range of about 1.2 to 2.0 times the live load at collapse mechanism as was required to form the first plastic hinge.

In addition, for all bridges, when dealing with a moving load, the critical

longitudinal position of vehicles at collapse mechanism found after the formation of the first plastic hinge may not coincide with the critical position in the elastic analysis. This would create a reduction in the strength reserve and the longitudinal redistribution. The longitudinal position of the vehicles also influenced the patterns of transverse redistribution. The transverse redistribution was always initially completed for the section where the maximum moment occurred, i.e at the most critical longitudinal position.

Transverse Position

The transverse position of the vehicles was maintained constant. However, in order to consider its effect, many trials should be considered at different distances of the load from the edge of the bridge. A critical position can decrease the multiple load factor and increase the strength reserve between the first hinge and failure.

6.12.4 Number of Lanes Loaded

This analysis was conducted on the simply supported box girder bridge. For this bridge, two conclusions can be made regarding the effect of the number of loaded lanes. First, a reduced number of loaded lanes would not govern the design of these bridges at ULS based on any critical stage. Second, a collapse mechanism is achieved more frequently when all lanes are loaded. It is highly improbable to reach the failure mechanism when a reduced number of lanes are loaded, due to the significant decline in

the stiffness and the rapid increase in deflections before the achievement of any transverse distribution. This transverse redistribution would be complete only if the transverse stiffness were increased significantly. These conclusions can be generalized for all other bridges.

6.13 Evaluation of the Analytical Method

The discussion of this post-elastic analysis would not be complete without an evaluation of the post-elastic analytical method. The purpose of this study was not to develop or refine an analytical method, but rather to investigate the redistribution characteristics of slab-on-girder bridges or box girder bridges. The method was more successful as a research aid in predicting the formation of the hinges, collapse mechanism etc. than previous research. However, as a design tool, the method lacks efficiency, especially when dealing with highly redundant structures such as bridges. Many stages are required before the formation of the collapse mechanism, making this method time consuming and very expensive.

6.14 Implications for the Post-elastic Design of Bridges

This study has shown that reserves of capacity can exist beyond those given by elastic strength calculations. It also identified certain properties which must be better defined before these strength reserves can be measured.

If analytical methods similar to those used in this study are required to take advantage of this surplus capacity, they would never become general practice. Simplified methods have to be developed. This study has revealed that, although the longitudinal and transverse patterns of redistribution are not independent of each other, the distribution of moment at any phase elastic or plastic, can be considered separately. This means that simplified methods of elasto-plastic analysis could be developped similar to those used in the elastic analysis of bridges. A post-elastic longitudinal distribution of moments could be determined, then post-elastic transverse load distribution factors applied to determine the actual moments in the individual beams. These could vary anywhere between the elastic distributions to the fully plastic distributions corresponding to a global collapse mechanism depending on the extent of redistribution that can realistically be achieved. As yet, only elastic transverse load distribution factors are applied.

Because of the substantial increase in capacity permitted by plastic design, new designs may be governed by serviceability rather than the ultimate limit states. In that case, better use of the post-elastic behavior of the structure would have to be included at the SLS if real benefits are to be seen from a plastic design. In addition, the true shakedown load levels would have to be determined. If the probability of a progressive plastic failure is large enough to be of concern, then an additional ULS may have to be established. The load factors associated with a shakedown failure would be less than those for simple plastic collapse since:

- Plastic collapse requires a single occurrence of an extreme load, while progressive plastic failure involves several occurrences of a lighter ve-

hicle. The more frequent event is assigned a smaller load factor on the basis of the live load probability distribution.

- Progressive failure provides additional warning between passages of the critical loads than would be possible from a simple plastic collapse. Less risk is associated with each passage of the vehicle, and hence a smaller load factor.

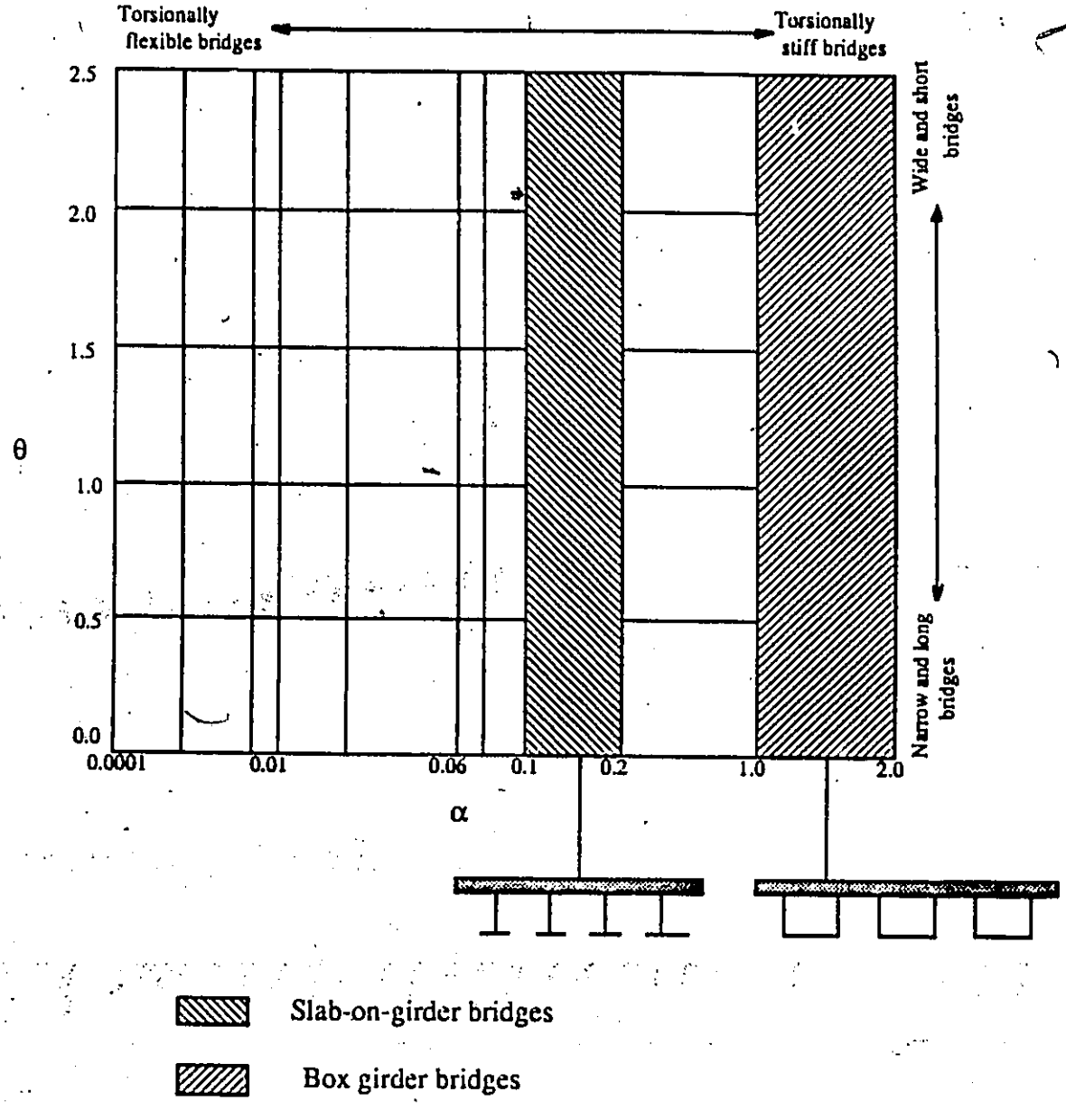

Figure 6.1: $\alpha - \theta$ Plane Showing Bridges Analyzed in this Study

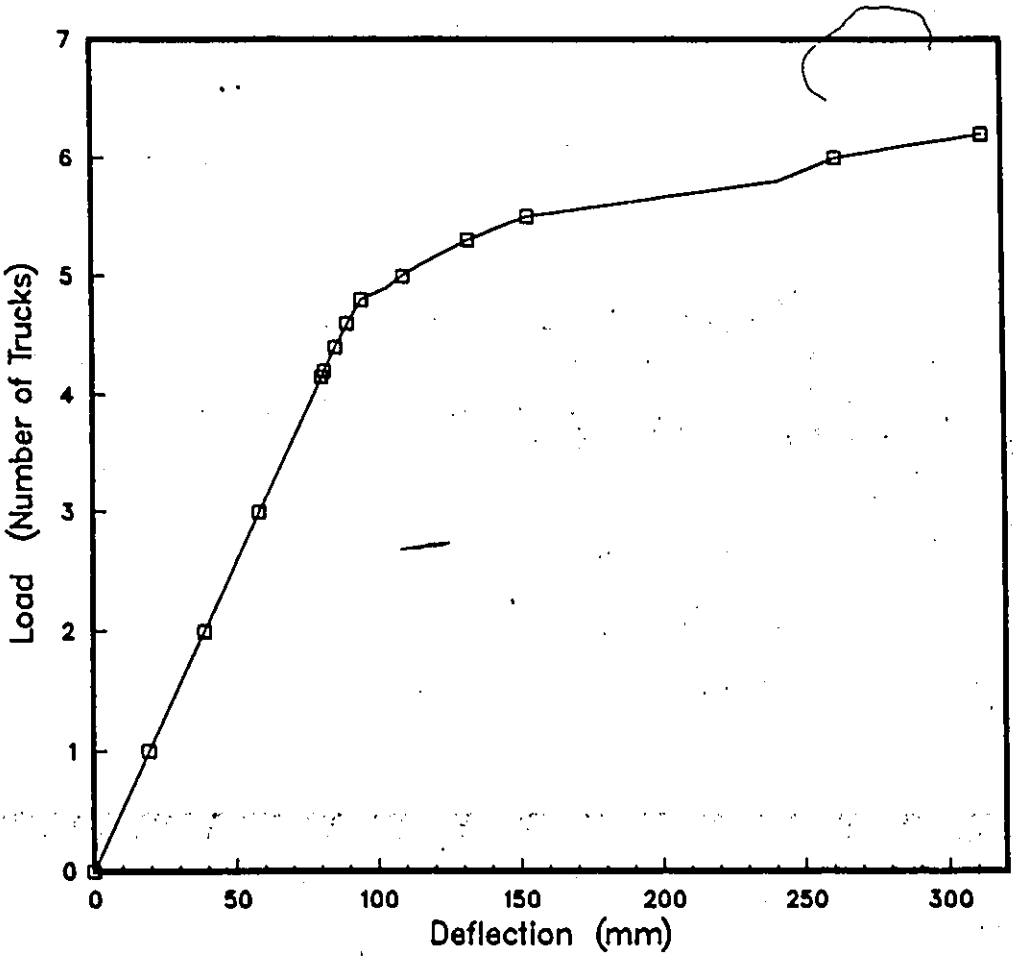

Figure 6.2: Load vs Deflection Curve for SSSGB-3P

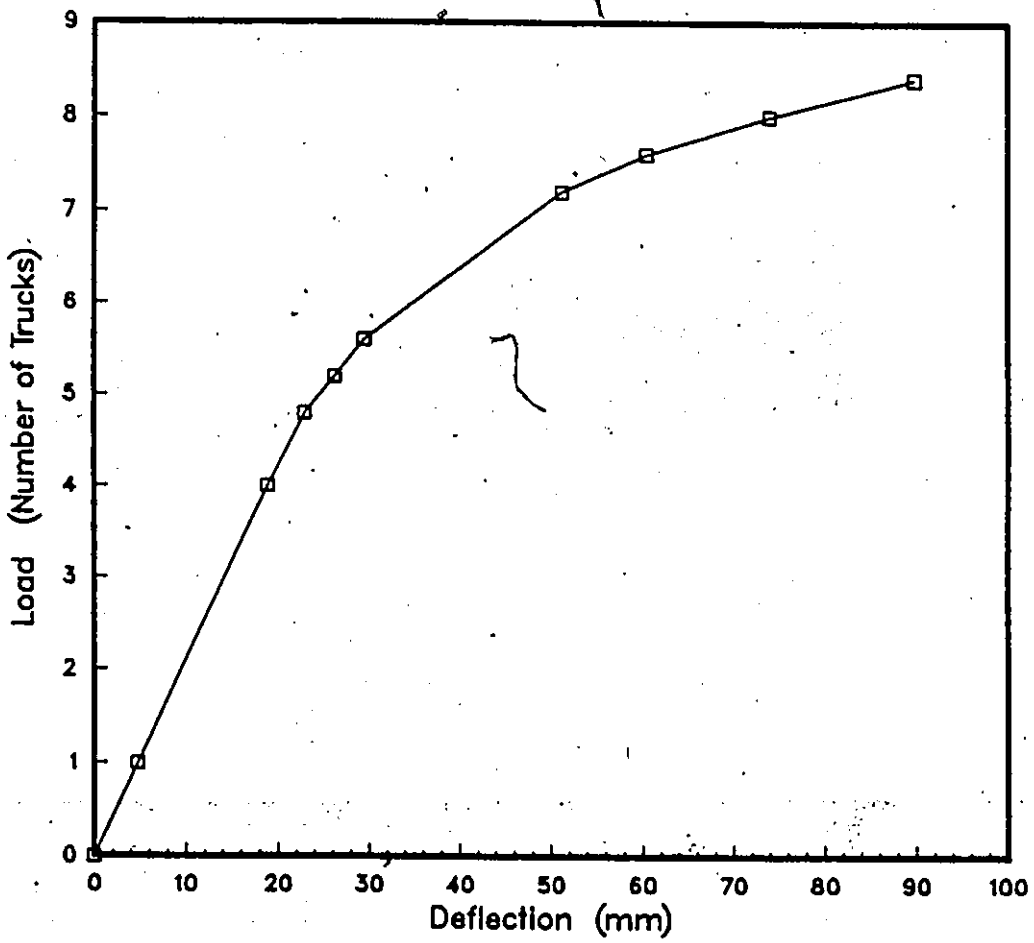

Figure 6.3: Load vs Deflection Curve for CSGB-3N

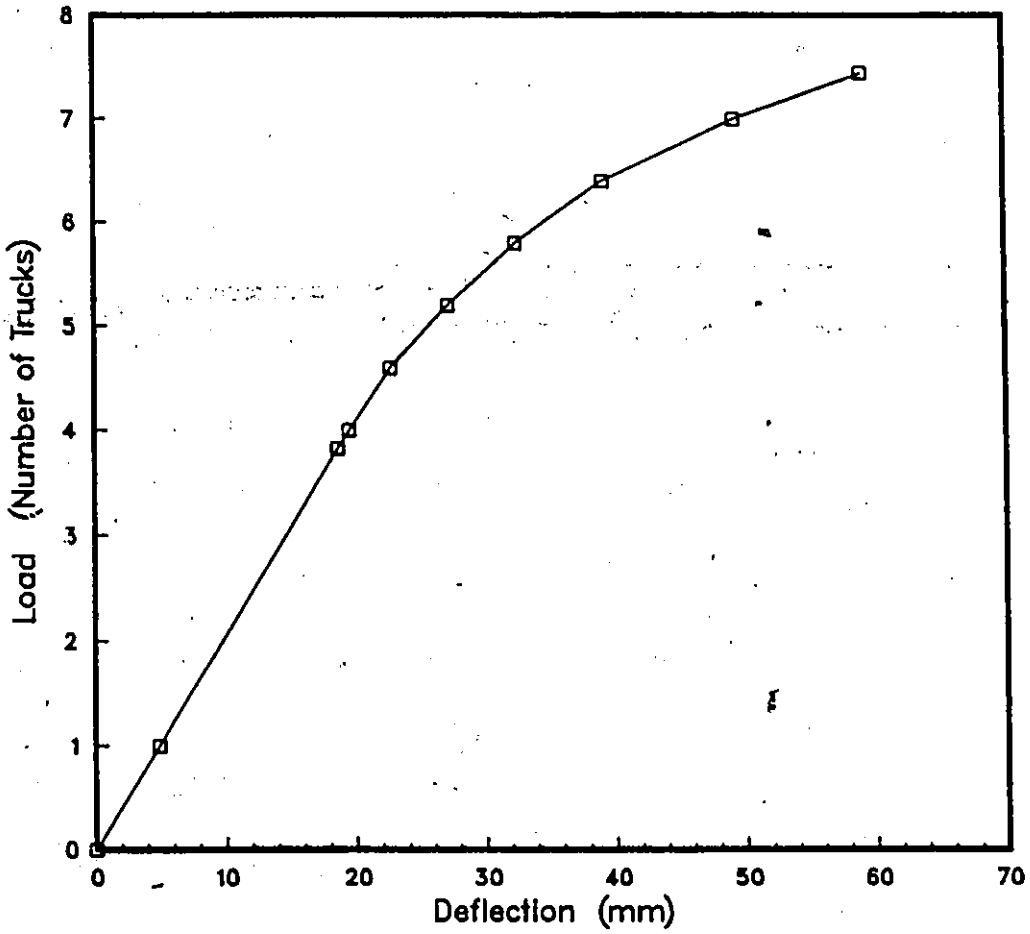

Figure 6.4: Load vs Deflection Curve for CSGB-3P

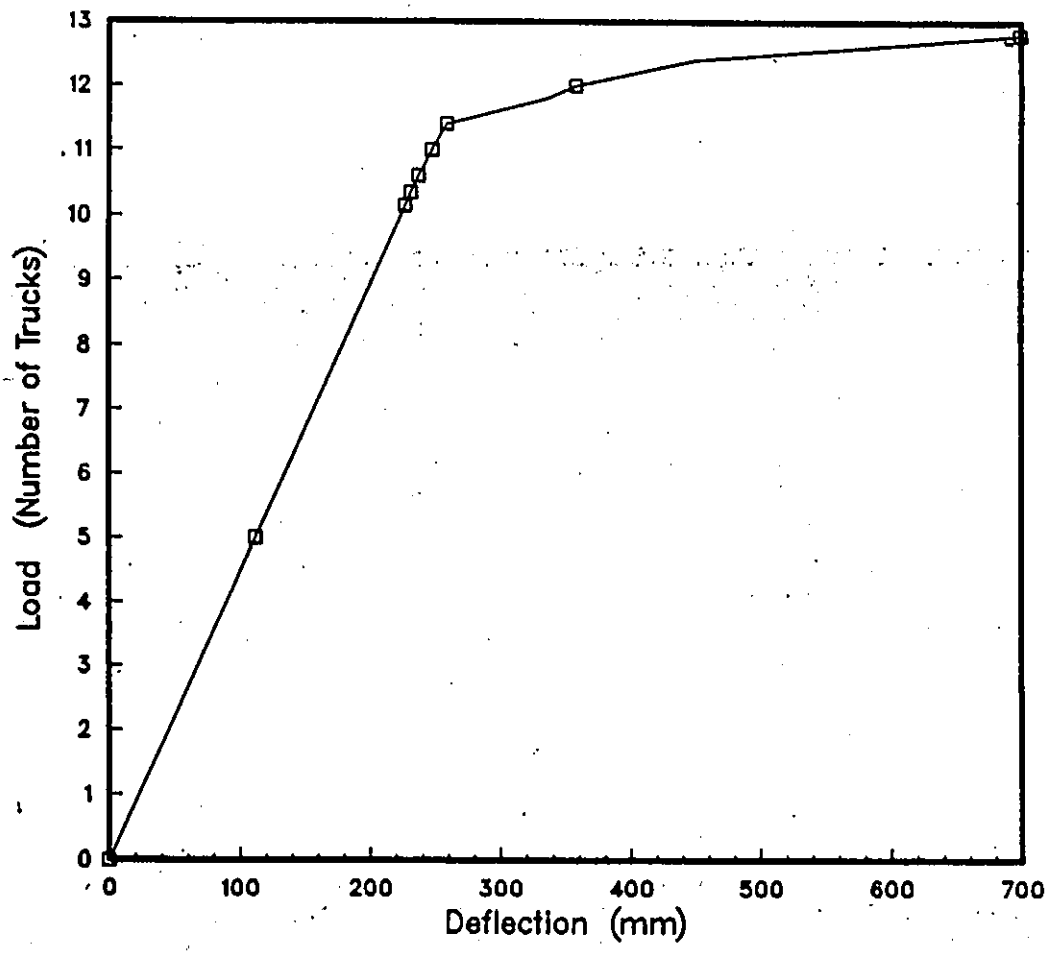

Figure 6.5: Load vs Deflection Curve for SSBGB-2P

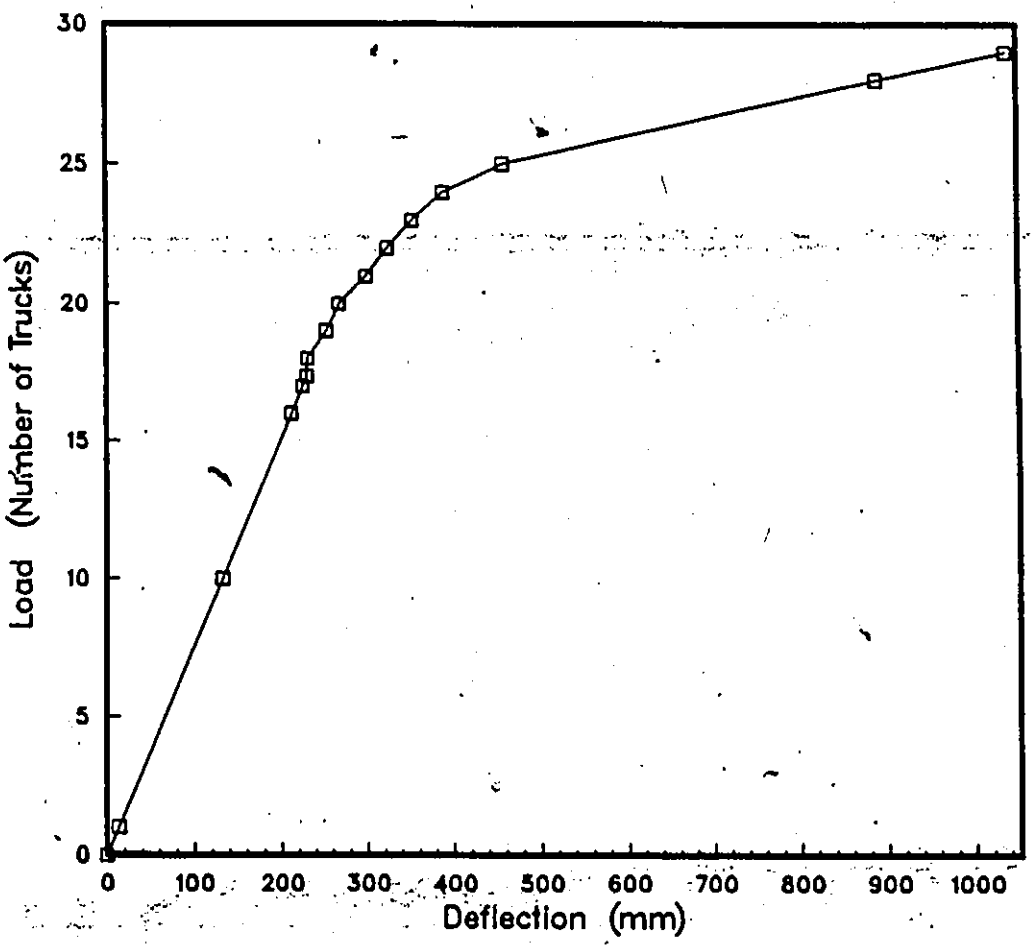

Figure 6.6: Load vs Deflection Curve for SSBGB-1P

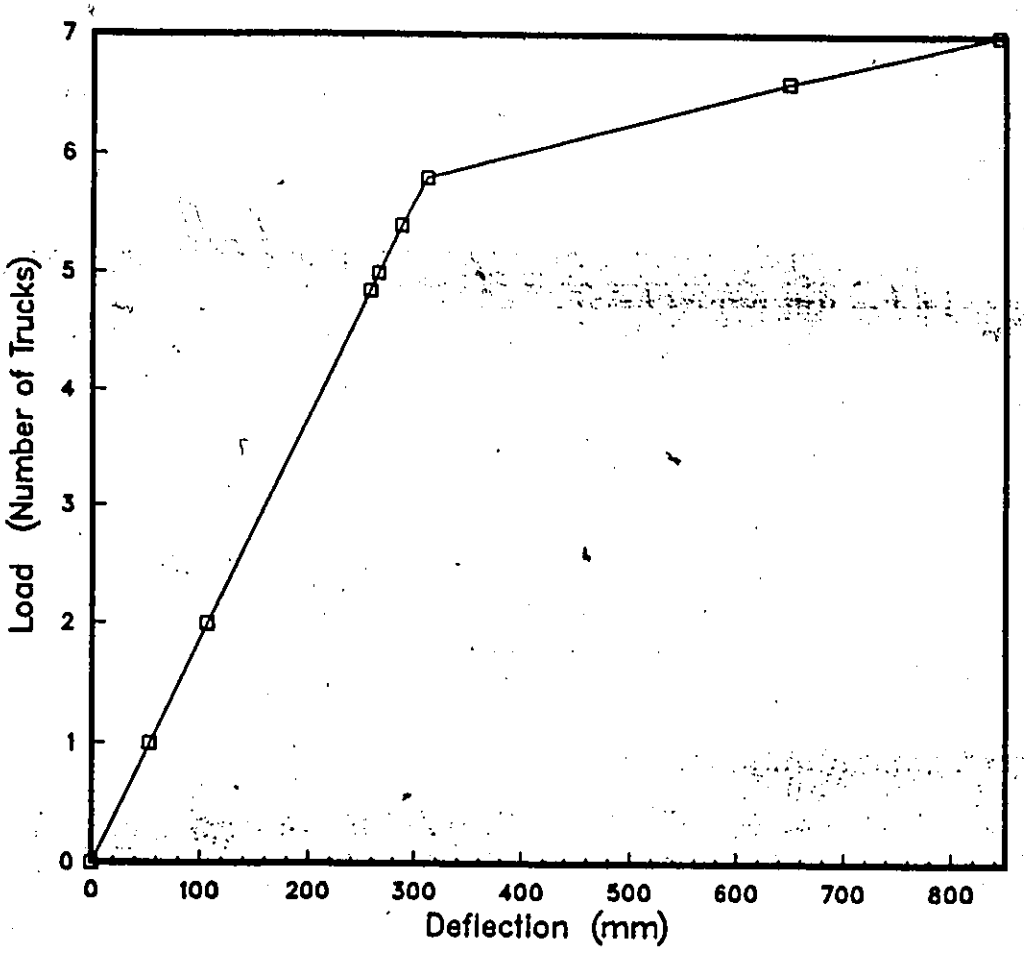

Figure 6.7: Load vs Deflection Curve for CBGB-3N

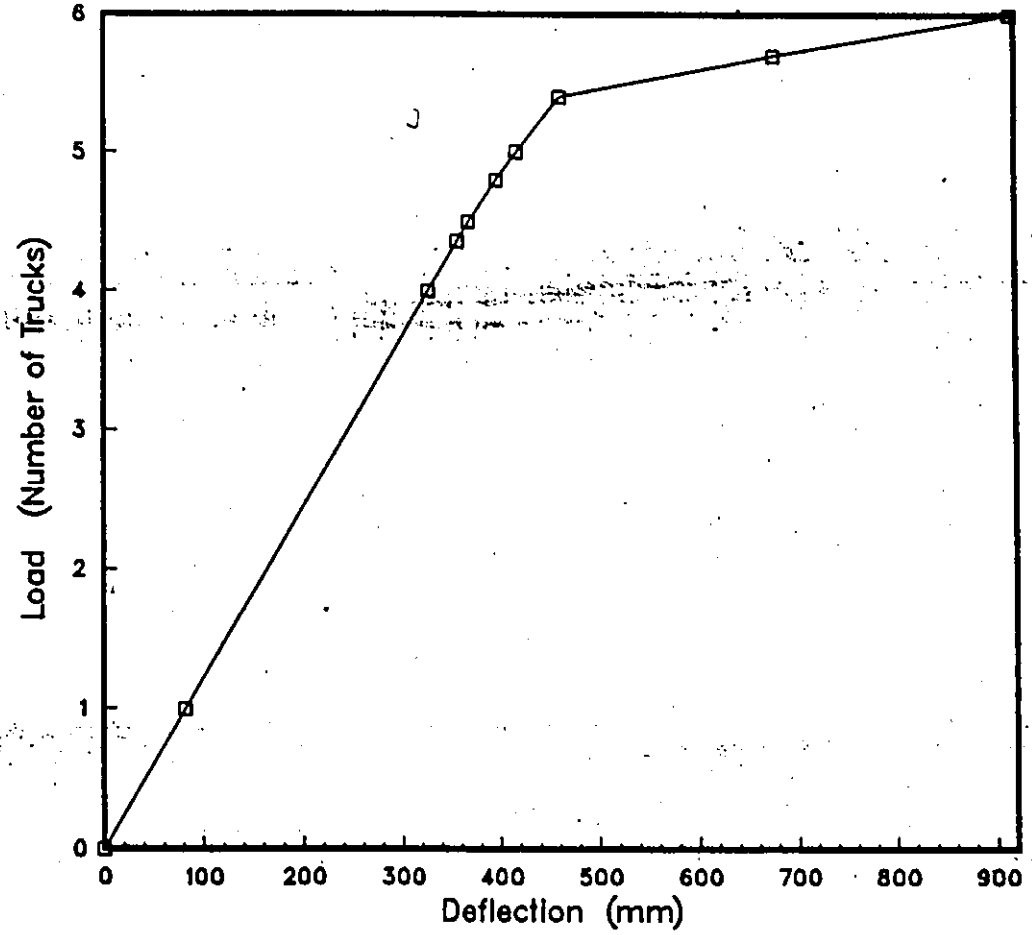

Figure 6.8: Load vs Deflection Curve for CBGB-3P

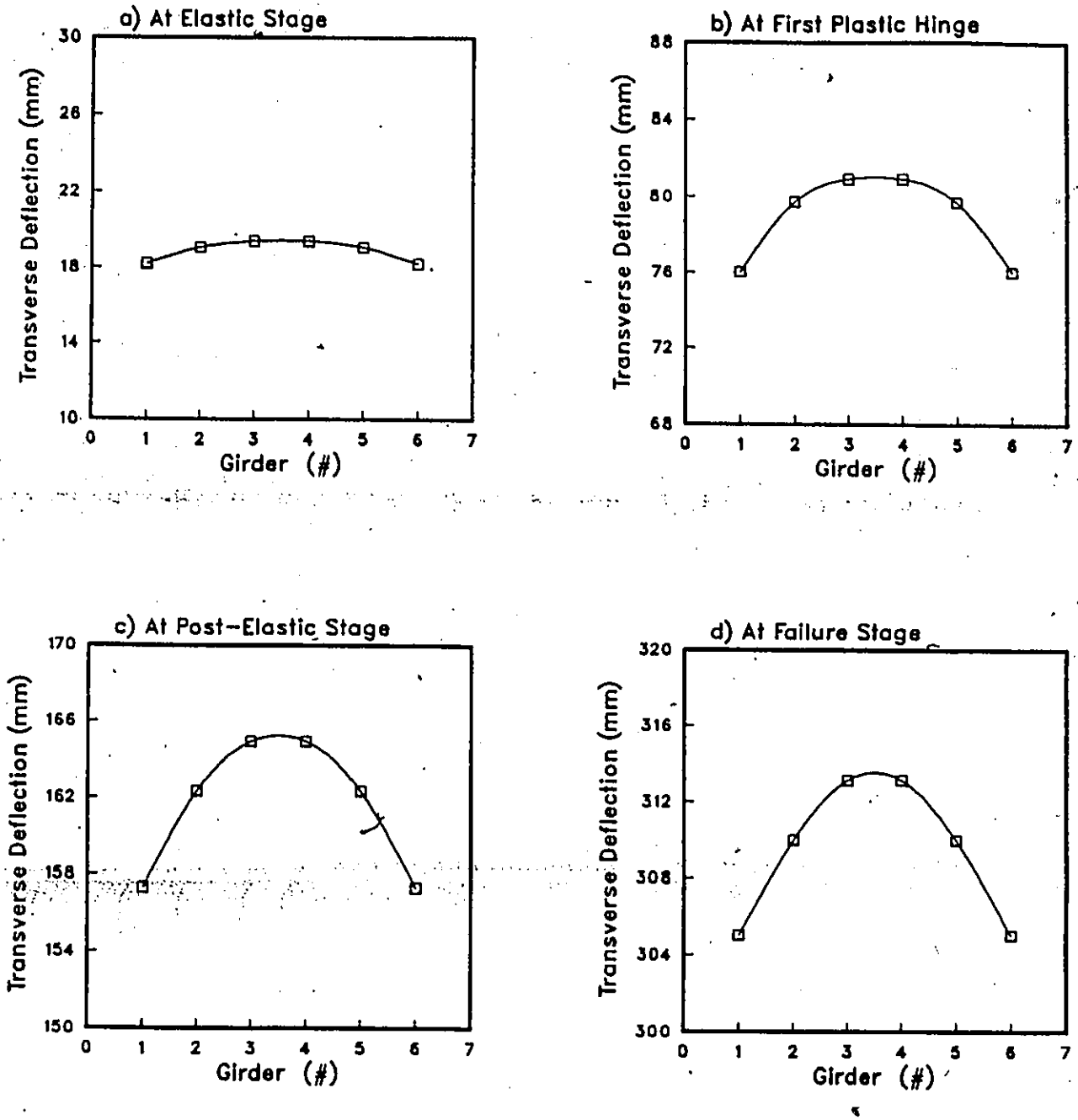

Figure 6.9: Transverse Deflection vs Girder Position Curve for SSSGB-3P

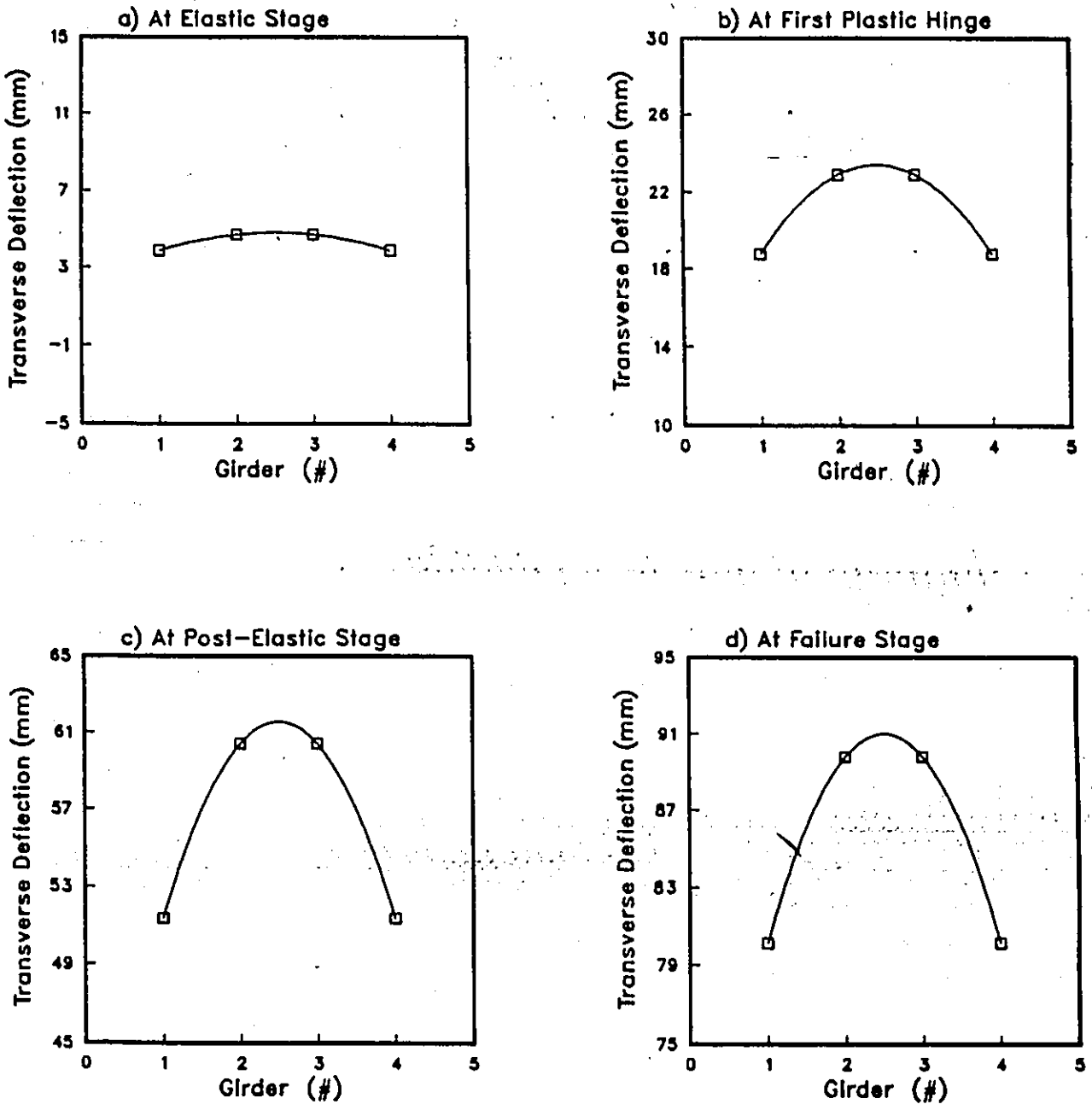

Figure 6.10: Transverse Deflection vs Girder Position Curve for CSGB-3N

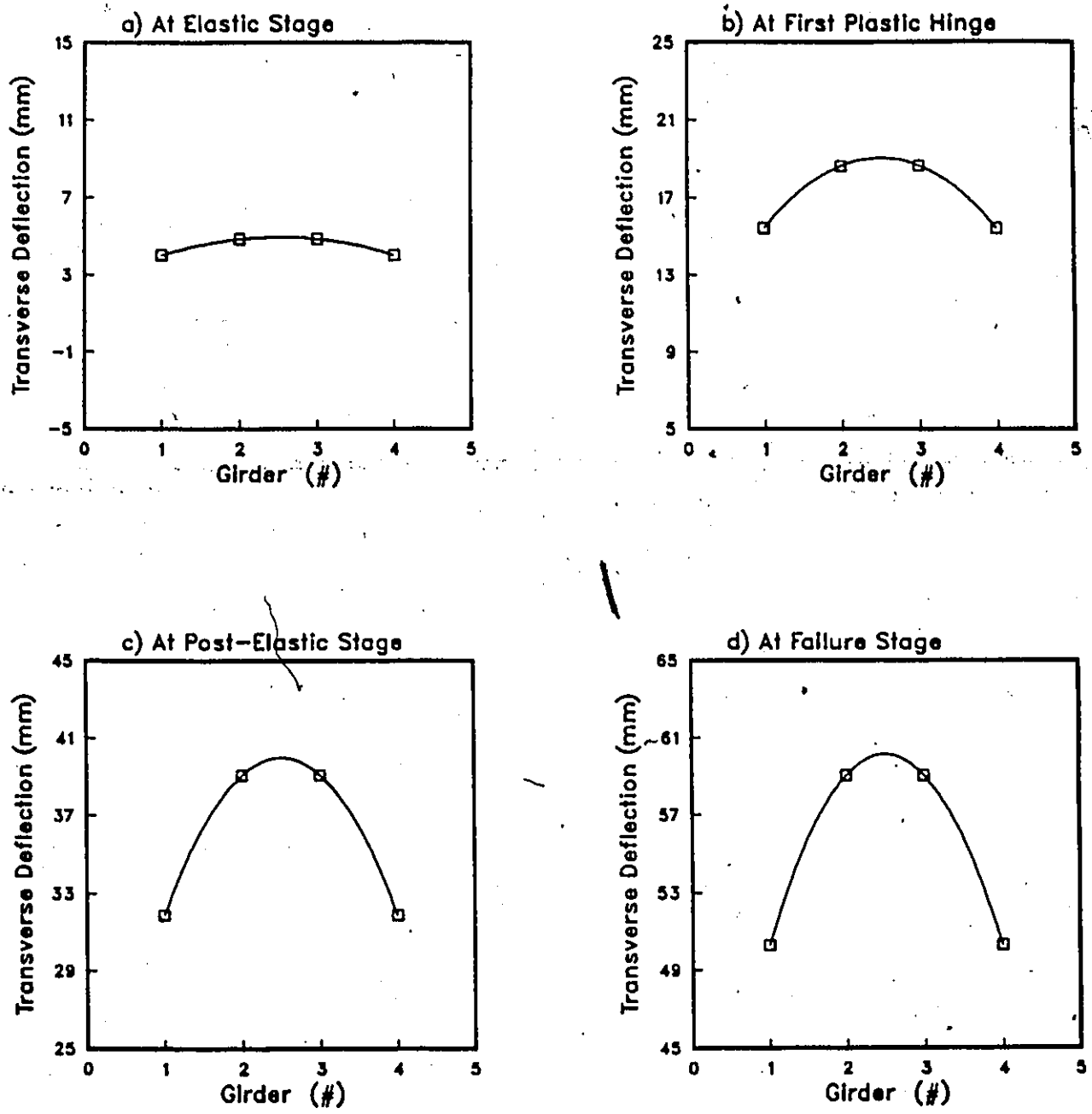

Figure 6.11: Transverse Deflection vs Girder Position Curve for CSGB-3P

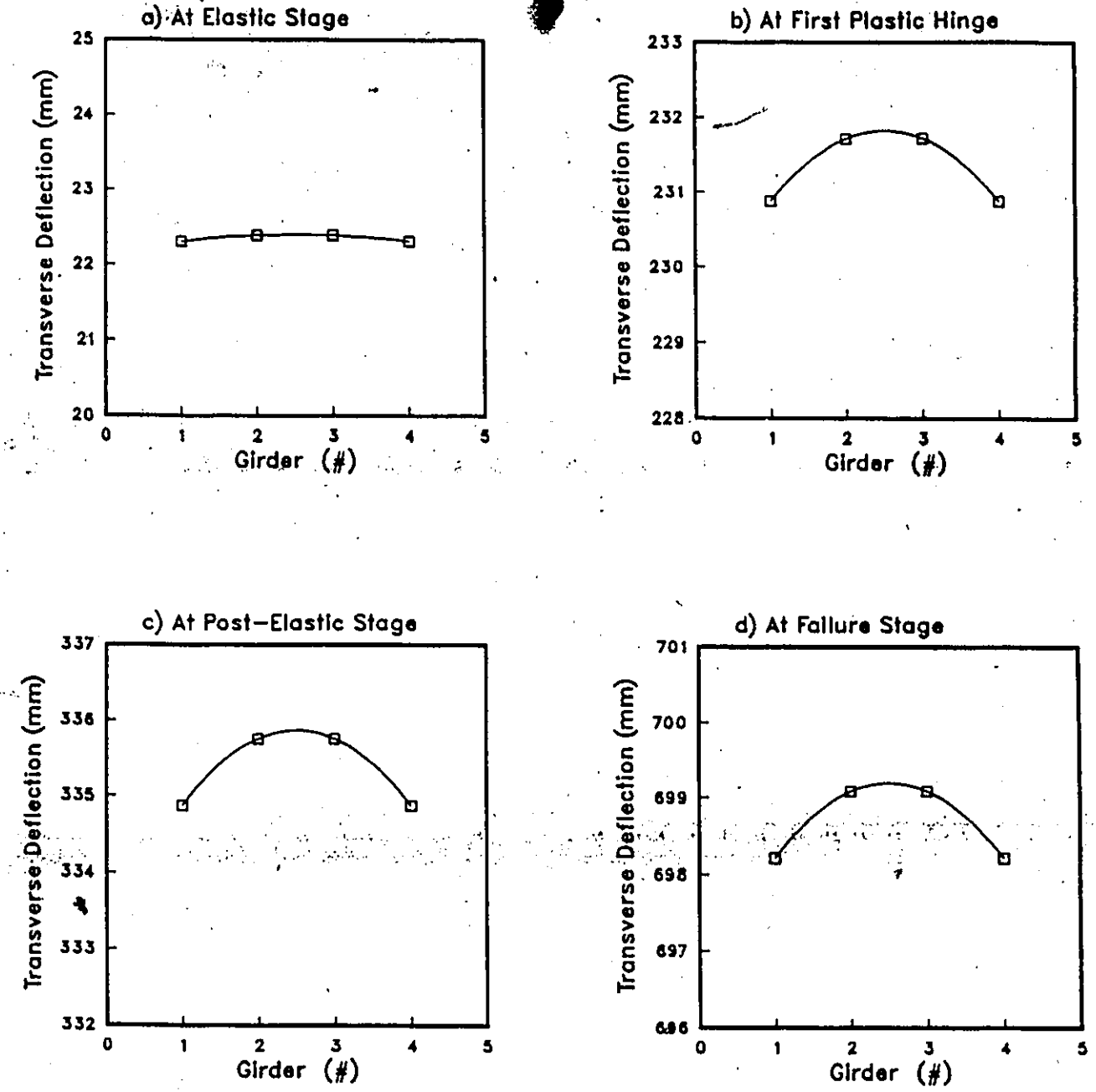

Figure 6.12: Transverse Deflection vs Girder Position Curve for SSBGB-2P

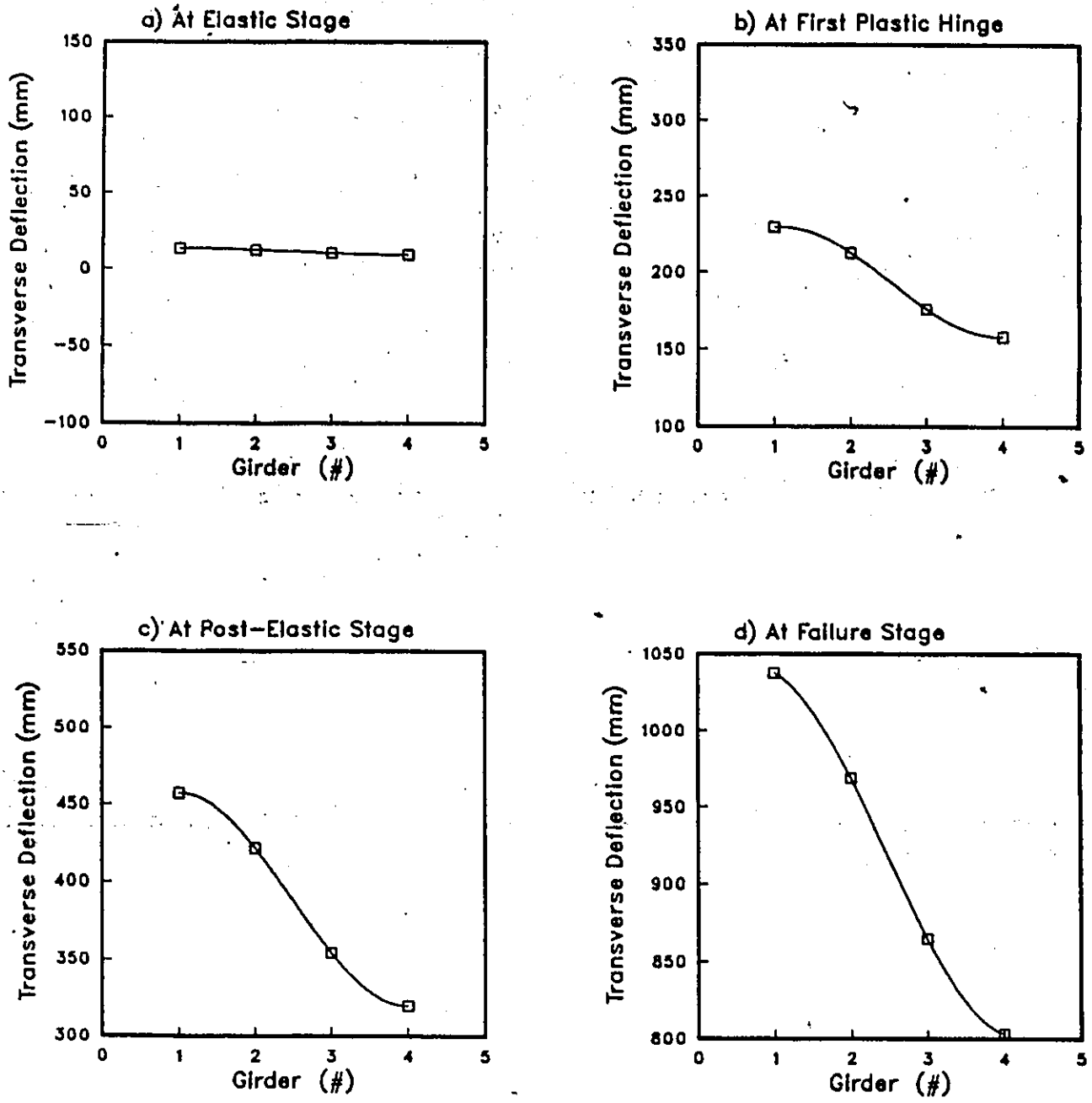

Figure 6.13: Transverse Deflection vs Girder Position Curve for SSBGB-1P

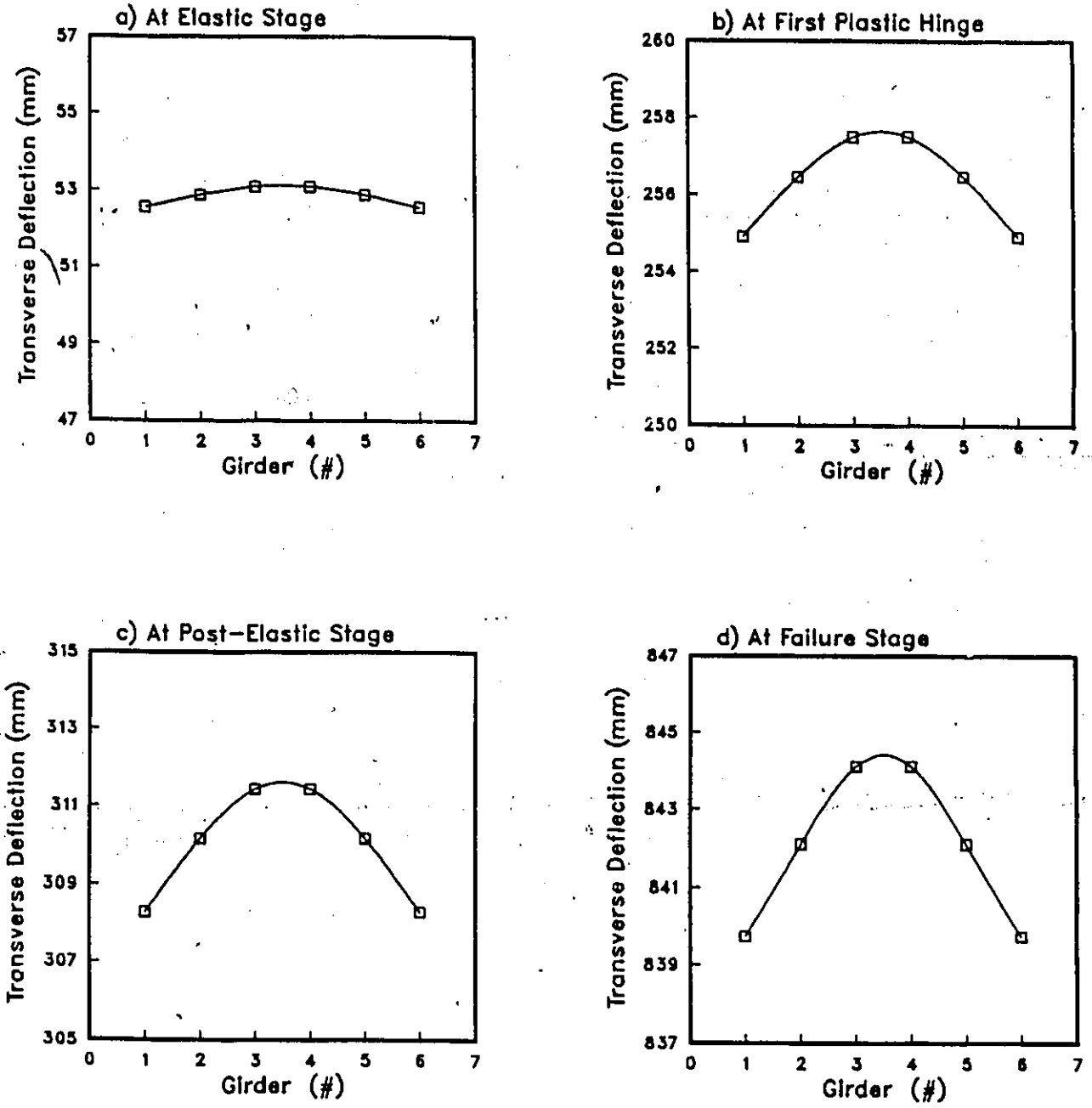

Figure 6.14: Transverse Deflection vs Girder Position Curve for CBGB-3N

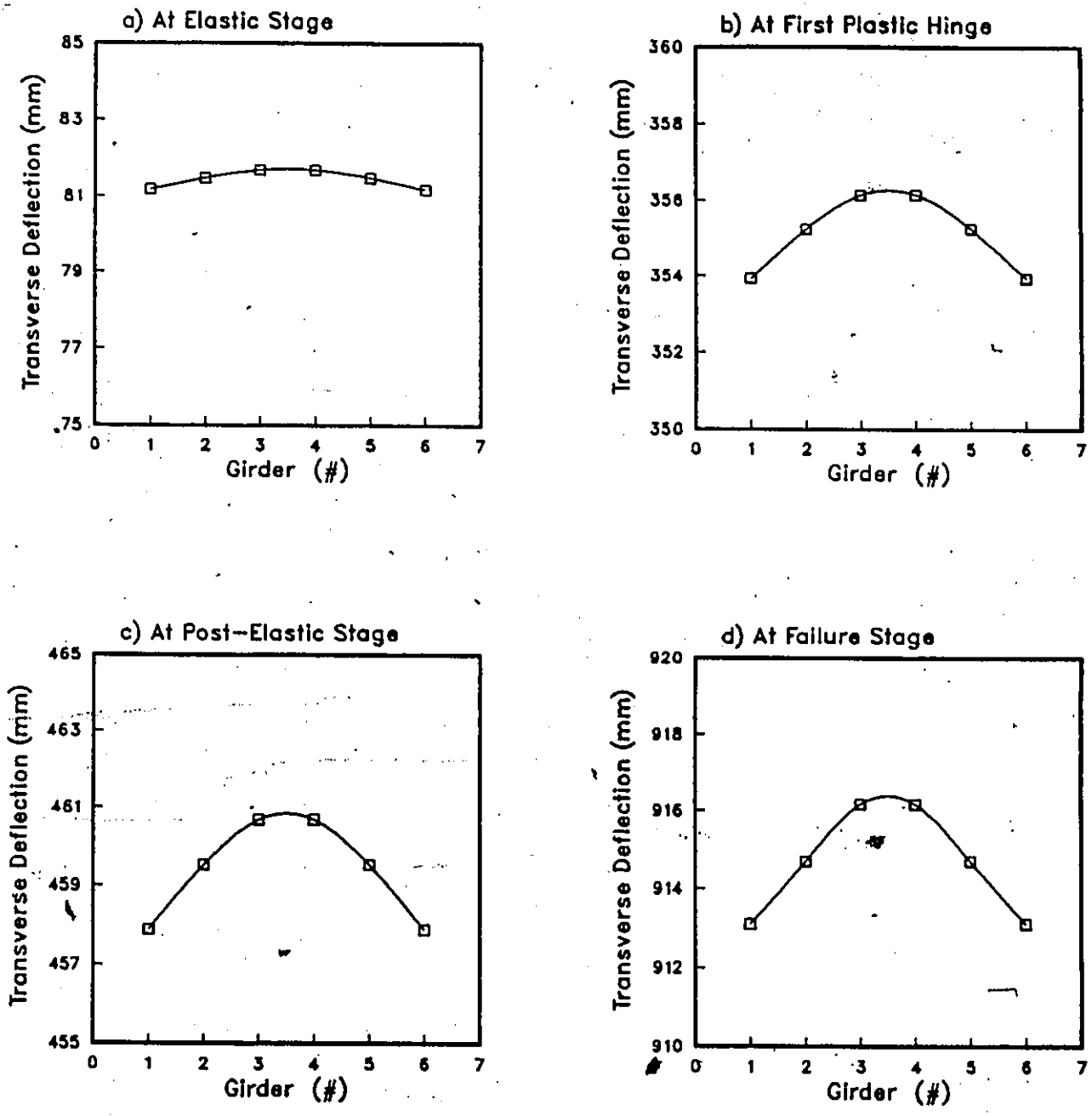

Figure 6.15: Transverse Deflection vs Girder Position Curve for CBGB-3P

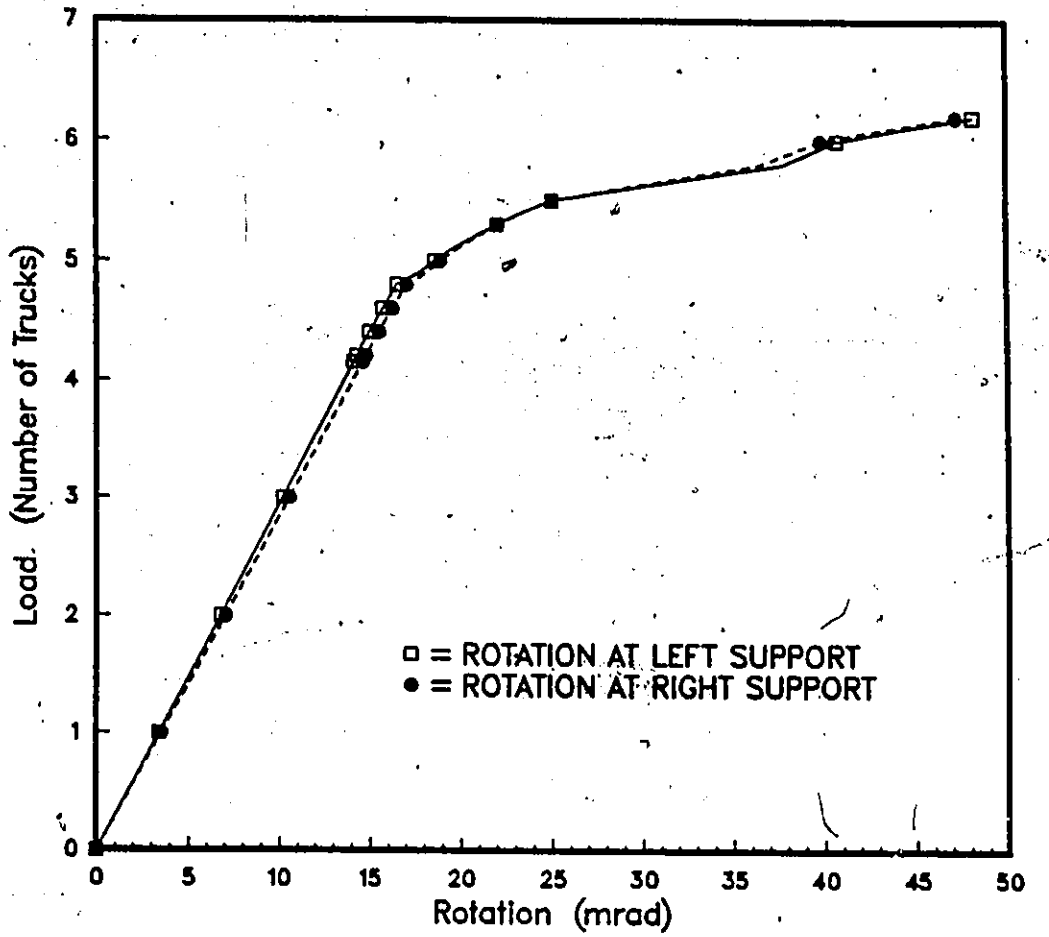

Figure 6.16: Load vs Support Rotation Curve for SSSGB-3P

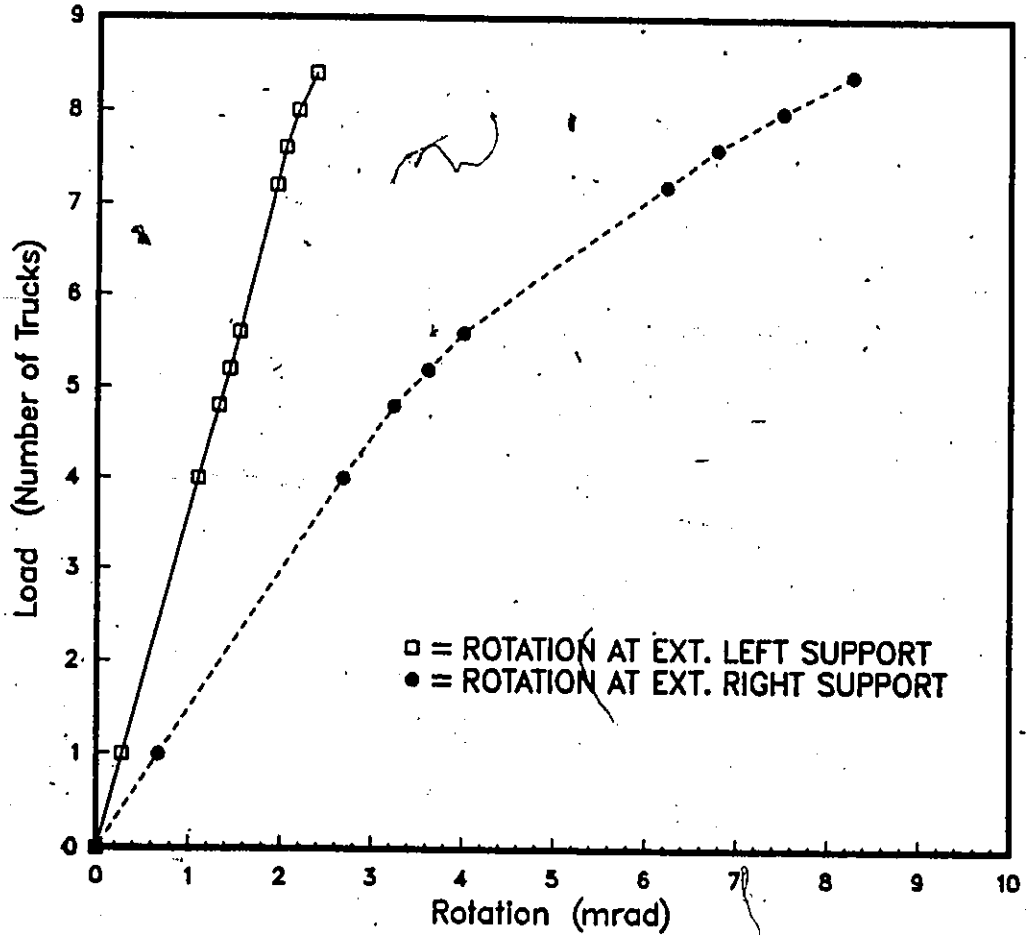

Figure 6.17: Load vs Ext. Support Rotation Curve for CSGB-3N

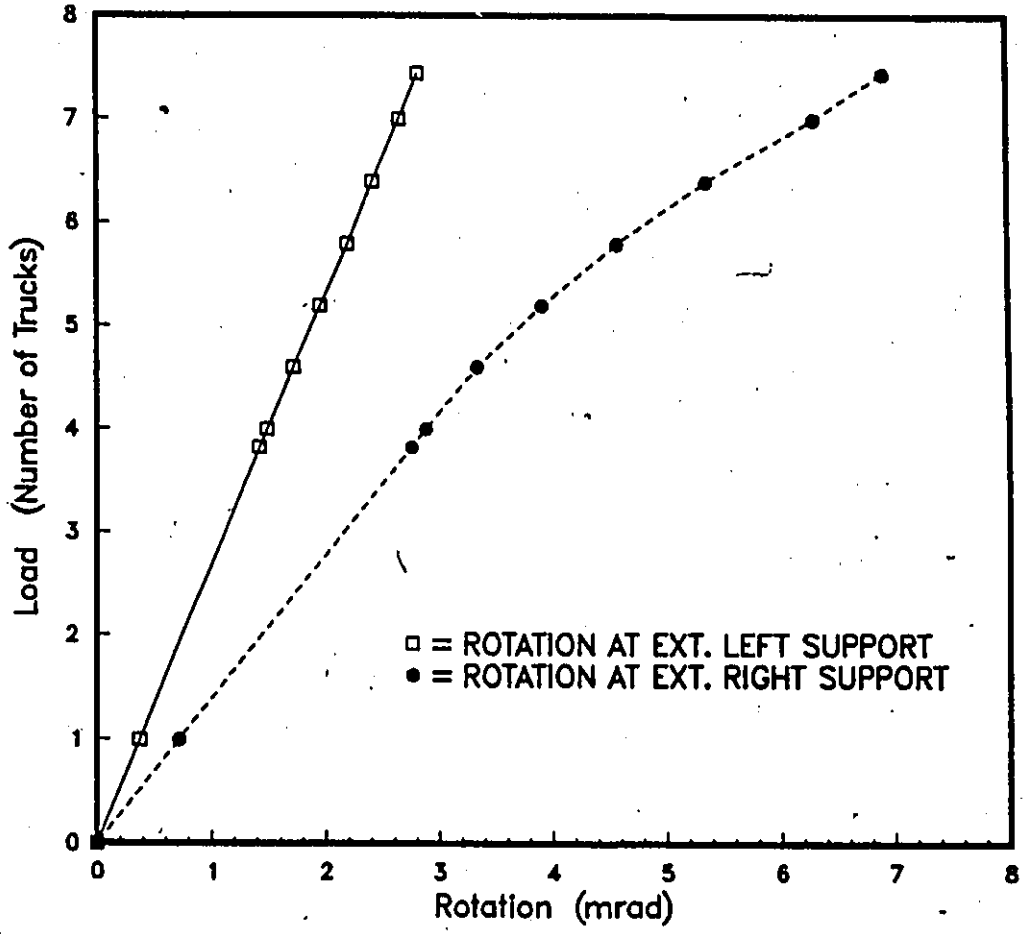

Figure 6.18: Load vs Ext. Support Rotation Curve for CSGB-3P

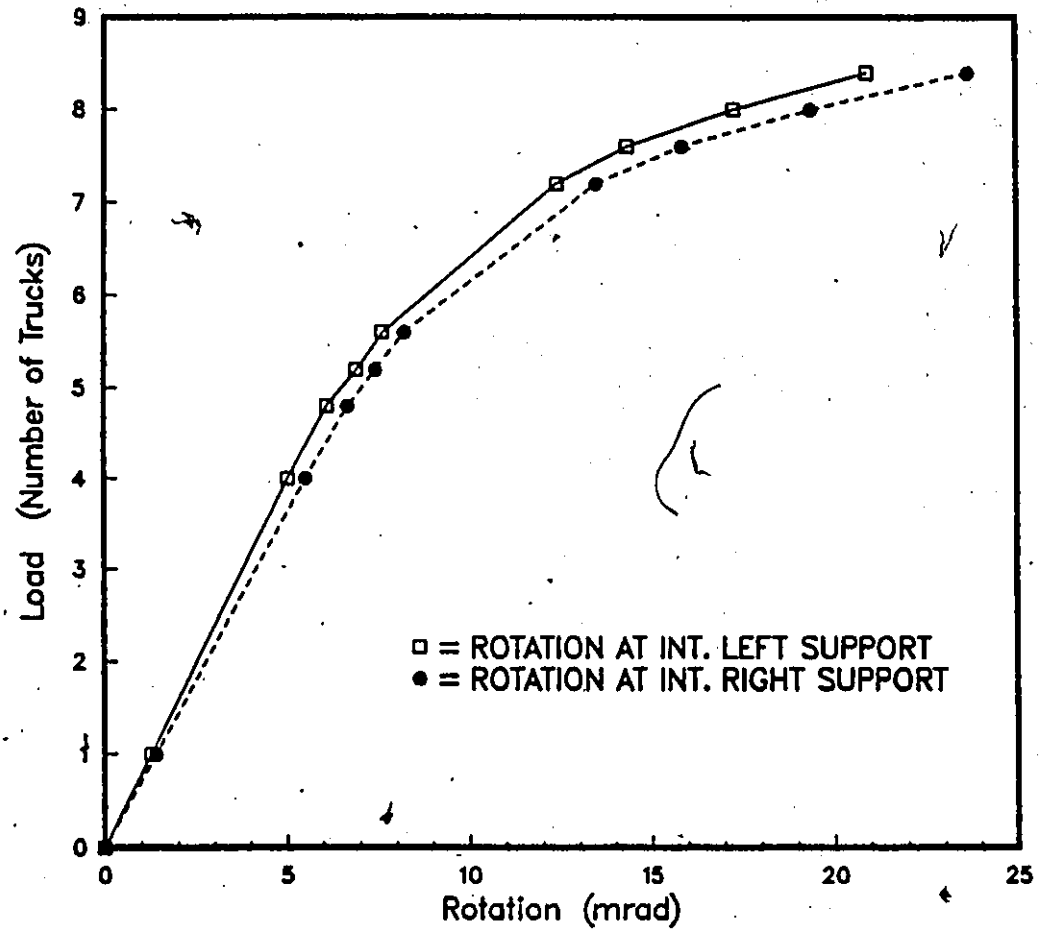

Figure 6.19: Load vs Int. Support Rotation Curve for CSGB-3N

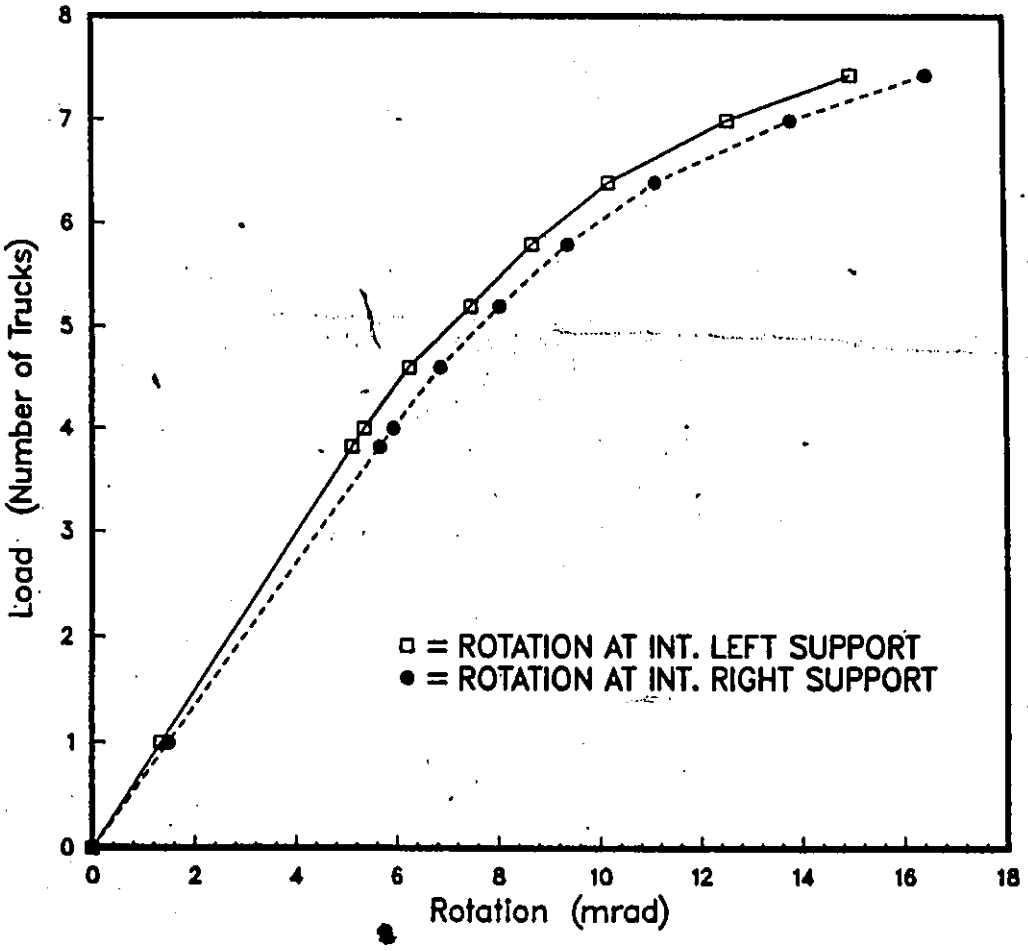

Figure 6.20: Load vs Int. Support Rotation Curve for CSGB-3P

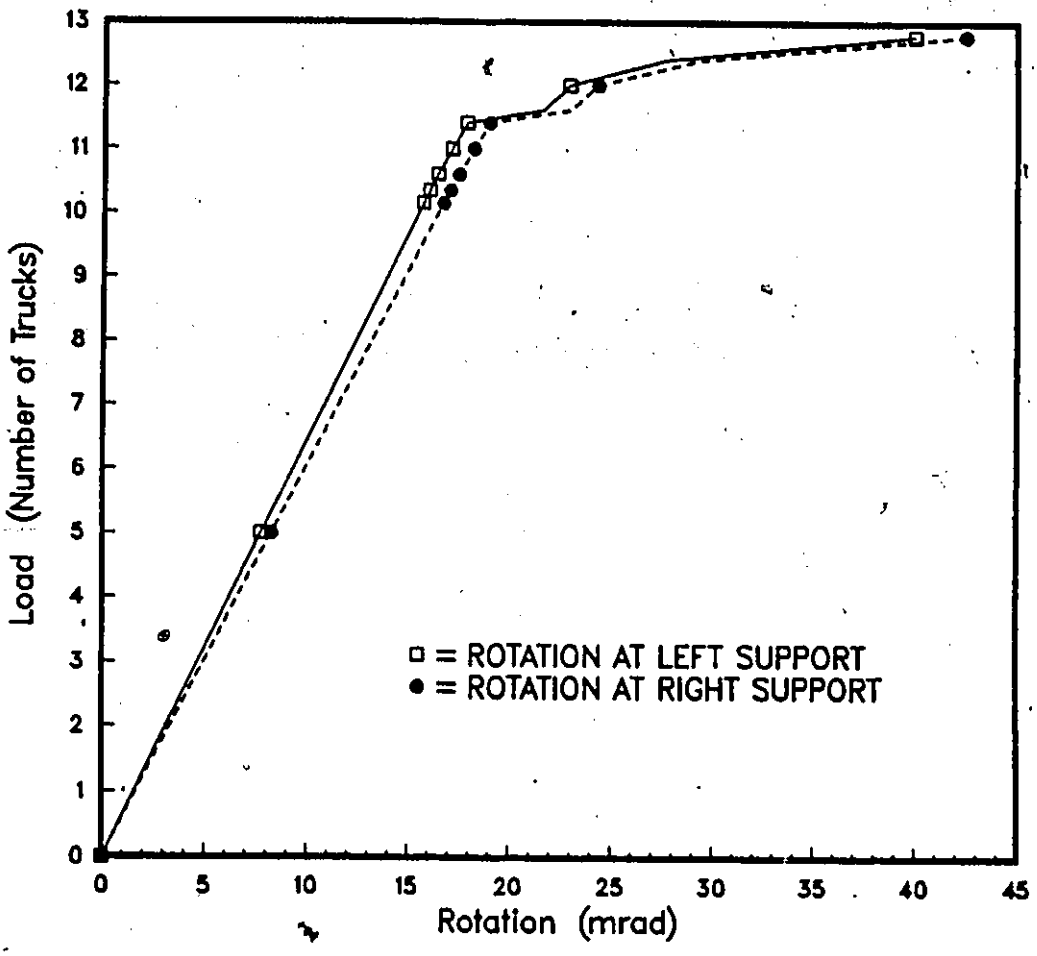

Figure 6.21: Load vs Support Rotation Curve for SSBGB-2P

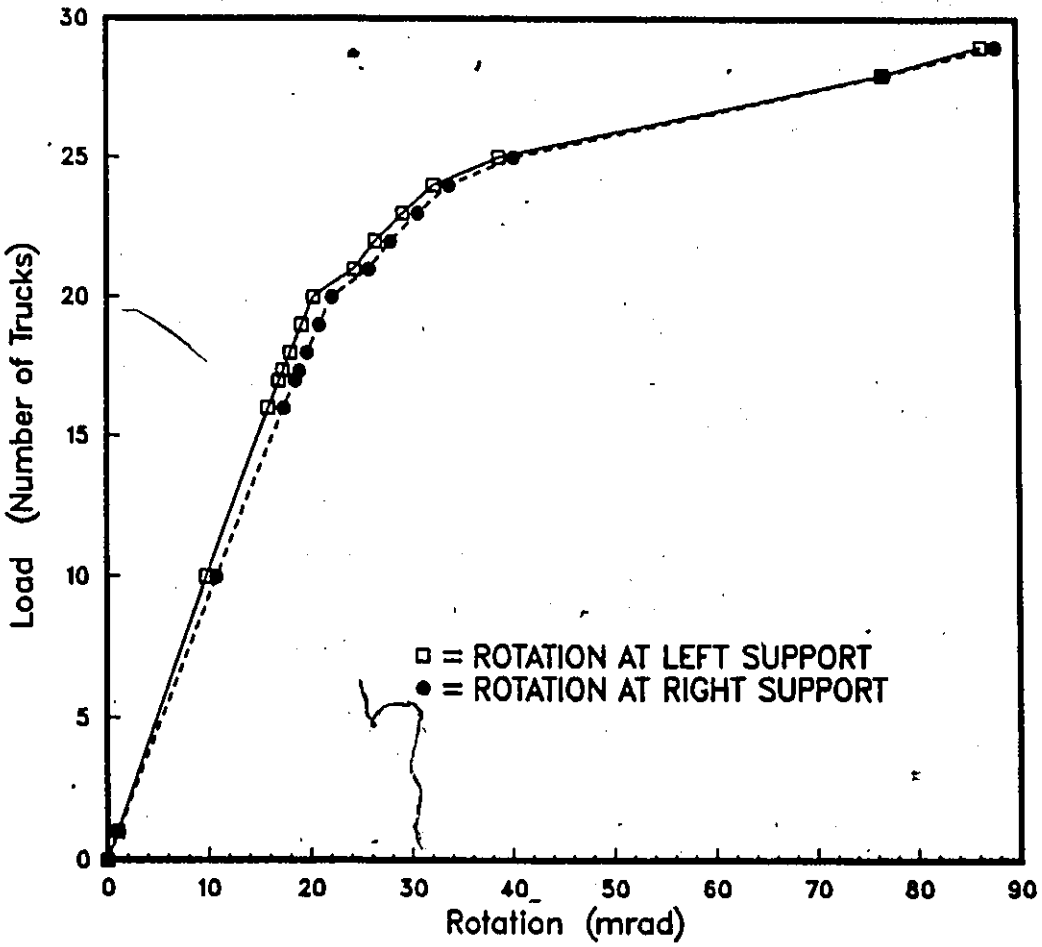

Figure 6.22: Load vs Support Rotation Curve for SSBGB-1P

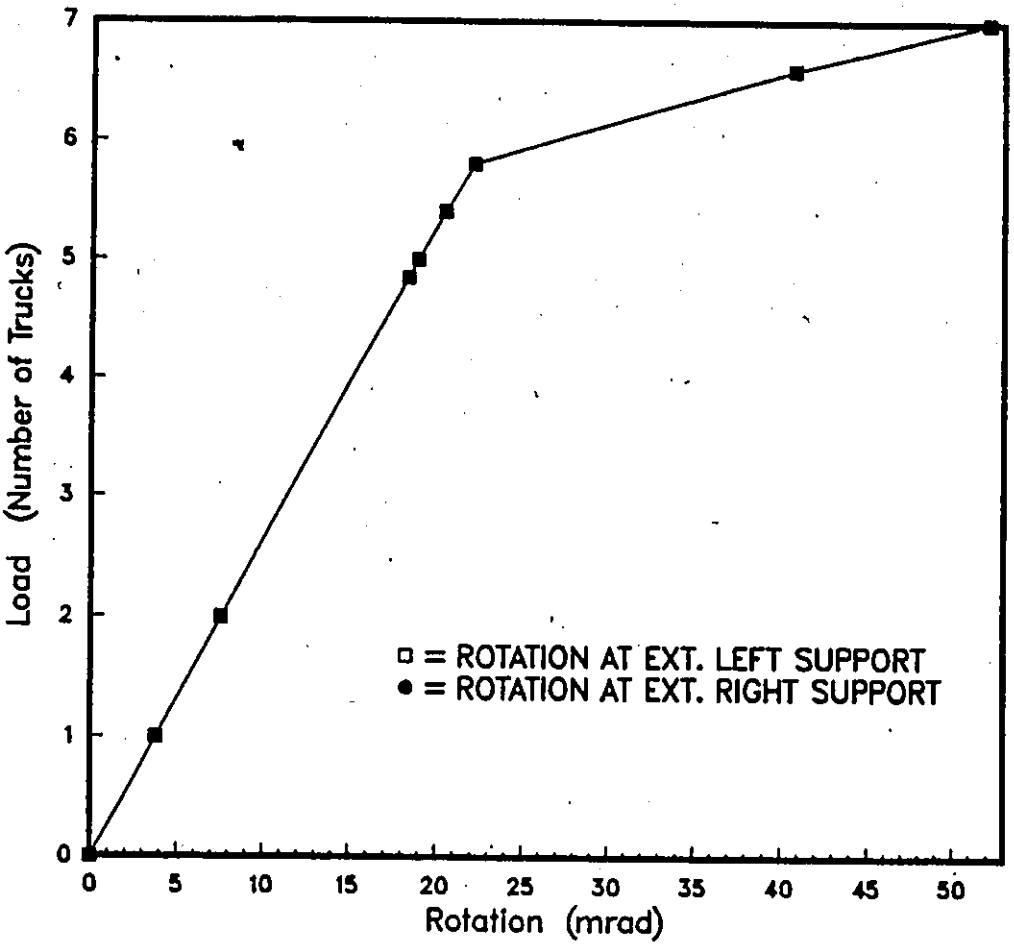

Figure 6.23: Load vs Ext. Support Rotation Curve for CBGB-3N

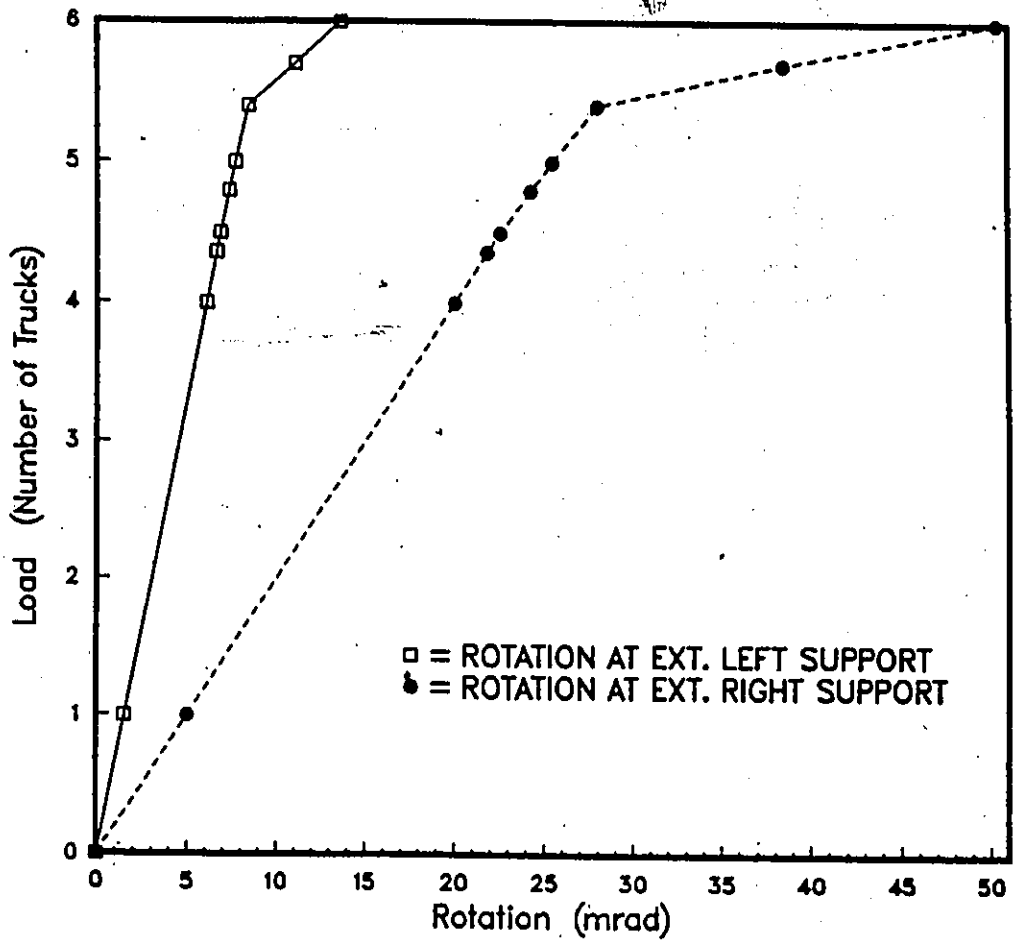

Figure 6.24: Load vs Ext. Support Rotation Curve for CBGB-3P

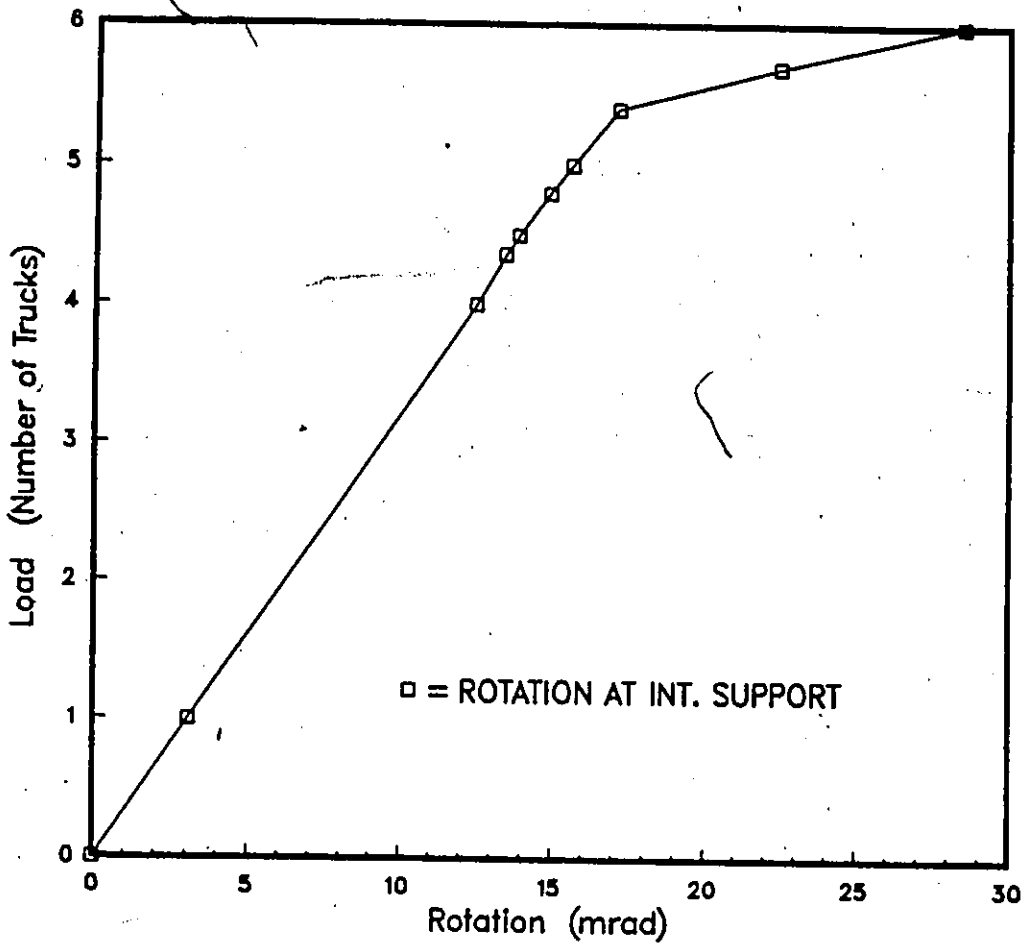

Figure 6.25: Load vs Int. Support Rotation Curve for CBGB-3P

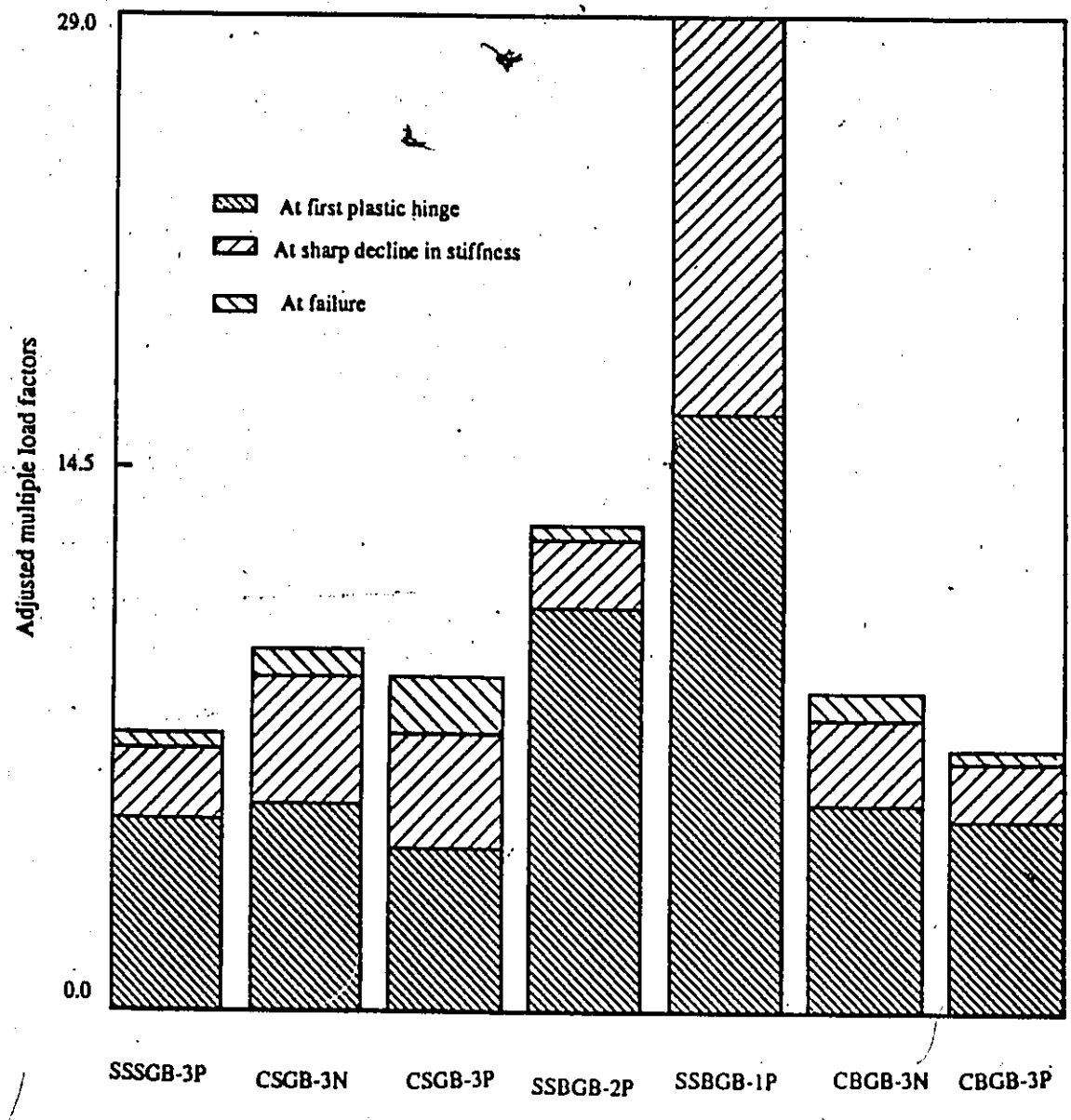

Figure 6.26: Adjusted Multiple Load Factors

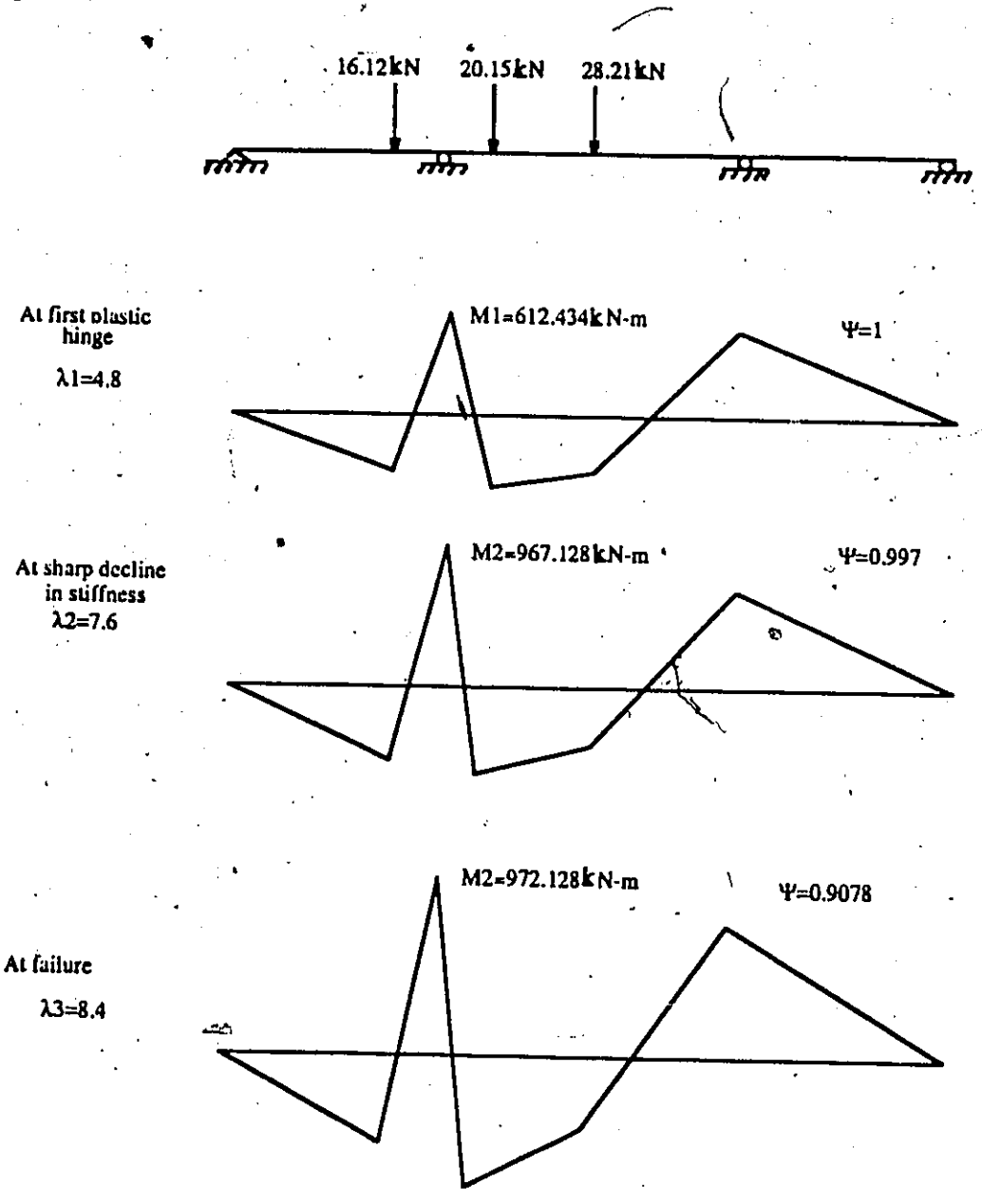

Figure 6.27: Longitudinal Distribution of the Load in CSGB-3N

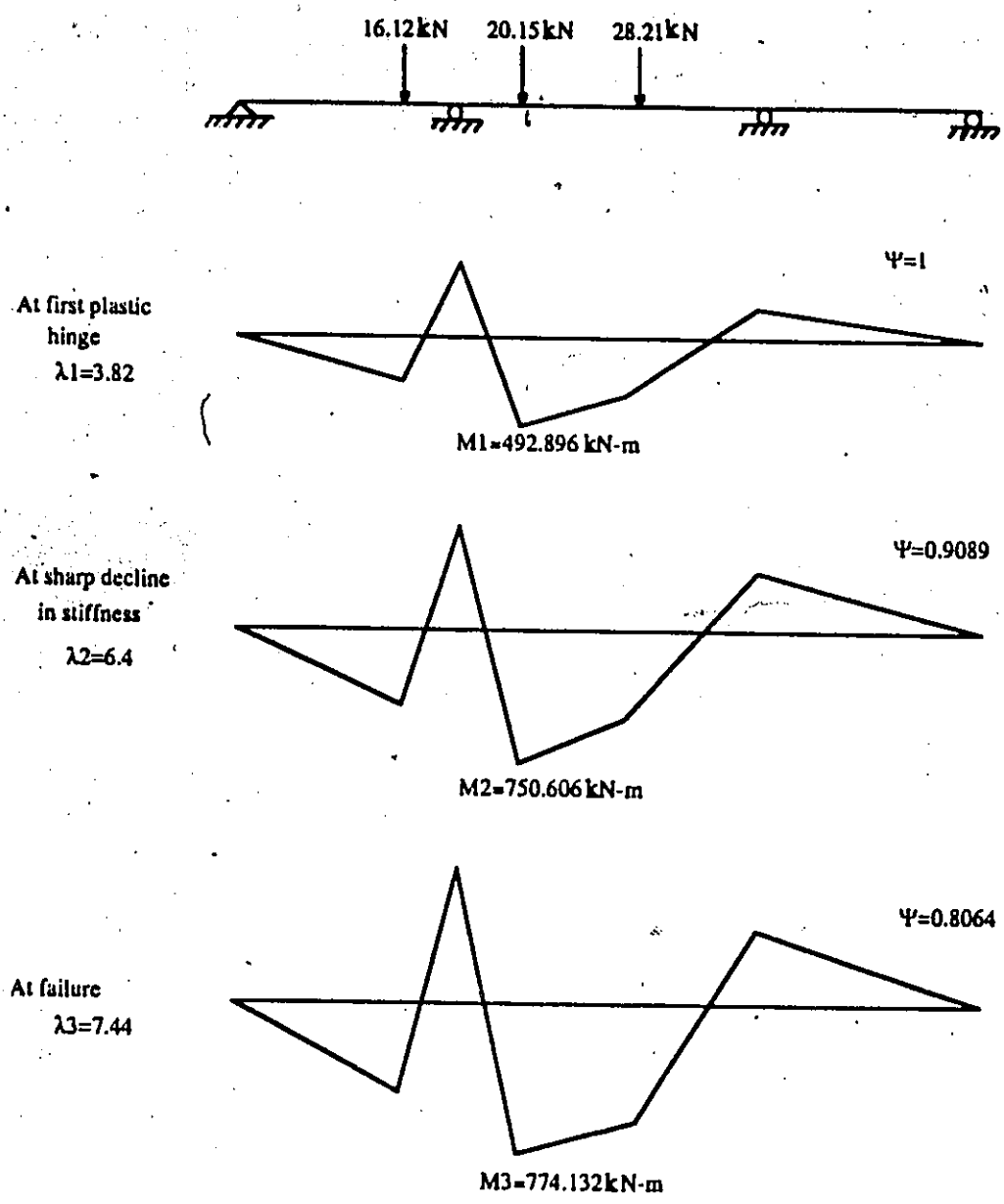

Figure 6.28: Longitudinal Distribution of the Load in CSGB-3P

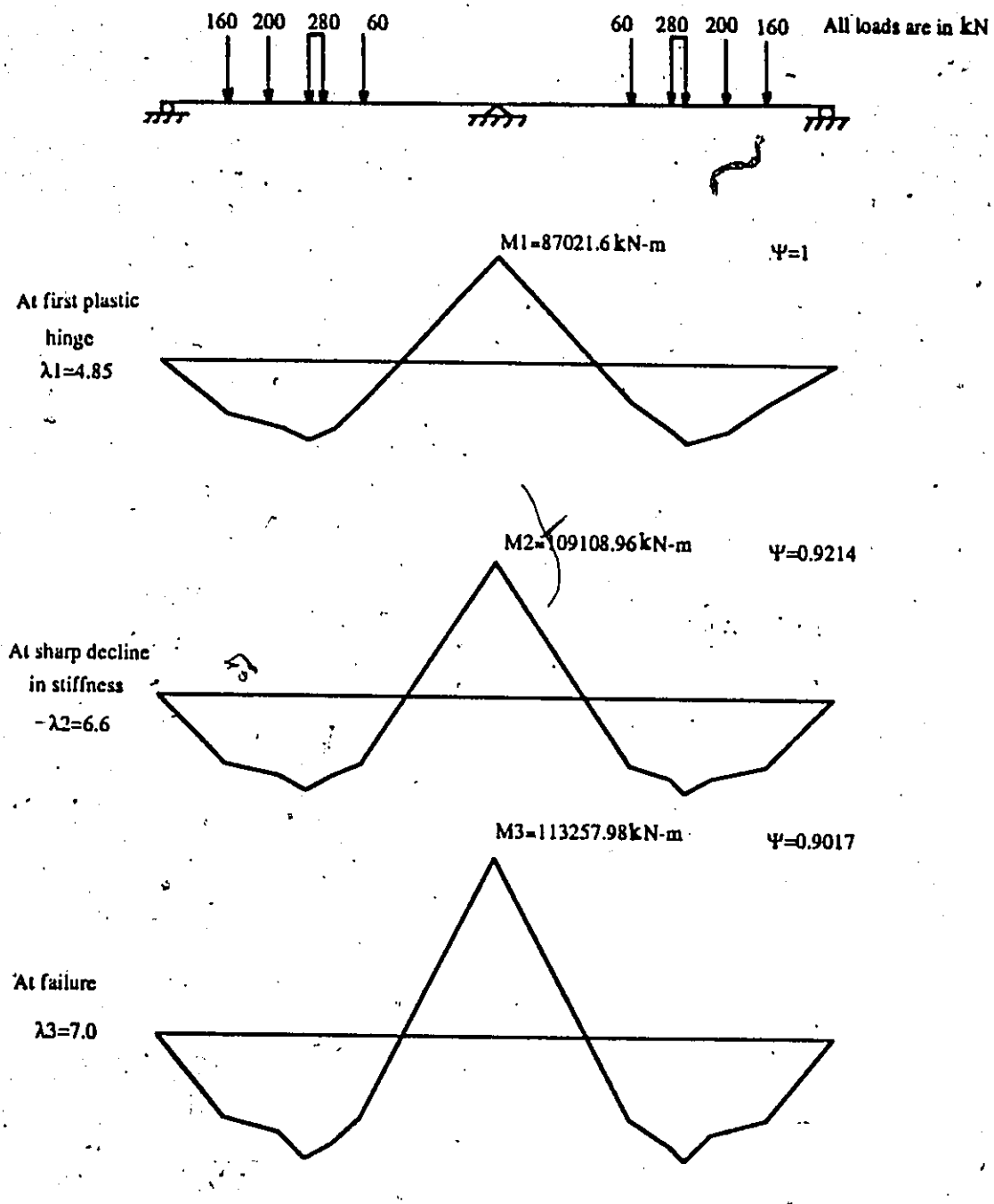

Figure 6.29: Longitudinal Distribution of the Load in CBGB-3N

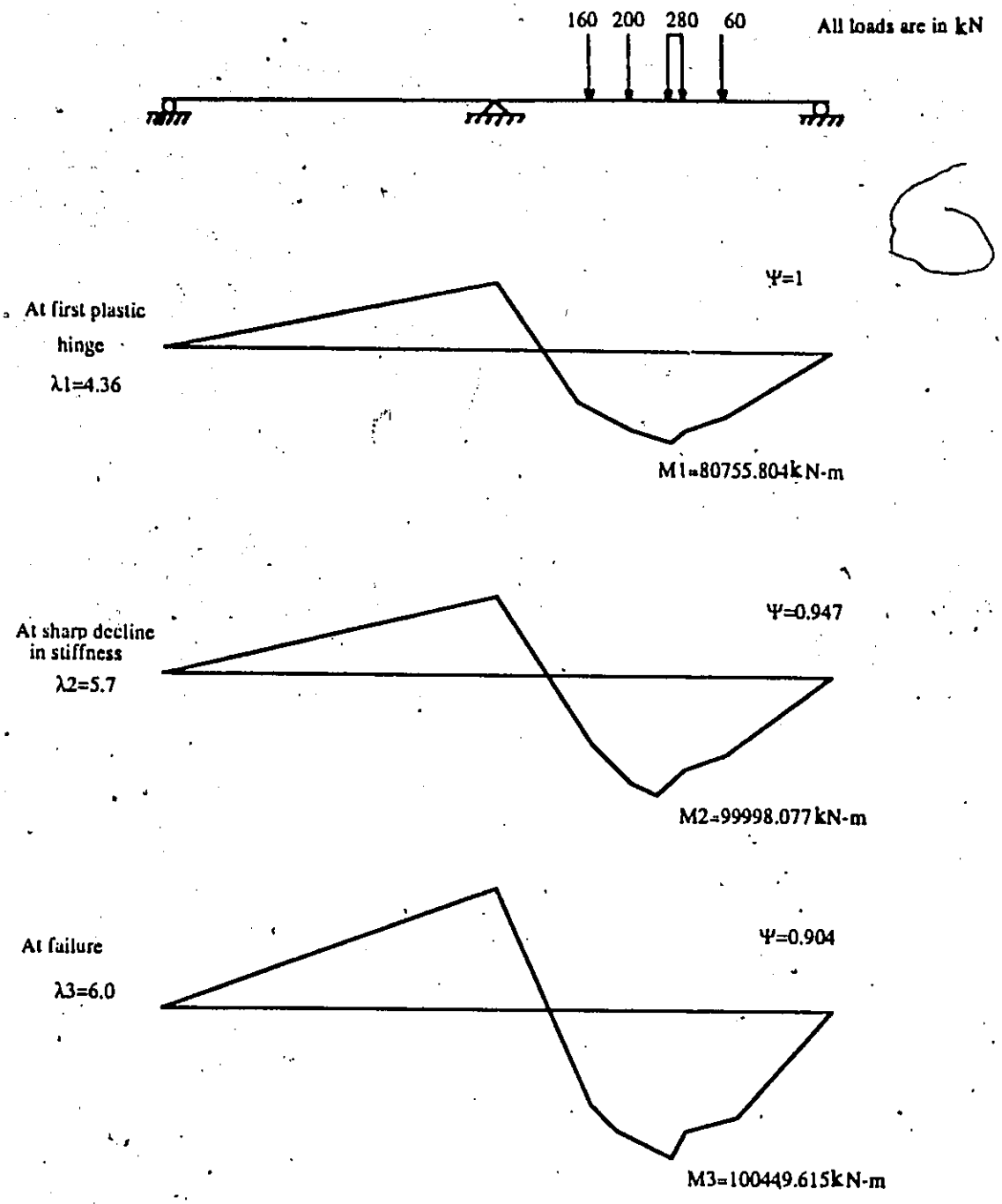

Figure 6.30: Longitudinal Distribution of the Load in CBGB-3P

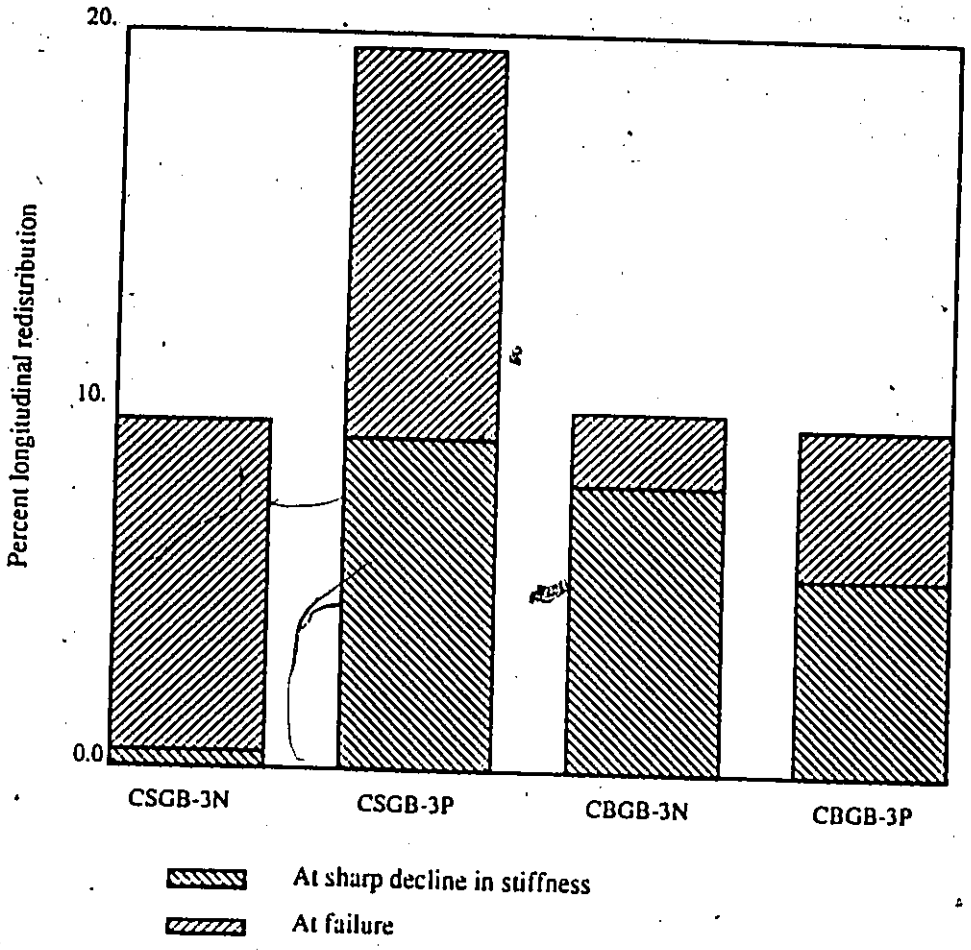

Figure 6.31: Percent Longitudinal Distribution Graphically

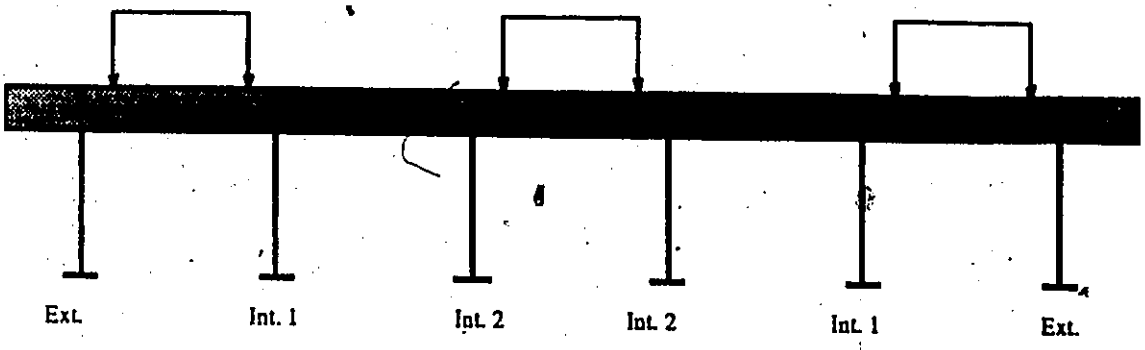

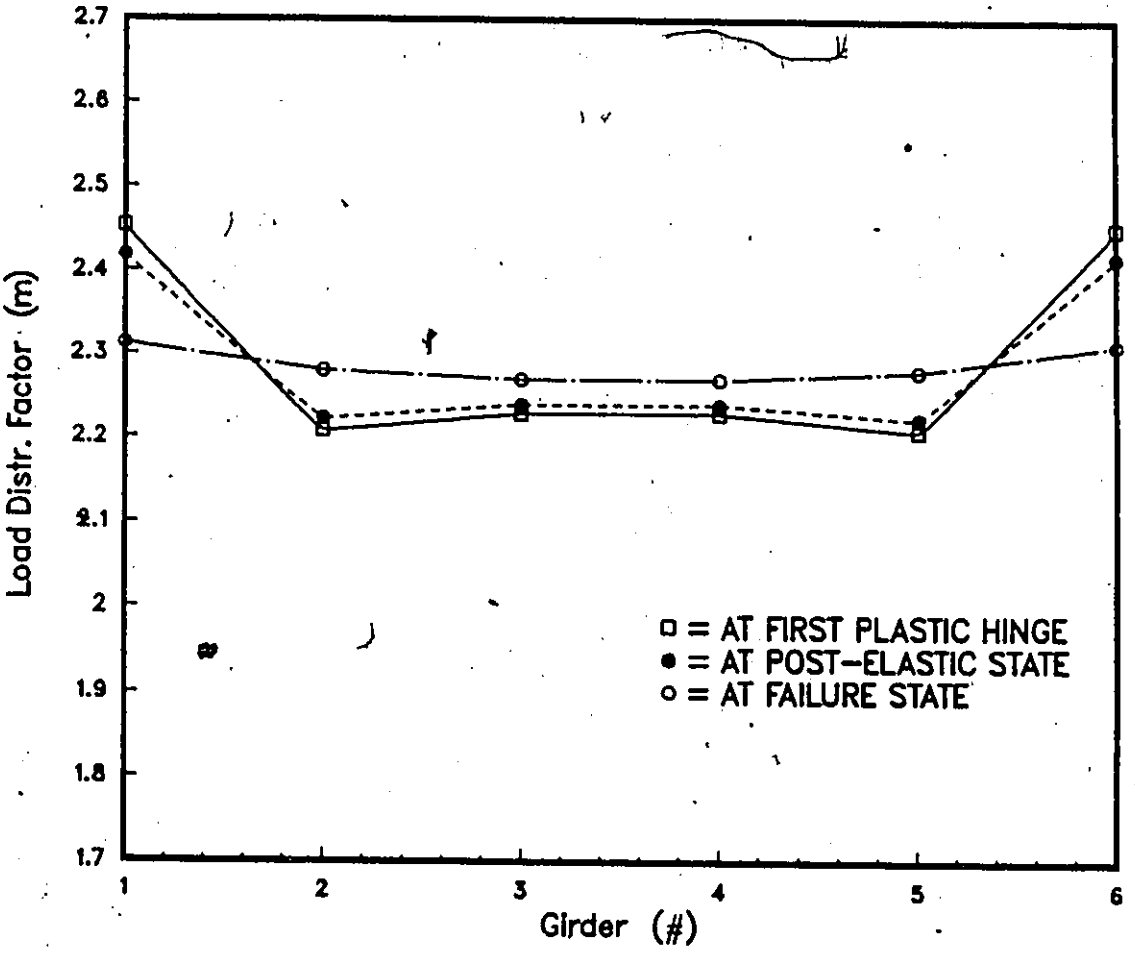

Figure 6.32: Transverse Distribution of the Moment in SSSGB-3P

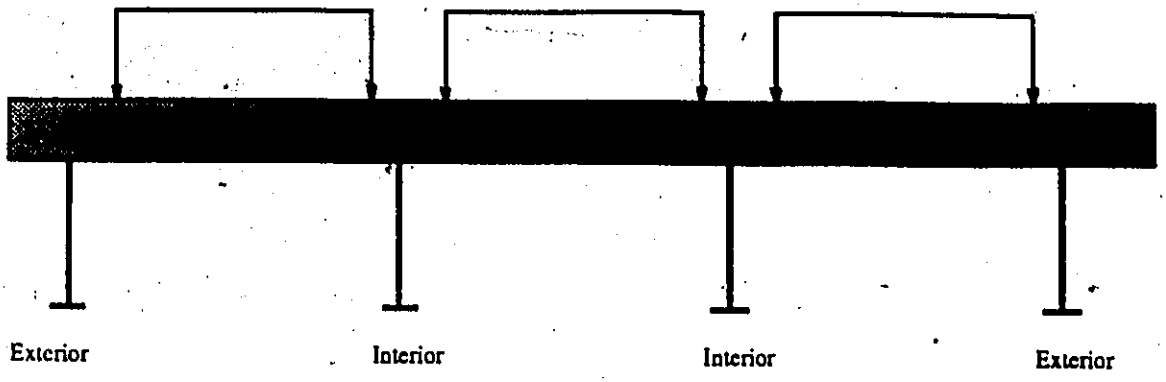

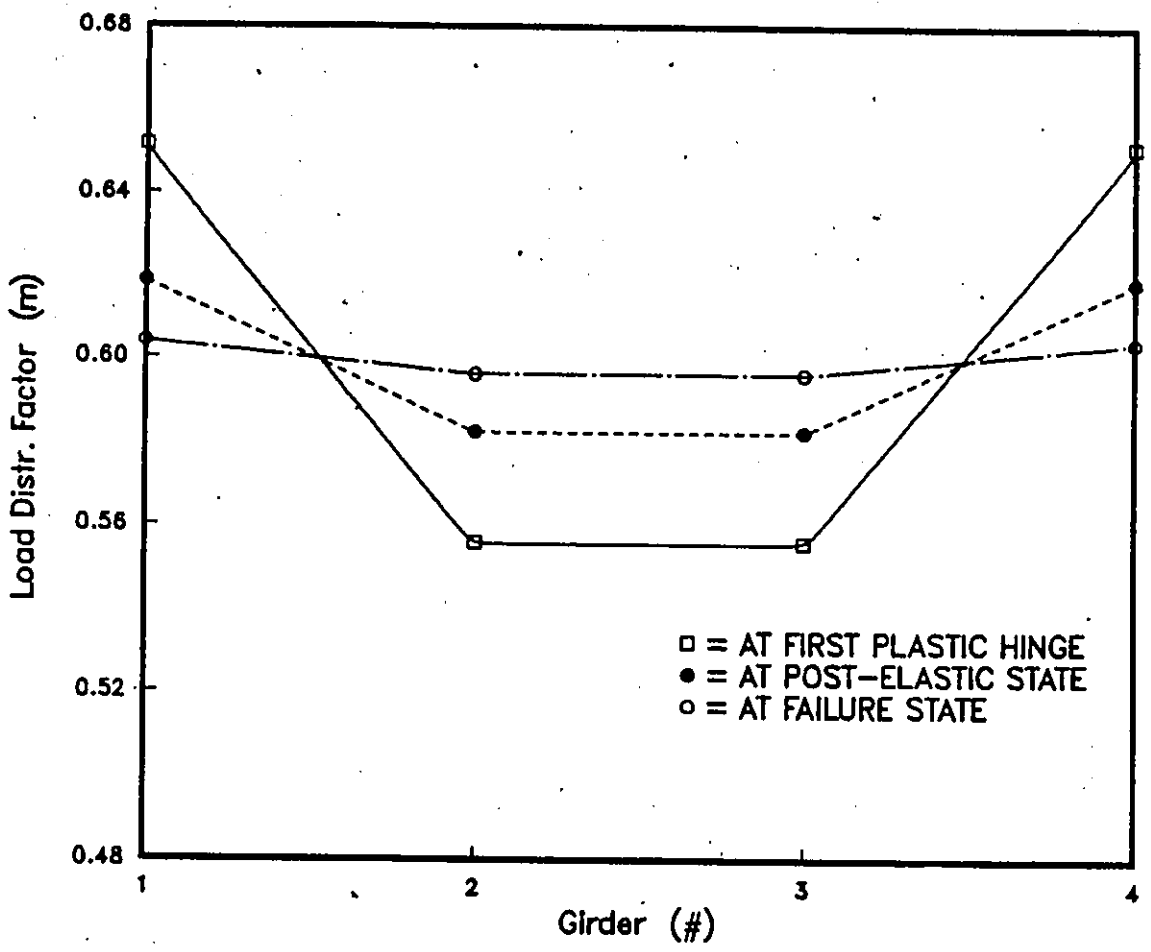

Figure 6.33: Transverse Distribution of the Moment in ¢SGB-3N

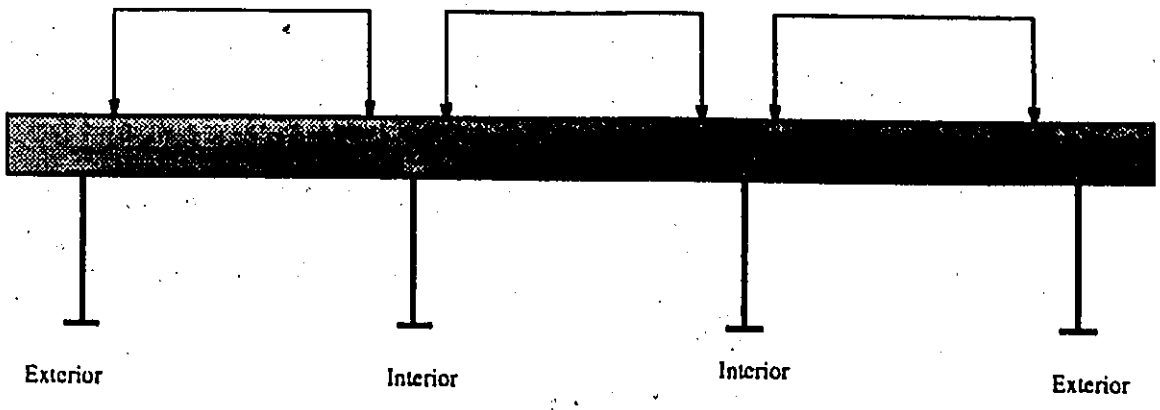

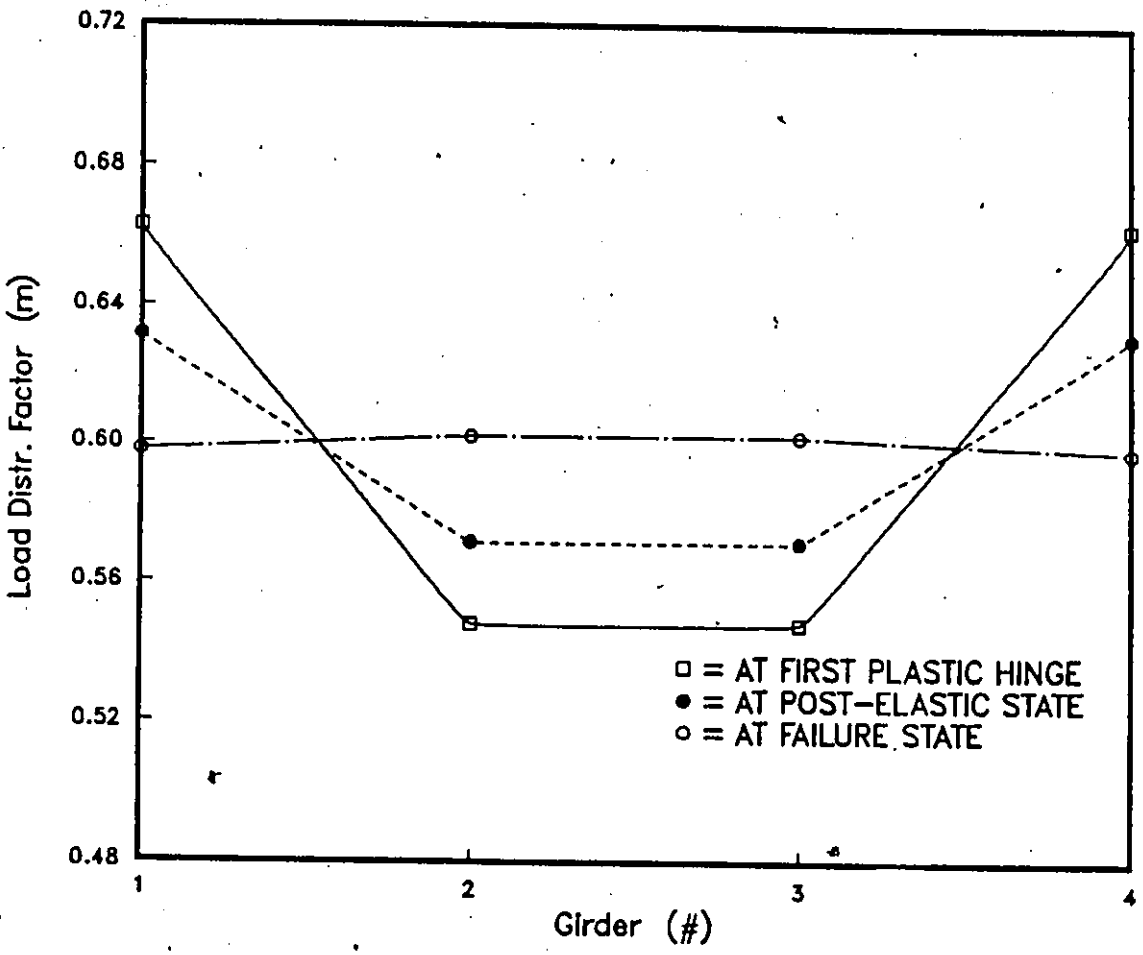

Figure 6.34: Transverse Distribution of the Moment in CSGB-3P

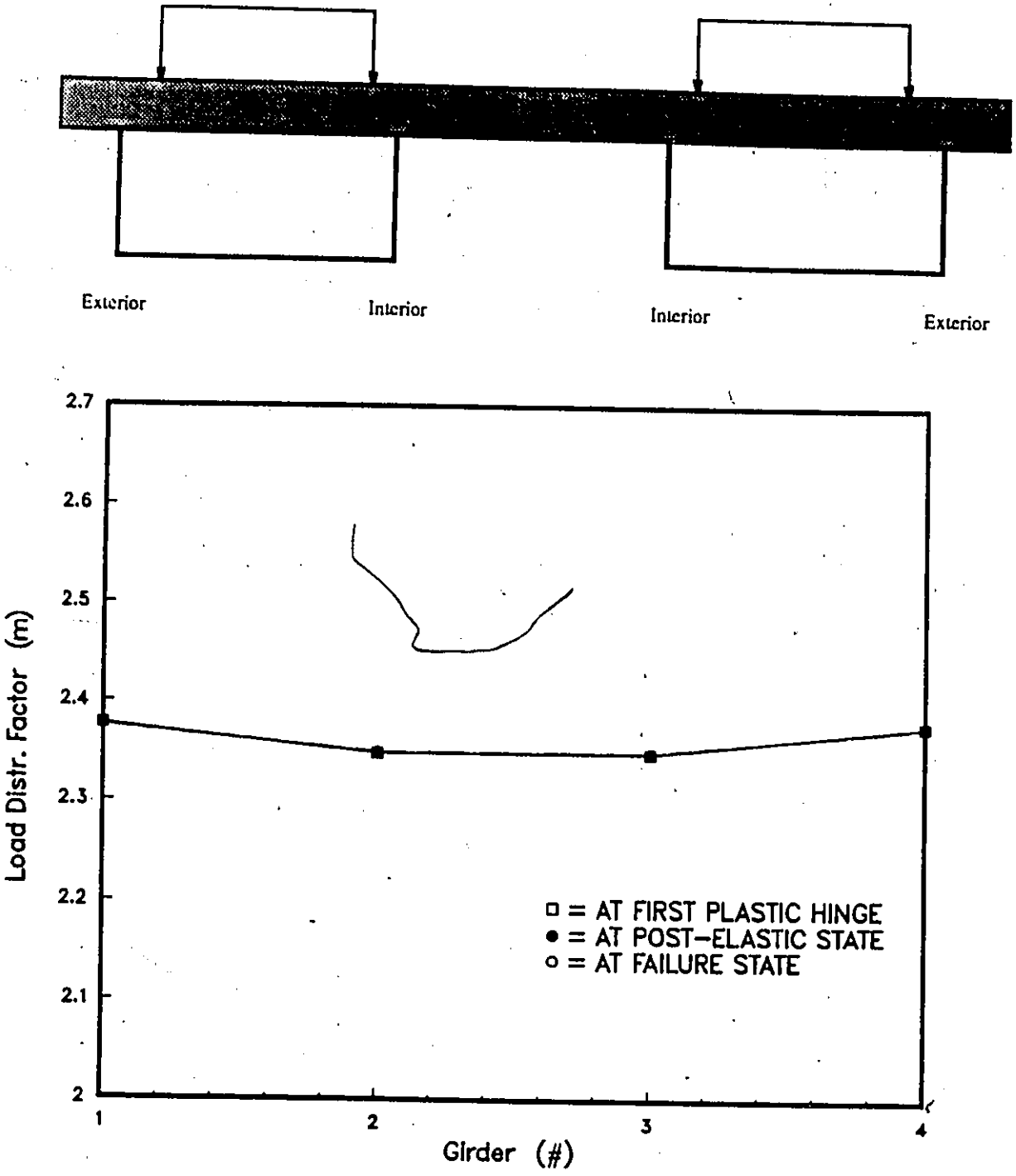

Figure 6.35: Transverse Distribution of the Moment in SSBGB-2P

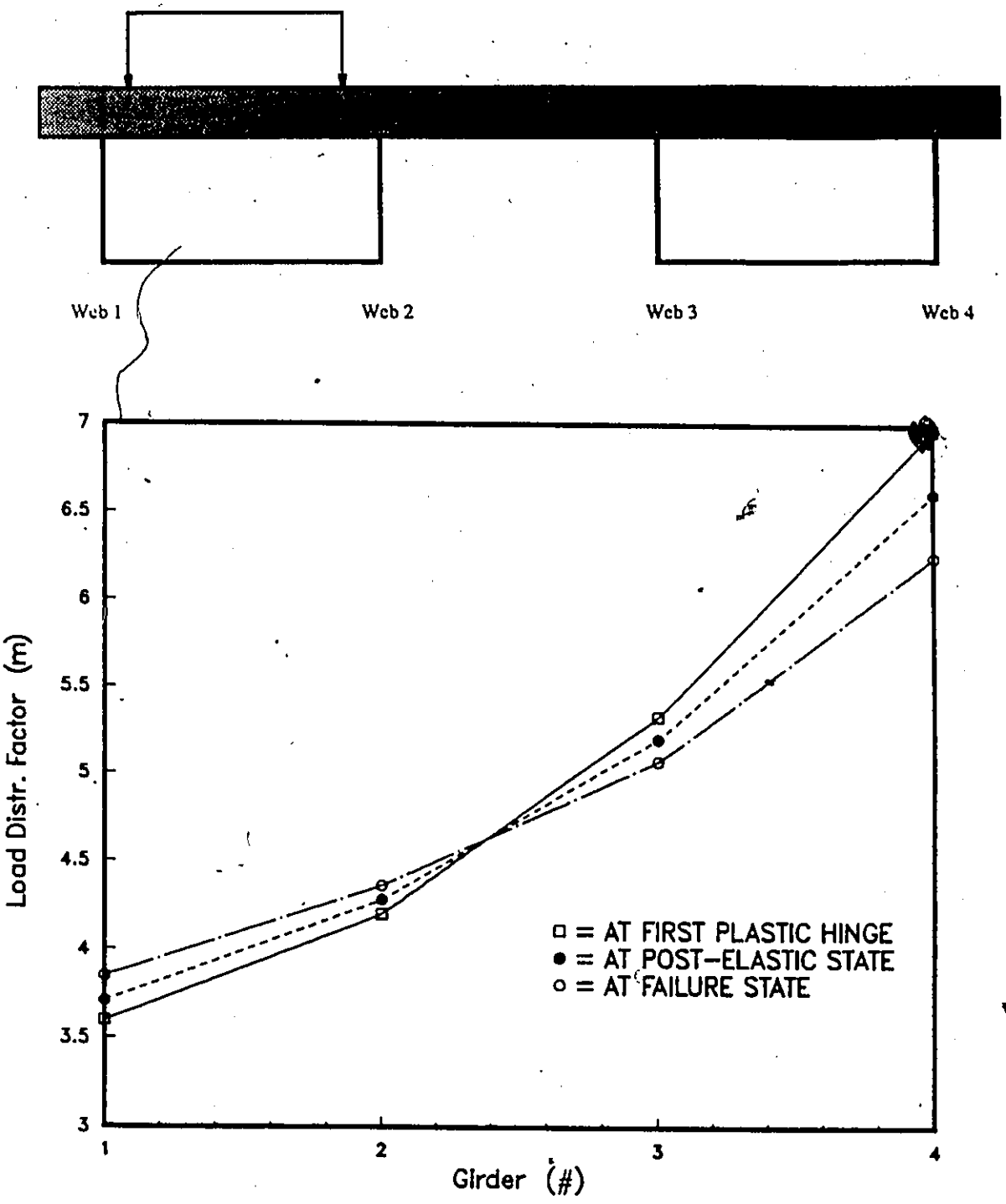

Figure 6.36: Transverse Distribution of the Moment in SSBGB-1P

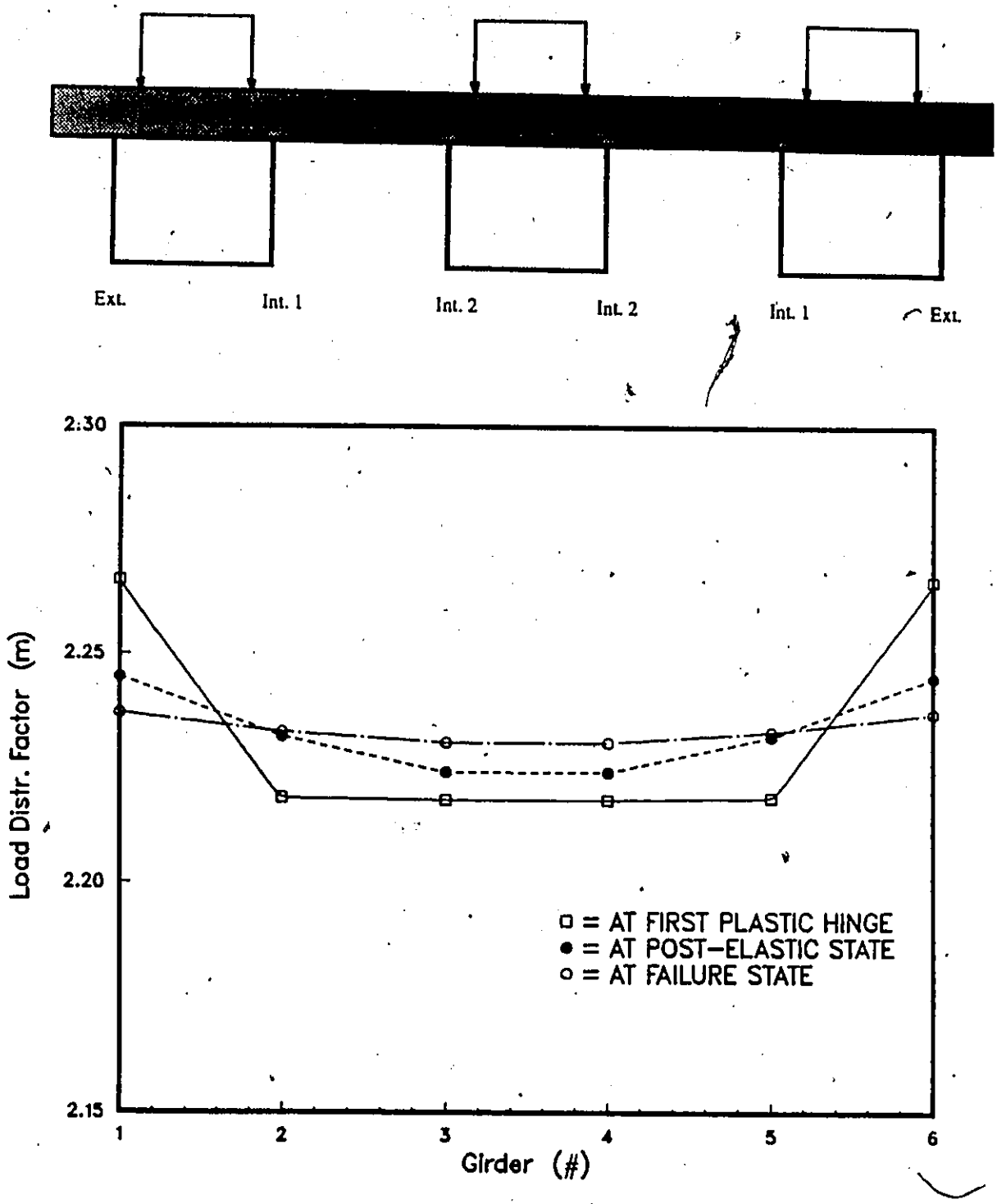

Figure 6.37: Transverse Distribution of the Moment in CBGB-3N

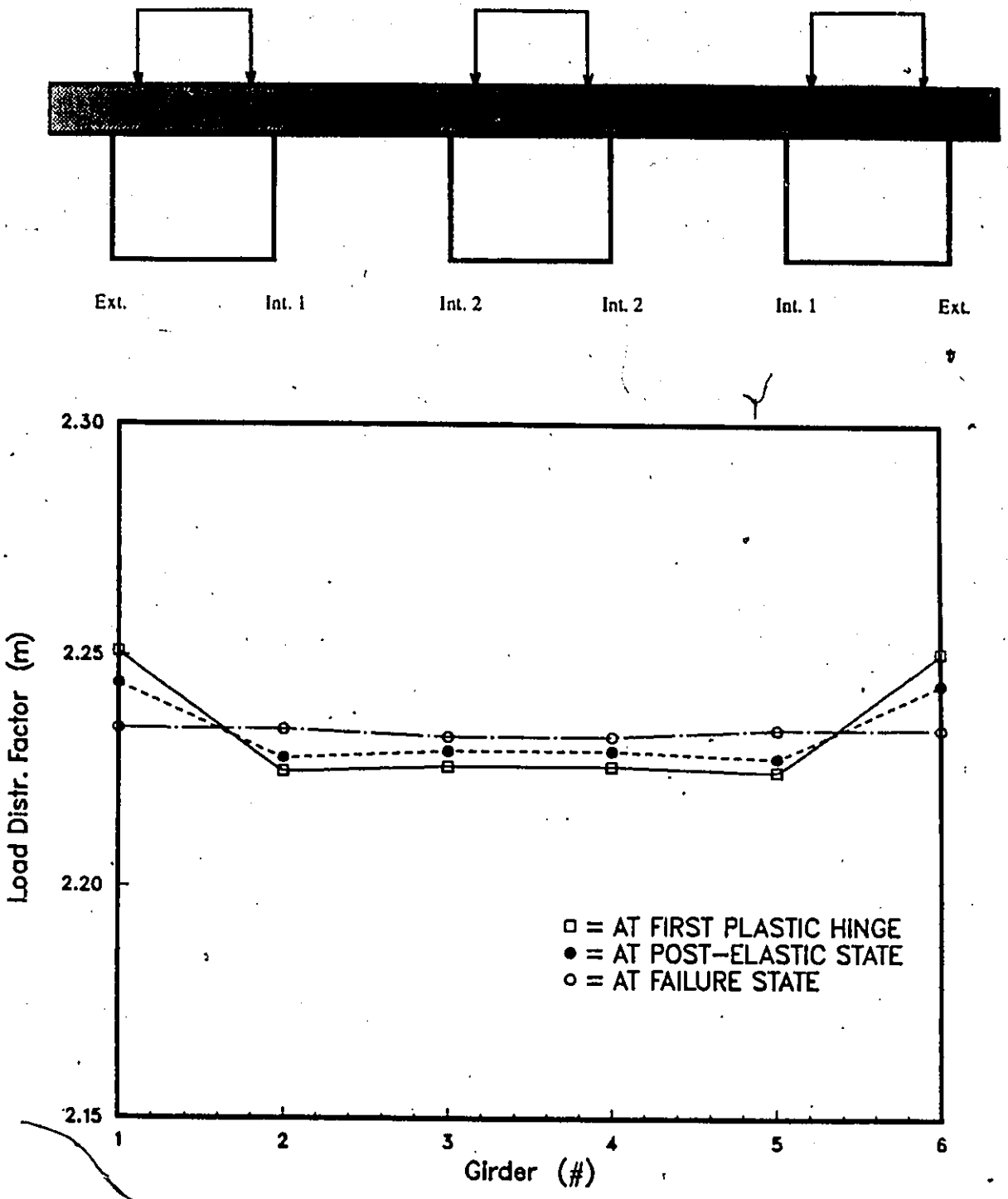

Figure 6.38: Transverse Distribution of the Moment in CBGB-3P

Table 6.1: Multiple Load Factors

	At elastic stage	At first plastic hinge	At sharp decline in stiffness	At failure
SSSGB-3P	1.00 (1.25)	4.15 (5.19)	5.80 (7.25)	6.20 (7.75)
CSGB-3N	1.00 (1.25)	4.80 (6.00)	7.60 (9.50)	8.40 (10.50)
CSGB-3P	1.00 (1.25)	3.82 (4.78)	6.40 (8.00)	7.44 (9.30)
SSBGB-2P	1.00 (1.11)	10.35 (11.50)	12.40 (13.78)	12.80 (14.22)
SSBGB-1P	1.00	17.35	29.00	N.A.
CBGB-3N	1.00 (1.25)	4.85 (6.06)	6.60 (8.25)	7.00 (8.75)
CBGB-3P	1.00 (1.25)	4.36 (5.45)	5.70 (7.13)	6.00 (7.50)

Table 6.2: Strength Reserves of the Analyzed Bridges

	$AMLF_{mcf}$	$AMLF_{mpf}$	SR
S.S. Slab-on-Girder	5.19	7.75	1.50
Cont. Slab-on-Girder	4.48	9.30	1.95
S.S. Box Girder	11.50	14.22	1.24
Cont. Box Girder	5.45	7.50	1.38

Table 6.3: Values of Ψ and $\%R$ in CSGB-3N

Multiple load factor	CSGB-3N	
	Ψ	$\%R$
4.8	1.000	0.00
5.2	1.005	-0.50
5.6	1.001	-0.10
7.2	1.019	-1.90
7.6	0.997	0.26
8.0	0.955	4.46
8.4	0.908	9.20

Table 6.4: Values of Ψ and $\%R$ in CSGB-3P

Multiple load factor	CSGB-3P	
	Ψ	$\%R$
3.82	1.000	0.00
4.00	0.998	0.19
4.60	0.995	0.50
5.20	0.991	0.90
5.80	0.978	2.17
6.40	0.909	9.10
7.00	0.848	15.20
7.44	0.806	19.40

Table 6.5: Values of Ψ and $\%R$ in CBGB-3N

Multiple load factor	CBGB-3N	
	Ψ	$\%R$
4.85	1.000	0.00
5.00	0.999	0.10
5.40	0.993	0.70
5.80	0.985	1.50
6.60	0.921	7.80
7.00	0.902	9.80

Table 6.6: Values of Ψ and $\%R$ in CSGB-3P

Multiple load factor	CSGB-3P	
	Ψ	$\%R$
4.36	1.000	0.00
4.50	0.999	0.10
4.80	0.996	0.40
5.00	0.994	0.60
5.40	0.989	1.10
5.70	0.947	5.20
6.00	0.904	9.60

Table 6.7: Moments and Load Distribution Factors for SSSGB-3P

Multiple load factor	Moment (kN-m)			D (m)		
	Ext.	Int.1	Int.2	Ext.	Int.1	Int.2
1.00	869.715	966.494	957.489	2.4536	2.2079	2.2287
4.00	3480.134	3866.896	3830.089	2.4532	2.2079	2.2290
4.15*	3609.780	4010.439	3973.372	2.4532	2.2081	2.2287
4.30	3741.127	4154.270	4116.201	2.4524	2.2085	2.2289
4.50	3917.962	4343.731	4304.174	2.4497	2.2096	2.2299
4.70	4096.497	4532.858	4491.948	2.4464	2.2109	2.2310
5.00	4482.344	4901.565	4864.752	2.4273	2.2198	2.2366
5.40	4912.313	5272.218	5236.322	2.3962	2.2326	2.2479
5.60	5087.214	5405.972	5380.458	2.3813	2.2409	2.2515
5.80	5293.759	5465.340	5480.350	2.3399	2.2664	2.2602
6.20**	5505.230	5583.322	5609.251	2.3127	2.2827	2.2698

[1] * At first plastic hinge

[2] ** All girders are yielded

Table 6.8: Moments and Load Distribution Factors for CSGB-3N

Multiple load factor	Moment (kN.m)		D (m)	
	Exterior	Interior	Exterior	Interior
1.00	28.986	34.970	0.6619	0.5487
4.00	115.948	139.881	0.6619	0.5487
4.80*	140.980	165.237	0.6516	0.5559
5.20	155.165	178.360	0.6448	0.5610
5.60	169.955	187.818	0.6315	0.5715
7.20	233.442	248.078	0.6188	0.5823
7.60	236.732	246.832	0.6128	0.5848
8.00	242.189	245.404	0.6039	0.5961
8.40**	245.901	240.585	0.5935	0.6066

Table 6.9: Moments and Load Distribution Factors for CSGB-3P

Multiple load factor	Moment (kN.m)		D (m)	
	Exterior	Interior	Exterior	Interior
1.00	29.185	35.317	0.6630	0.5479
2.00	58.371	70.635	0.6630	0.5479
3.82*	111.525	134.923	0.6630	0.5479
4.00	116.726	140.844	0.6620	0.5486
4.60	134.573	160.657	0.6581	0.5513
5.20	153.633	178.901	0.6493	0.5576
5.80	173.933	192.168	0.6315	0.5715
6.40	184.576	190.727	0.6100	0.5903
7.00	192.116	190.800	0.5979	0.6020
7.44**	195.599	191.467	0.5937	0.6065

Table 6.10: Moments and Load Distribution Factors for SSBGB-2P

Multiple load factor	Moment (kN.m)		D (m)	
	Exterior	Interior	Exterior	Interior
1.00	3180.002	3219.349	2.3773	2.3482
10.00	31800.020	32193.490	2.3773	2.3482
10.35*	32912.123	33319.930	2.3773	2.3482
10.60	33698.248	34115.850	2.3773	2.3482
11.20	35556.511	36000.328	2.3774	2.3481
11.60	37425.607	37954.103	2.3794	2.3462
12.00	38595.571	39117.441	2.3787	2.3469
12.40	40459.880	40948.991	2.3763	2.3491
12.80**	41609.324	42084.643	2.3761	2.3492

Table 6.11: Moments and Load distribution Factors for SSBGB-1P

Multiple load factor	Moment (kN-m)				D (m)			
	Web1	Web2	Web3	Web4	Web1	Web2	Web3	Web4
10.00	19680.36	18022.74	14196.76	10185.46	3.6058	4.1999	5.3318	6.9671
16.00	31501.76	28831.56	22716.94	16290.12	3.6044	4.2008	5.3315	6.9702
17.35[†]	34165.17	31267.99	24629.96	17665.73	3.6040	4.2006	5.3326	6.9702
19.00	37458.45	34101.65	27010.16	19360.81	3.5985	4.2163	5.3232	6.9623
20.00	39285.79	35768.91	28527.53	20504.35	3.6102	4.2295	5.3032	6.9171
21.00	40256.19	37171.26	30636.54	22571.50	3.7091	4.2848	5.1987	6.6152
22.00	41568.71	38589.11	32684.41	24271.38	3.7702	4.3320	5.1146	6.4570
23.00	42938.58	40162.36	34324.32	25801.93	3.8126	4.3479	5.0874	6.3448
24.00	44353.25	41854.63	35946.78	27344.50	3.8526	4.3548	5.0705	6.2491
25.00	46629.24	44399.31	37342.24	28641.93	3.8488	4.3115	5.1264	6.2658
29.00[††]	64139.85	51665.70	43506.68	34548.73	3.4547	4.5747	5.4326	6.4136

[3†] At first plastic hinge

[4††] At sharp decline in stiffness

Table 6.12: Moments and Load Distribution Factors for CBGB-3N

Multiple load factor	Moment (kN-m)			D (m)		
	Ext.	Int.1	Int.2	Ext.	Int.1	Int.2
1.00	3000.258	3071.351	3084.194	2.2726	2.2199	2.2107
2.00	6000.516	6142.702	6168.388	2.2726	2.2199	2.2107
4.85*	14552.107	14896.100	14956.281	2.2724	2.2199	2.2110
5.00	14991.632	15336.685	15391.378	2.2711	2.2200	2.2121
5.40	16110.746	16464.918	16519.291	2.2693	2.2205	2.2132
5.80	17177.139	17547.337	17604.058	2.2686	2.2207	2.2136
6.60	18469.154	18576.954	18642.456	2.2449	2.2319	2.2240
7.00**	19240.034	19274.737	19295.856	2.2369	2.2329	2.2304

Table 6.13: Moments and Load Distribution Factors for CBGB-3P

Multiple load factor	Moment (kN-m)			D (m)		
	Ext.	Int.1	Int.2	Ext.	Int.1	Int.2
1.00	3126.862	3163.784	3162.245	2.2509	2.2246	2.2257
4.36*	13633.305	13794.354	13787.503	2.2509	2.2246	2.2257
4.50	14062.945	14227.496	14210.578	2.2502	2.2242	2.2268
4.80	14952.616	15132.416	15110.398	2.2505	2.2238	2.2270
5.00	15545.623	15723.038	15704.907	2.2498	2.2244	2.2270
5.40	16722.997	16901.700	16882.666	2.2487	2.2249	2.2274
5.70	16933.721	17058.295	17046.529	2.2440	2.2276	2.2291
6.00**	17086.326	17087.941	17100.089	2.2340	2.2338	2.2322

Chapter 7

CONCLUSIONS AND RECOMMENDATIONS

7.1 General

An extensive analytical work was undertaken to study the load distribution characteristics of simply supported and continuous slab-on-girder and box girder composite bridges over the entire loading range up to failure.

A detailed literature review was conducted to establish the current state of the art. It was found out that with respect to load distribution at ultimate state there is a paucity of relevant material. This has led to the work described in this thesis.

In view of its versatility, the non-linear finite element was adopted as the

method of analysis. An existing program of analysis (ADINA) was used to determine the materially non-linear response of slab-on-girder and box girder bridges to overloading.

The conclusions made are strictly applicable to those bridge configurations analyzed. Since only a few variations of a limited number of parameters were included, no design recommendations as such will be made. It is hoped that the findings of this study will be incorporated in a comprehensive procedure for the plastic analysis of slab-on-girder and box girder bridges.

7.2 Conclusions

1. The non-linear finite element method is an accurate and powerful tool for the analysis of slab-on-girder and box girder composite bridges, including the study of their load distribution characteristics.

2. The load distribution characteristics of these types of bridges are affected by many parameters, including the position of the truck on the bridge and the number of lanes loaded.

3. The load distribution characteristics improve with increased level of loading. The best load sharing generally occurs just prior to failure. At this stage all the girders or box girders attain their ultimate capacity.

4. The governing case for design purposes is generally a symmetrical one in which all lanes are loaded.

5. Significant reserves of capacity can exist between that based on an elastic strength calculation for the most heavily loaded member and collapse of the entire structure.

6. The magnitude of that reserve capacity for a specific positioning of the design vehicle will depend on the amount of longitudinal redistribution which is required before a collapse mechanism is complete.

7. The amount of longitudinal redistribution that will be required depends on the longitudinal position of the vehicle and the relative capacities of the bridge in sagging and hogging bending sections. These determine the ratios of the live load flexural capacities to the elastic live load bending moments at the critical sagging and hogging sections. The more equal these values are, the less longitudinal redistribution will be required.

8. The patterns of transverse redistribution are directly related to those of longitudinal redistribution, and therefore the vehicle position. Where a large amount of longitudinal redistribution from the hogging to the sagging region is required, the hogging moments will be redistributed transversely before any significant redistribution of the sagging moments occurs. At a post-elastic stage prior to collapse, different transverse load distribution would apply in the two regions. In the sagging, only a marginal improvement in transverse distribution was observed at any of the critical post-elastic stages prior to the actual collapse, and possibly a marginal decline in the early stages. Where little or no longitudinal redistribution is possible, the transverse redistribution of both the sagging and hogging moments occurs at a similar rate. Sim-

ilar transverse load distribution would apply in both regions. Prior to collapse, only marginal improvements in transverse distribution were observed. At the formation of a global collapse mechanism, for any longitudinal position of the vehicles, the transverse distribution will equal the relatively uniform distribution of live load flexural capacities at all sections.

9. A reduced number of lanes loaded should not govern the design at ULS, regardless of whether capacity is based on elastic strength calculations, plastic collapse, or any intermediate post-elastic stage.

7.3 Recommendations For Future Work

The current study was restricted to straight simply supported and continuous concrete slab on compact steel girders or box girders bridges. Although such bridges constitute a large number of actual bridges, it is recommended to study the load distribution properties of

- Skew bridges
- Curved bridges
- Bridges with non-compact sections
- Composite concrete slab-on-girder or box girder bridges.

Additional experimental studies are required to better understand the post-elastic behavior and capacities of certain composite bridge components.

Further analytical work should be undertaken to consider the effect of the following in more details:

- The effect of different transverse positions of the design vehicle on the redistribution patterns and the reserve capacities.
- Additional variations in the bridge configurations considered, including the number and spacing of longitudinal members, the ratio of the width to the span length, and relative rigidity of slab to girder or box girder.

We restricted our attention in this thesis to the longitudinal moments. It may also be interesting to investigate the longitudinal shear and transverse bending moment in the slab. These are not, however, generally as important as longitudinal moments.

Bibliography

[1] *ADINA-IN-Users mgnual,* Report AE 84-5, ADINA Engineering, December 1984.

[2] *ADINA-Theory and modelling guide,* Report AE 84-5, ADINA Engineering, December 1984.

[3] American Association of Highway and Transportation Officials (AASHTO), *Standard specification for highway bridges,* 13^{th}, Washington D.C., 1983.

[4] Bakht, B., Cheung, M.S., and Aziz, T.S., *Application of a simplified method of calculating longitudinal moments to the Ontario highway bridge design code,* Canadian Journal of Civil Engineering, Vol. 6, pp. 36-50, 1979.

[5] Bakht, B., Jaeger, L.G., and Cheung, M.S., *Cellular and voided slab bridges,* American Society of Civil Engineers, Vol. 107, No. ST9, pp. 1797-1813, 1981.

[6] Bakht, B., and Jaeger, L.G., *Effect of vehicle eccentricity on longitudinal moments in bridges,* Canadian Journal of Civil Engineering, Vol. 10, pp. 582-599, 1983.

[7] Bakht, B., and Jaeger, L.G., *Bridge analysis simplified,* McGraw-Hill, New York, 1985.

[8] Bathe, K.J., *Finite element procedures in engineering analysis,* Prentice-Hall, Inc., Englewood Cliffs, New Jersey, 1982.

[9] Botzler, P.W., and Colville, J., *Continuous composite bridge model tests,* American Society of Civil Engineers, Vol. 105, No. ST9, pp. 1741-1755, 1979.

[10] Canadian Standards Association, *Code for design of highway bridges (CAN3-S6-M78),* Rexdale, Canada, 1978.

[11] Chapman, J.C., and Balakrishnan, S, *Experiments on composite beams,* the Structural Engineer, Vol. 42, pp. 369-383, 1964.

[12] Cheung, M.S., Bakht, B., and Jaeger, L.G., *Analysis of box girder bridges by grillage and orthotropic plate methods,* Canadian Journal of Civil Engineering, Vol. 9, No. 4, pp. 595-601, 1982.

[13] Cheung, M.S., Gardner, N.J., and Ng, S.F., *Load distribution characteristics of slab-on-girder bridges at ultimate,* Second International Conference on Short and Medium Span Bridges, Proceedings, Vol. 2, pp. 461-485, Ottawa, 1986.

[14] Cusens, A.R., and Pama, R.P., *Bridge deck analysis,* John Widey and sons, London, 1975.

[15] Hambley , E.C., *Bridge deck behavior,* Chapman and Hall, London, 1976.

[16] Hardy, C, *Method of elastic moment distribution,* Publications, 1932.

[17] Heins, C.P., and Looney, C.T.G., *Bridge analysis using orthotropic plate theory,* American Society for Civil Engineers, Vol. 94, No. ST2, pp. 565-592, 1968.

[18] Heins, C.P., and Kerzweil, B.S., *Analytical study of different failure mechanisms in slab-on-girder bridges,* American Society for Civil Engineers, Vol. 97, No. ST4, pp. 1010-1043, 1971.

[19] Heins, C.P., and Kuo, T.C., *The ultimate live load distribution factors for bridges,* American Society for Civil Engineers, Vol. 101, No. ST7, pp. 1481-1496, 1975.

[20] Heins, C.P., *LDF criteria for composite steel I-beam bridges,* American Society of Civil Engineers, Vol. 106, No. ST11, pp. 2297-2312, 1980.

[21] Jategaontar, R., Jaeger, L.G., and Cheung, M.S., *Bridge analysis using finite elements,* Canadian Society of Civil Engineering, 1985.

[22] Kennedy, J.B., and Grace, N.F., *Load distribution in continuous composite bridges,* Canadian Journal of Civil Engineering, Vol. 10, pp. 384-395, 1983.

[23] Lash, S.D., and Nagaraja, R., *The ultimate load capacity of beam and slab bridges,* Department of Highway Report No. RR-159, Department of Highway, Ontario, 1970.

[24] Lowe, P.A., and Flint, A.R., *Prediction of collapse loading for composite highway bridges,* Institution of Civil Engineers, Part 2, Vol. 48, pp. 645-659, 1971.

[25] MacGregor, J.E., *Safety and limit states for reinforced concrete,* Canadian Journal of Civil Engineering, Vol. 3, No. 4, pp. 484-513, 1976.

[26] Maheu, J.M., *Redistribution of moments in slab-on-girder bridges,* M.A.Sc. Thesis, University of Toronto, 1987.

[27] Mattock, A.H., and Johnston, S.B., *Behavior under load of composite box girder bridges,* American Society of Civil Engineers, Vol. 94, No. ST10, pp. 2351-2370, 1968.

[28] MTC, *Ontario highway bridge design code,* Downsview, 1983.

[29] Newmark, N.M., *A distribution procedure for the analysis of slabs continuous over flexible beams,* University of Illinois, Eng. Exp. Sta., Bul. 304, 1938.

[30] Nofal, M.E., *Inelastic load distribution of composite concrete-steel slab-on-girder bridges,* M.A.Sc. Thesis, University of Carleton, 1988.

[31] Owen, D.R.J., and Hinton, E., *Finite element in plasticity,* Pineridge Press Limited, Swansea, U.K., 1980.

[32] Percy, R., *A design method for grillages,* Institution of Civil Engineering, Part 2, Vol. 23, pp. 409-422, 1962.

[33] Rowe, R.E., *Concrete bridge design,* C.R. Books, London, 1962.

[34] Scordelis, A.C., *Analysis of simply supported box girder bridges,* Report SESM66-17, University of California, Berkeley, 1966.

[35] Seible, F., and Scordelis, A.C., *Nonlinear behavior and failure of multicell reinforced concrete box girder bridges,* Canadian Journal of Civil Engineering, Vol. 11, pp. 411-422, 1984.

[36] Shanmugan, N.E., and Evans, H.R., *A grillage analysis of the non-linear and ultimate load behavior of cellular structures under bending loads,* Institution of Civil Engineers, Part 2, Vol. 71, pp. 705-719, 1981.

[37] Shaw, R., *Limit analysis of grid frameworks,* American Society of Civil Engineers, Vol. 89, No. ST5, pp. 1-14, 1983.

[38] Slutter, R.G., and Driscoll, G.C., *Flexural strength of steel-concrete composite beams,* American Society of Civil Engineers, Vol. 91, No. ST2, pp. 71-99, 1965.

[39] Tharmabala, T., *Nonlinear analysis of grid system,* Canadian Journal of Civil Engineering Centennial Conference, Proceedings, Vol. 1, pp. 65-82, Montreal 1987.

[40] Walsh, R., *Limit analysis of grids including torsion,* Tr.I.E.Aust., Vol. CE12, No. 1, pp. 90-93, 1970.

[41] Wegmuller, A.W., *Overload behavior of composite steel-concrete bridges,* American Society of Civil Engineers, Vol. 103, No. ST9, pp. 1799-1819, 1977.

[42] Zienkiewicz, O.C., *The finite element method,* McGraw-Hill, U.K., 1978.

Appendix A

Calculation of Elastic Load Distribution Factors at ULS and SLS II

Table A.1: Values of D_d in the S.S. Slab-on-Girder Bridge

Parameter Notation	Parameter Value
L (meters)	18.28
$2b$ (meters)	13.72
S (meters)	2.36
NL (no units)	3
D_x (Newton-meters)	628.46×10^6
D_y (Newton-meters)	25.90×10^6
$D_{xy} = D_{yx}$ (Newton-meters)	22.00×10^6
$D_1 = D_2$ (Newton-meters)	38.85×10^5
α (no units)	0.203
θ (no units)	0.832
W_e (meters)	4.26
μ (no units)	1.00
$D_{ext.}$ (meters)	2.03
$D_{int.}$ (meters)	2.09
C_f (percent)	7.50
$D_{d,ext.}$ (meters)	2.18
$D_{d,int.}$ (meters)	2.25

Table A.2: Values of D_d in the S.S. Box Girder Bridge

Parameter Notation	Parameter Value
L (meters)	45.72
$2b$ (meters)	9.45
S (meters)	2.44
$N.L$ (no units)	2
D_x (Newton-meters)	12.24×10^9
D_{xy} (Newton-meters)	45.69×10^8
β (no units)	1.063
W_e (meters)	4.27
μ (no units)	1.00
D (meters)	2.10
C_f (percent)	16.00
D_d (meters)	2.44
α (no units)	2.000
θ (no units)	0.338
$D_{ext.}$ (meters)	2.05
$D_{int.}$ (meters)	2.10
C_f (percent)	20.00
$D_{d,ext.}$ (meters)	2.46
$D_{d,int.}$ (meters)	2.52

Table A.3: Values of D_d in the Cont. Box Girder Bridge for the Negative Regions

Parameter Notation	Parameter Value
L (meters)	21.60
$2b$ (meters)	13.40
S (meters)	2.28
NL (no units)	3
D_x (Newton-meters)	43.36×10^8
D_{xy} (Newton-meters)	21.10×10^8
β (no units)	2.790
W_e (meters)	4.45
μ (no units)	1.00
D (meters)	2.20
C_f (percent)	13.50
D_d (meters)	2.487
α (no units)	2.000
θ (no units)	0.888
$D_{ext.}$ (meters)	2.39
$D_{int.}$ (meters)	2.38
C_f (percent)	11.50
$D_{d,ext.}$ (meters)	2.665
$D_{d,int.}$ (meters)	2.654

Table A.4: Values of D_d in the Cont. Box Girder Bridge for the Positive Regions

Parameter Notation	Parameter Value
L (meters)	43.20
$2b$ (meters)	13.40
S (meters)	2.28
NL (no units)	3
D_x (Newton-meters)	43.36×10^8
D_{xy} (Newton-meters)	21.10×10^8
β (no units)	1.397
W_c (meters)	4.45
μ (no units)	1.00
D (meters)	2.15
C_f (percent)	16.00
D_d (meters)	2.494
α (no units)	2.000
θ (no units)	0.440
$D_{ext.}$ (meters)	2.57
$D_{int.}$ (meters)	2.50
C_f (percent)	15.00
$D_{d,ext.}$ (meters)	2.955
$D_{d,int.}$ (meters)	2.875

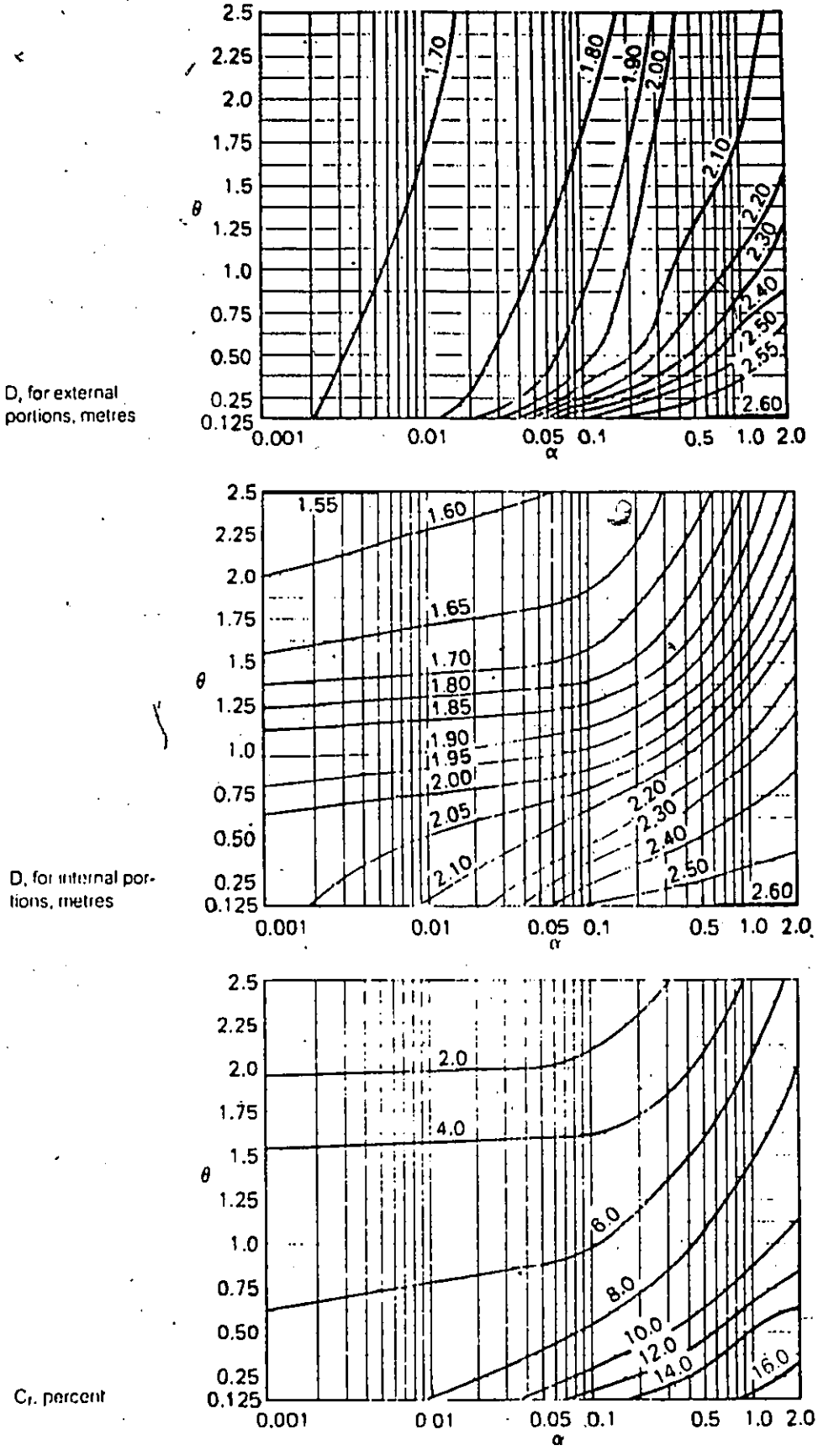

Figure A.1: D Values for Longitudinal Moments from OHBDC

Charts for ULS and SLS II Cases in Two-Lane Bridges **3 7.1.2.1(a)**

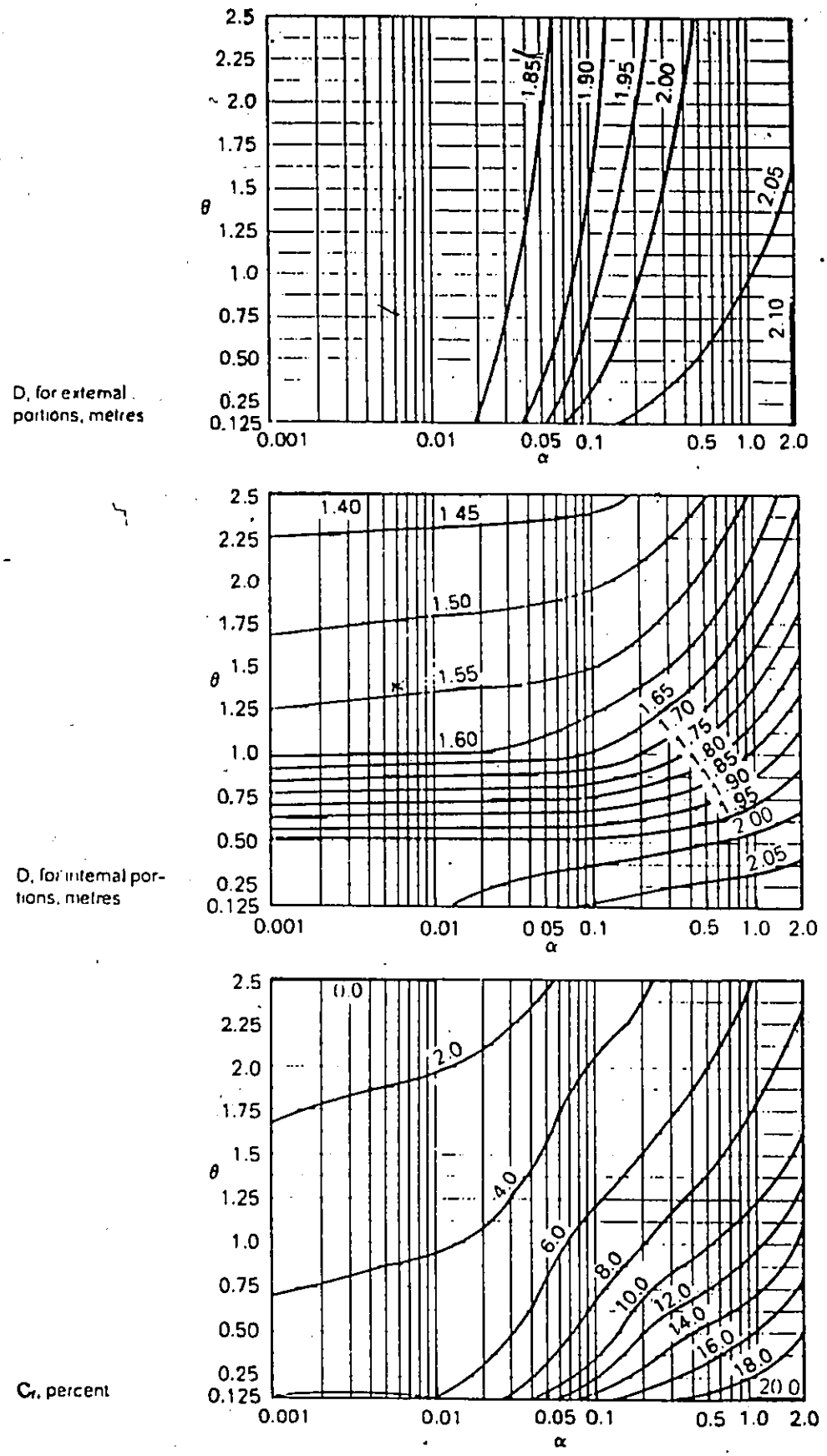

Figure A.2: D Values for Longitudinal Moments from OHBDC

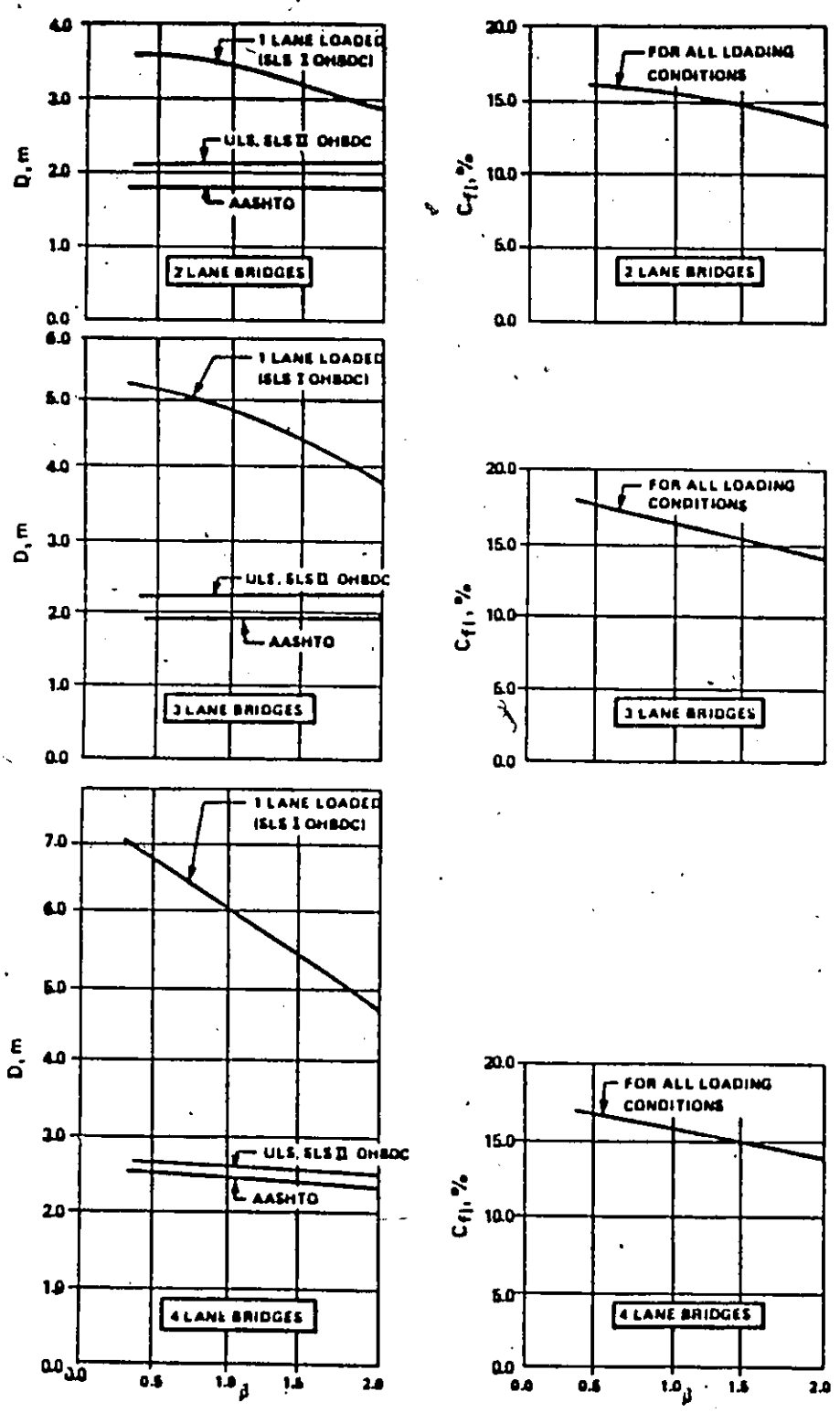

Figure A.3: D Values for Longitudinal Moments for Multispine Bridges

Appendix B

Sample Input Datasets for ADINA Analysis

```
'PLOTSIZE' 30.00 27.50'
DATABASE CREATE
HEAD 'Simply Supported Slab-on-Girder Bridge '
MASTER IDOF=000001 NSTEP=1
ITERATION METHOD=BFGS
STIFFNESS-STEPS
EQUILIBRIUM-STEPS
TIMEFUNCTION 1
0 0.
1 -1.0
PRINTOUT MINIMUM
PRINTNODES 1 899 1
COORDINATES
ENTRIES NODE X Y Z
*CONCRETE SLAB
1 -6860. 18300. 773.725
9 -6860. 12700. 773.725
13 -6860. 10300. 773.725
17 -6860. 8000. 773.725
21 -6860. 5600. 773.725
29 -6860. 0. 773.725
59 -5900. 18300. 773.725
87 -5900. 0. 773.725
349 0. 18300. 773.725
357 0. 12700. 773.725
361 0. 10300. 773.725
365 0. 8000. 773.725
369 0. 5600. 773.725
377 0. 0. 773.725
*BOTTOM STEEL FLANGES
465 -6079. 18300. 0.
473 -6079. 12700. 0.
477 -6079. 10300. 0.
481 -6079. 8000. 0.
485 -6079. 5600. 0.
493 -6079. 0. 0.
523 -5721. 18300. 0.
531 -5721. 12700. 0.
535 -5721. 10300. 0.
539 -5721. 8000. 0.
543 -5721. 5600. 0.
551 -5721. 0. 0.
639 -3719. 18300. 0.
647 -3719. 12700. 0.
651 -3719. 10300. 0.
655 -3719. 8000. 0.
659 -3719. 5600. 0.
667 -3719. 0. 0.
697 -3361. 18300. 0.
705 -3361. 12700. 0.
```

```
709 -3361. 10300. 0.
713 -3361. 8000. 0.
717 -3361. 5600. 0.
725 -3361. 0. 0.
813 -1359. 18300. 0.
821 -1359. 12700. 0.
825 -1359. 10300. 0.
829 -1359. 8000. 0.
833 -1359. 5600. 0.
841 -1359. 0. 0.
871 -1001. 18300. 0.
879 -1001. 12700. 0.
883 -1001. 10300. 0.
887 -1001. 8000. 0.
891 -1001. 5600. 0.
899 -1001. 0. 0.
LINE STRAIGHT 1 9 EL=4 MID=1 NF=2
LINE STRAIGHT 9 13 EL=2 MID=1 NF=10
LINE STRAIGHT 13 17 EL=2 MID=1 NF=14
LINE STRAIGHT 17 21 EL=2 MID=1 NF=18
LINE STRAIGHT 21 29 EL=4 MID=1 NF=22
LINE STRAIGHT 29 87 EL=1 MID=1 NF=58 NS=29
LINE STRAIGHT 87 377 EL=5 MID=1 NF=116 NS=29
LINE STRAIGHT 1 59 EL=1 MID=1 NF=30 NS=29
LINE STRAIGHT 59 349 EL=5 MID=1 NF=88 NS=29
LINE STRAIGHT 349 357 EL=4 MID=1 NF=350
LINE STRAIGHT 357 361 EL=2 MID=1 NF=358
LINE STRAIGHT 361 365 EL=2 MID=1 NF=362
LINE STRAIGHT 365 369 EL=2 MID=1 NF=366
LINE STRAIGHT 369 377 EL=4 MID=1 NF=370
LINE COMBINE 1 29 9 13 17 21
LINE COMBINE 29 377 87
LINE COMBINE 1 349 59
LINE COMBINE 349 377 357 361 365 369
LINE STRAIGHT 465 473 EL=4 MID=1 NF=466
LINE STRAIGHT 473 477 EL=2 MID=1 NF=474
LINE STRAIGHT 477 481 EL=2 MID=1 NF=478
LINE STRAIGHT 481 485 EL=2 MID=1 NF=482
LINE STRAIGHT 485 493 EL=4 MID=1 NF=486
LINE STRAIGHT 493 551 EL=1 MID=1 NF=522 NS=29
LINE STRAIGHT 465 523 EL=1 MID=1 NF=494  NS=29
LINE STRAIGHT 523 531 EL=4 MID=1 NF=524
LINE STRAIGHT 531 535 EL=2 MID=1 NF=532
LINE STRAIGHT 535 539 EL=2 MID=1 NF=536
LINE STRAIGHT 539 543 EL=2 MID=1 NF=540
LINE STRAIGHT 543 551 EL=4 MID=1 NF=544
LINE COMBINE 465 493 473 477 481 485
LINE COMBINE 523 551 531 535 539 543
LINE STRAIGHT 639 647 EL=4 MID=1 NF=640
LINE STRAIGHT 647 651 EL=2 MID=1 NF=648
```

```
LINE STRAIGHT 651 655 EL=2 MID=1 NF=652
LINE STRAIGHT 655 659 EL=2 MID=1 NF=656
LINE STRAIGHT 659 667 EL=4 MID=1 NF=660
LINE STRAIGHT 667 725 EL=1 MID=1 NF=696 NS=29
LINE STRAIGHT 639 697 EL=1 MID=1 NF=668 NS=29
LINE STRAIGHT 697 705 EL=4 MID=1 NF=698
LINE STRAIGHT 705 709 EL=2 MID=1 NF=706
LINE STRAIGHT 709 713 EL=2 MID=1 NF=710
LINE STRAIGHT 713 717 EL=2 MID=1 NF=714
LINE STRAIGHT 717 725 EL=4 MID=1 NF=718
LINE COMBINE 639 667 647 651 655 659
LINE COMBINE 697 725 705 709 713 717
LINE STRAIGHT 813 821 EL=4 MID=1 NF=814
LINE STRAIGHT 821 825 EL=2 MID=1 NF=822
LINE STRAIGHT 825 829 EL=2 MID=1 NF=826
LINE STRAIGHT 829 833 EL=2 MID=1 NF=830
LINE STRAIGHT 833 841 EL=4 MID=1 NF=834
LINE STRAIGHT 841 899 EL=1 MID=1 NF=870 NS=29
LINE STRAIGHT 813 871 EL=1 MID=1 NF=842 NS=29
LINE STRAIGHT 871 879 EL=4 MID=1 NF=872
LINE STRAIGHT 879 883 EL=2 MID=1 NF=880
LINE STRAIGHT 883 887 EL=2 MID=1 NF=884
LINE STRAIGHT 887 891 EL=2 MID=1 NF=888
LINE STRAIGHT 891 899 EL=4 MID=1 NF=892
LINE COMBINE 813 841 821 825 829 833
LINE COMBINE 871 899 879 883 887 891
*CONCRETE SLAB AND STEEL GIRDERS
MATERIAL 1 ELASTIC E=26500. NU=.15 D=0. K=.833
MATERIAL 2 PLASTIC H=I E=2.E5 NU=.3 Y=300. ET=0. D=0.
EGROUP 1 SHELL M=1 RINT=3 SINT=3 TINT=2
GSURFACE 1 29 377 349 EL1=14 EL2=6 NODES=9 NF=2 EF=1
THICKNESS 1 225.45
STRESSTABLE 1 1 2 3 4 5 6 7 8 17 18
EDATA
ENTRIES EL NTH TABLE
1 1 1
TO
84 1 1
EGROUP 2 SHELL M=2 RINT=5 SINT=3 TINT=-3
GSURFACE 465 493 551 523 EL1=14 EL2=1 NODES=9 NF=466 EF=15
GSURFACE 639 667 725 697 EL1=14 EL2=1 NODES=9 NF=640 EF=43
GSURFACE 813 841 899 871 EL1=14 EL2=1 NODES=9 NF=814 EF=71
COORDINATES
ENTRIES NODE X Y Z
*STEEL WEBS
378 -5900. 18300. 773.725
407 -5900. 18300. 386.8625
436 -5900. 18300. .0
552 -3540. 18300. 773.725
581 -3540. 18300. 386.8625
```

```
610 -3540. 18300. .0
726 -1180. 18300. 773.725
755 -1180. 18300. 386.8625
784 -1180. 18300. .0
NGENERATION TIMES=8 NSTEP=1 YSTEP=-700.
378 407 436 552 581 610 726 755 784
NGENERATION TIMES=4 NSTEP=1 YSTEP=-600.
386 415 444 560 589 618 734 763 792
NGENERATION TIMES=4 NSTEP=1 YSTEP=-575.
390 419 448 564 593 622 738 767 796
NGENERATION TIMES=4 NSTEP=1 YSTEP=-600.
394 423 452 568 597 626 742 771 800
NGENERATION TIMES=8 NSTEP=1 YSTEP=-700.
398 427 456 572 601 630 746 775 804
ENODES
ENTRIES EL N1 N8 N4 N5 N13 N7 N2 N6 N3
1 378 379 380 407 408 409 436 437 438
29 552 553 554 581 582 583 610 611 612
57 726 727 728 755 756 757 784 785 786
EGENERATION TIMES=13 ESTEP=1 NSTEP1=2
1 STEP 28 TO 57
THICKNESS 1 30.
THICKNESS 2 18.
EDATA
ENTRIES EL NTH TABLE
1 2 1
TO
14 2 1
15 1 1
TO
28 1 1
29 2 1
TO
42 2 1
43 1 1
TO
56 1 1
57 2 1
TO
70 2 1
71 1 1
TO
84 1 1
BOUNDARIES IDOF=111001
493 STEP 29 TO 551/464
667 STEP 29 TO 725/638
841 STEP 29 TO 899/812
BOUNDARIES IDOF=100011
349 TO 377
BOUNDARIES IDOF=101001
```

```
465 STEP 29 TO 523/436
639 STEP 29 TO 697/610
813 STEP 29 TO 871/784
LIST BOUNDARIES
CONSTRAINT
378 1 59 1/TO/406 1 87 1
378 2 59 2/TO/406 2 87 2
378 3 59 3/TO/406 3 87 3
378 5 59 5/TO/406 5 87 5
552 1 175 1/TO/580 1 203 1
552 2 175 2/TO/580 2 203 2
552 3 175 3/TO/580 3 203 3
552 5 175 5/TO/580 5 203 5
726 1 291 1/TO/754 1 319 1
726 2 291 2/TO/754 2 319 2
726 3 291 3/TO/754 3 319 3
726 5 291 5/TO/754 5 319 5
437 1 495 1/TO/463 1 521 1
437 2 495 2/TO/463 2 521 2
437 3 495 3/TO/463 3 521 3
437 5 495 5/TO/463 5 521 5
436 2 494 2
436 5 494 5
464 5 522 5
611 1 669 1/TO/637 1 695 1
611 2 669 2/TO/637 2 695 2
611 3 669 3/TO/637 3 695 3
611 5 669 5/TO/637 5 695 5
610 2 668 2
610 5 668 5
638 5 696 5
785 1 843 1/TO/811 1 869 1
785 2 843 2/TO/811 2 869 2
785 3 843 3/TO/811 3 869 3
785 5 843 5/TO/811 5 869 5
784 2 842 2
784 5 842 5
812 5 870 5
LOADS CONCENTRATED
77 3 113700. 1
193 3 183485. 1
309 3 149305. 1
66 3 81215. 1
182 3 131065. 1
298 3 106650. 1
FRAME
MESH
ADINA OPTIM=YES
END
```

```
'PLOTSIZE' 30.00 27.50
DATABASE CREATE
HEAD 'Continuous Slab-on-Girder Bridge'
MASTER IDOF=000001 NSTEP=1
ITERATION M=BFGS
STIFFNESS-STEPS
EQUILIBRIUM-STEPS
PRINTOUT VOLUME=MIN IVC=0 IAC=0
TIMEFUNCTION 1
0 0.0
1 1.0
PRINTNODES 1 1659 1
COORDINATES
ENTRIES NODE X Y Z
1 -1610 16186 277.75
21 -1610 11330 277.75
37 -1610 8534.6 277.75
49 -1610 6198.2 277.75
55 -1610 4856 277.75
63 -1610 3649.2 277.75
79 -1610 0 277.75
159 -1350 16186 277.75
237 -1350 0 277.75
633 0 16186 277.75
653 0 11330 277.75
669 0 8534.6 277.75
681 0 6198.2 277.75
687 0 4856 277.75
695 0 3649.2 277.75
711 0 0 277.75
949 -1401 16186 0
969 -1401 11330 0
985 -1401 8534.6 0
997 -1401 6198.2 0
1003 -1401 4856 0
1011 -1401 3649.2 0
1027 -1401 0 0
1107 -1299 16186 0
1127 -1299 11330 0
1143 -1299 8534.6 0
1155 -1299 6198.2 0
1161 -1299 4856 0
1169 -1299 3649.2 0
1185 -1299 0 0
1423 -501 16186 0
1443 -501 11330 0
1459 -501 8534.6 0
1471 -501 6198.2 0
1477 -501 4856 0
1485 -501 3649.2 0
```

```
1501 -501 0 0
1581 -399 16186 0
1601 -399 11330 0
1617 -399 8534.6 0
1629 -399 6198.2
1635 -399 4856 0
1643 -399 3649.2 0
1659 -399 0 0
LINE STRAIGHT N1=1 N2=21 EL=10 MID=1 NF=2 NS=1 R=1
LINE STRAIGHT N1=21 N2=37 EL=8 MID=1 NF=22 NS=1 R=1
LINE STRAIGHT N1=37 N2=49 EL=6 MID=1 NF=38
LINE STRAIGHT N1=49 N2=55 EL=3 MID=1 NF=50
LINE STRAIGHT N1=55 N2=63 EL=4 MID=1 NF=56
LINE STRAIGHT N1=63 N2=79 EL=8 MID=1 NF=64
LINE STRAIGHT N1=1 N2=159 EL=1 MID=1 NF=80 NS=79 R=1
LINE STRAIGHT N1=159 N2=633 EL=3 MID=1 NF=238 NS=79
LINE S N1=79 N2=237 EL=1 M=1 NF=158 NS=79
LINE S N1=237 N2=711 EL=3 M=1 NF=316 NS=79
LINE S N1=633 N2=653 EL=10 M=1 NF=634
LINE S N1=653 N2=669 EL=8 M=1 NF=654
LINE S N1=669 N2=681 EL=6 M=1 NF=670
LINE S N1=681 N2=687 EL=3 M=1 NF=682
LINE S N1=687 N2=695 EL=4 M=1 NF=688
LINE S N1=695 N2=711 EL=8 M=1 NF=696
LINE S N1=949 N2=969 EL=10 M=1 NF=950
LINE S N1=969 N2=985 EL=8 M=1 NF=970
LINE S N1=985 N2=997 EL=6 M=1 NF=986
LINE S N1=997 N2=1003 EL=3 M=1 NF=998
LINE S N1=1003 N2=1011 EL=4 M=1 NF=1004
LINE S N1=1011 N2=1027 EL=8 M=1 NF=1012
LINE S N1=1107 N2=1127 EL=10 M=1 NF=1108
LINE S N1=1127 N2=1143 EL=8 M=1 NF=1128
LINE S N1=1143 N2=1155 EL=6 M=1 NF=1144
LINE S N1=1155 N2=1161 EL=3 M=1 NF=1156
LINE S N1=1161 N2=1169 EL=4 MID=1 NF=1162
LINE STRAIGHT N1=1169 N2=1185 EL=8 MID=1 NF=1170
LINE STRAIGHT N1=1423 N2=1443 EL=10 MID=1 NF=1424
LINE STRAIGHT N1=1443 N2=1459 EL=8 MID=1 NF=1444
LINE STRAIGHT N1=1459 N2=1471 EL=6 MID=1 NF=1460
LINE STRAIGHT N1=1471 N2=1477 EL=3 MID=1 NF=1472
LINE S N1=1477 N2=1485 EL=4 M=1 NF=1478
LINE S N1=1485 N2=1501 EL=8 M=1 NF=1486
LINE S N1=1581 N2=1601 EL=10 M=1 NF=1582
LINE S N1=1601 N2=1617 EL=8 M=1 NF=1602
LINE S N1=1617 N2=1629 EL=6 M=1 NF=1618
LINE S N1=1629 N2=1635 EL=3 M=1 NF=1630
LINE S N1=1635 N2=1643 EL=4 M=1 NF=1636
LINE S N1=1643 N2=1659 EL=8 M=1 NF=1644
LINE COMBINED 1 79 21 37 49 55 63
LINE COMBINED 1 633 159
```

```
LINE C 79 711 237
LINE C 633 711 653 669 681 687 695
LINE C 949 1027 969 985 997 1003 1011
LINE C 1107 1185 1127 1143 1155 1161 1169
LINE C 1423 1501 1443 1459 1471 1477 1485
LINE C 1581 1659 1601 1617 1629 1635 1643
MATERIAL 1 ELASTIC E=4.358E4 NU=0.15 D=0. K=0.83333
MATERIAL 2 PLASTIC H=I E=2E5 NU=0.3 Y=304. ET=0. D=0.
EGROUP N=1 SHELL D=S M=1 RINT=3 SINT=3 TINT=2
GSURFACE 1 79 711 633 EL1=39 EL2=4 NO=9 NF=2 EF=1
THICKNESS 1 65.5
STRESSTABLE 1 1 2 3 4 5 6 7 8
EDATA
ENTRIES EL NTH TABLE
1 1 1
TO
156 1 1
EGROUP N=2 SHELL D=S M=2 RINT=3 SINT=5 TINT=2
GSURFACE 949 1027 1185 1107 EL1=39 EL2=1 NO=9 NF=950 EF=40
GSURFACE 1423 1501 1659 1581 EL1=39 EL2=1 NO=9 NF=1424 EF=118
COORDINATES
ENTRIES NODE X Y Z
712 -1350 16186 277.75
791 -1350 16186 138.875
870 -1350 16186 0
732 -1350 11330 277.75
811 -1350 11330 138.875
890 -1350 11330 0
748 -1350 8534.6 277.75
827 -1350 8534.6 138.875
906 -1350 8534.6 0
760 -1350 6198.2 277.75
839 -1350 6198.2 138.875
918 -1350 6198.2 0
766 -1350 4856 277.75
845 -1350 4856 138.875
924 -1350 4856 0
774 -1350 3649.2 277.75
853 -1350 3649.2 138.875
932 -1350 3649.2 0
1186 -450 16186 277.75
1265 -450 16186 138.875
1344 -450 16186 0
1206 -450 11330 277.75
1285 -450 11330 138.875
1364 -450 11330 0
1222 -450 8534.6 277.75
1301 -450 8534.6 138.875
1380 -450 8534.6 0
1234 -450 6198.2 277.75
```

```
1313 -450 6198.2 138.875
1392 -450 6198.2 0
1240 -450 4856 277.75
1319 -450 4856 138.875
1398 -450 4856 0
1248 -450 3649.2 277.75
1327 -450 3649.2 138.875
1406 -450 3649.2 0
NGENERATION TIMES=20 NSTEP=1 YSTEP=-242.8
712 STEP 79 TO 870
1186 STEP 79 TO 1344
ENODES
ENTRIES EL N1 N5 N2 N8 N13 N6 N4 N7 N3
1 712 713 714 791 792 793 870 871 872
79 1186 1187 1188 1265 1266 1267 1344 1345 1346
EGENERATION TIMES=9 ESTEP=1 NSTEP1=2
1 79
NGENERATION TIMES=16 NSTEP=1 YSTEP=-174.7125
732 STEP 79 TO 890
1206 STEP 79 TO 1364
ENODES
ENTRIES EL N1 N5 N2 N8 N13 N6 N4 N7 N3
11 732 733 734 811 812 813 890 891 892
89 1206 1207 1208 1285 1286 1287 1364 1365 1366
EGENERATION TIMES=7 ESTEP=1 NSTEP1=2
11 89
NGENERATION TIMES=12 NSTEP=1 YSTEP=-194.7
748 STEP 79 TO 906
1222 STEP 79 TO 1380
ENODES
ENTRIES EL N1 N5 N2 N8 N13 N6 N4 N7 N3
19 748 749 750 827 828 829 906 907 908
97 1222 1223 1224 1301 1302 1303 1380 1381 1382
EGENERATION TIMES=5 ESTEP=1 NSTEP1=2
19 97
NGENERATION TIMES=8 NSTEP=1 YSTEP=-223.7
760 STEP 79 TO 918
1234 STEP 79 TO 1392
ENODES
ENTRIES EL N1 N5 N2 N8 N13 N6 N4 N7 N3
25 760 761 762 839 840 841 918 919 920
103 1234 1235 1236 1313 1314 1315 1392 1393 1394
EGENERATION TIMES=2 ESTEP=1 NSTEP1=2
25 103
NGENERATION TIMES=8 NSTEP=1 YSTEP=-150.85
766 STEP 79 TO 924
1240 STEP 79 TO 1398
ENODES
ENTRIES EL N1 N5 N2 N8 N13 N6 N4 N7 N3
28 766 767 768 845 846 847 924 925 926
```

```
106 1240 1241 1242 1319 1320 1321 1398 1399 1400
EGENERATION TIMES=3 ESTEP=1 NSTEP1=2
28 106
NGENERATION TIMES=16 NSTEP=1 YSTEP=-228.075
774 STEP 79 TO 932
1248 STEP 79 TO 1406
ENODES
ENTRIES EL N1 N5 N2 N8 N13 N6 N4 N7 N3
32 774 775 776 853 854 855 932 933 934
110 1248 1249 1250 1327 1328 1329 1406 1407 1408
EGENERATION TIMES=7 ESTEP=1 NSTEP1=2
32 110
THICKNESS 2 6.3.
EDATA
ENTRIES EL NTH TABLE
1 2 2
TO
156 2 2
BOUNDARY IDOF=101001
949 STEP 79 TO 1107/870
1423 STEP 79 TO 1581/1344
969 STEP 79 TO 1127/890
1443 STEP 79 TO 1601/1364
1003 STEP 79 TO 1161/924
1477 STEP 79 TO 1635/1398
BOUNDARY IDOF=111001
1027 STEP 79 TO 1185/948
1501 STEP 79 TO 1659/1422
BOUNDARY IDOF=100011
633 TO 711
LIST BOUNDARY
CONSTRAINTS
712 1 159 1/TO/790 1 237 1
712 2 159 2/TO/790 2 237 2
712 3 159 3/TO/790 3 237 3
712 5 159 5/TO/790 5 237 5
1186 1 475 1/TO/1264 1 553 1
1186 2 475 2/TO/1264 2 553 2
1186 3 475 3/TO/1264 3 553 3
1186 5 475 5/TO/1264 5 553 5
871 1 1029 1/TO/947 1 1105 1
871 2 1029 2/TO/947 2 1105 2
871 3 1029 3/TO/947 3 1105 3
871 5 1029 5/TO/947 5 1105 5
DELETE 890 924
1345 1 1503 1/TO/1421 1 1579 1
1345 2 1503 2/TO/1421 2 1579 2
1345 3 1503 3/TO/1421 3 1579 3
1345 5 1503 5/TO/1421 5 1579 5
DELETE 1364 1398
```

```
870 2 1028 2
870 5 1028 5
890 2 1048 2
890 5 1048 5
924 2 1082 2
924 5 1082 5
948 5 1106 5
1344 2 1502 2
1344 5 1502 5
1364 2 1522 2
1364 5 1522 5
1398 2 1556 2
1398 5 1556 5
1422 5 1580 5
LOAD CONCENTRATED
195 3 -13150.
207 3 -9395.
221 3 -7515.
511 3 -29165.
523 3 -20830.
537 3 -16665.
FRAME
MESH NODES=11 ELEMENTS=1
ADINA
END
```

```
'PLOTSIZE' 30.00 27.50
DATABASE CREATE
HEAD 'Simply Supported Box Girder Bridge'
MASTER IDOF=000001 NSTEP=1
ITERATION METHOD=BFGS
TOLERANCES TYPE=E ETOL=0.01 ITEMAX=30
STIFFNESS-STEPS
EQUILIBRIUM-STEPS
TIMEFUNCTION 1
0 0.
1 -1.00
PRINTOUT MINIMUM
PRINTNODES 1 1155 1
COORDINATES
ENTRIES NODE X Y Z
*CONCRETE DECK SLAB
1   -4724.4 45720. 2376.65
7   -4724.4 34320. 2376.65
13  -4724.4 27120. 2376.65
19  -4724.4 20520. 2376.65
23  -4724.4 16320. 2376.65
33  -4724.4     0. 2376.65
67  -3657.6 45720. 2376.65
99  -3657.6     0. 2376.65
463  3657.6 45720. 2376.65
495  3657.6     0. 2376.65
529  4724.4 45720. 2376.65
535  4724.4 34320. 2376.65
541  4724.4 27120. 2376.65
547  4724.4 20520. 2376.65
551  4724.4 16320. 2376.65
561  4724.4     0. 2376.65
*STEEL FLANGES
661  -3657.6 45720. 0.
667  -3657.6 34320. 0.
673  -3657.6 27120. 0.
679  -3657.6 20520. 0.
683  -3657.6 16320. 0.
693  -3657.6     0. 0.
727  -1219.2 45720. 0.
733  -1219.2 34320. 0.
739  -1219.2 27120. 0.
745  -1219.2 20520. 0.
749  -1219.2 16320. 0.
759  -1219.2     0. 0.
958   1219.2 45720. 0.
964   1219.2 34320. 0.
970   1219.2 27120. 0.
976   1219.2 20520. 0.
980   1219.2 16320. 0.
```

```
990   1219.2     0. 0.
1024  3657.6 45720. 0.
1030  3657.6 34320. 0.
1036  3657.6 27120. 0.
1042  3657.6 20520. 0.
1046  3657.6 16320. 0.
1056  3657.6     0. 0.
LINE STRAIGHT    1    7    EL=3 MID=1 NF=2
LINE STRAIGHT    7   13    EL=3 MID=1 NF=8
LINE STRAIGHT   13   19    EL=3 MID=1 NF=14
LINE STRAIGHT   19   23    EL=2 MID=1 NF=20
LINE STRAIGHT   23   33    EL=5 MID=1 NF=24
LINE STRAIGHT   33   99    EL=1 MID=1 NF=66   NS=33
LINE STRAIGHT   99  495    EL=6 MID=1 NF=132  NS=33
LINE STRAIGHT  495  561    EL=1 MID=1 NF=528  NS=33
LINE STRAIGHT    1   67    EL=1 MID=1 NF=34   NS=33
LINE STRAIGHT   67  463    EL=6 MID=1 NF=100  NS=33
LINE STRAIGHT  463  529    EL=1 MID=1 NF=496  NS=33
LINE STRAIGHT  529  535    EL=3 MID=1 NF=530
LINE STRAIGHT  535  541    EL=3 MID=1 NF=536
LINE STRAIGHT  541  547    EL=3 MID=1 NF=542
LINE STRAIGHT  547  551    EL=2 MID=1 NF=548
LINE STRAIGHT  551  561    EL=5 MID=1 NF=552
LINE COMBINE     1   33    7   13   19   23
LINE COMBINE    33  561   99  495
LINE COMBINE     1  529   67  463
LINE COMBINE   529  561  535  541  547  551
LINE STRAIGHT  661  667    EL=3 MID=1 NF=662
LINE STRAIGHT  667  673    EL=3 MID=1 NF=668
LINE STRAIGHT  673  679    EL=3 MID=1 NF=674
LINE STRAIGHT  679  683    EL=2 MID=1 NF=680
LINE STRAIGHT  683  693    EL=5 MID=1 NF=684
LINE STRAIGHT  693  759    EL=1 MID=1 NF=726  NS=33
LINE STRAIGHT  661  727    EL=1 MID=1 NF=694  NS=33
LINE STRAIGHT  727  733    EL=3 MID=1 NF=728
LINE STRAIGHT  733  739    EL=3 MID=1 NF=734
LINE STRAIGHT  739  745    EL=3 MID=1 NF=740
LINE STRAIGHT  745  749    EL=2 MID=1 NF=746
LINE STRAIGHT  749  759    EL=5 MID=1 NF=750
LINE COMBINE   661  693  667  673  679  683
LINE COMBINE   727  759  733  739  745  749
LINE STRAIGHT  958  964    EL=3 MID=1 NF=959
LINE STRAIGHT  964  970    EL=3 MID=1 NF=965
LINE STRAIGHT  970  976    EL=3 MID=1 NF=971
LINE STRAIGHT  976  980    EL=2 MID=1 NF=977
LINE STRAIGHT  980  990    EL=5 MID=1 NF=981
LINE STRAIGHT  990 1056    EL=1 MID=1 NF=1023 NS=33
LINE STRAIGHT  958 1024    EL=1 MID=1 NF=991  NS=33
LINE STRAIGHT 1024 1030    EL=3 MID=1 NF=1025
LINE STRAIGHT 1030 1036    EL=3 MID=1 NF=1031
```

```
LINE STRAIGHT 1036 1042    EL=3 MID=1 NF=1037
LINE STRAIGHT 1042 1046    EL=2 MID=1 NF=1043
LINE STRAIGHT 1046 1056    EL=5 MID=1 NF=1047
LINE COMBINE   958  990  964  970  976  980
LINE COMBINE  1024 1056 1030 1036 1042 1046
*CONCRETE DECK AND STEEL BOXES
MATERIAL 1 ELASTIC E=26500. NU=.15 D=0. K=.833
MATERIAL 2 PLASTIC H=I E=2.E5 NU=.3 Y=350. ET=0. D=0.
EGROUP 1 SHELL M=1 RINT=3 SINT=3 TINT=2
GSURFACE 1 33 561 529 EL1=16 EL2=8 NODES=9 NF=2 EF=1
THICKNESS 1 270.2
STRESSTABLE 1 1 2 3 4 5 6 7 8
EDATA
ENTRIES EL NTH TABLE
1 1 1
TO
128 1 1
*LIST ENODES 1 128
EGROUP 2 SHELL M=2 RINT=5 SINT=3 TINT=-3
GSURFACE 661 693 759 727 EL1=16 EL2=1 NODES=9 NF=662 EF=17
GSURFACE 958 990 1056 1024 EL1=16 EL2=1 NODES=9 NF=959 EF=65
COORDINATES
ENTRIES NODE X Y Z
*STEEL WEBS
562  -3657.6 45720. 2376.650
595  -3657.6 45720. 1188.325
628  -3657.6 45720.    0.
760  -1219.2 45720. 2376.650
793  -1219.2 45720. 1188.325
826  -1219.2 45720.    0.
859   1219.2 45720. 2376.650
892   1219.2 45720. 1188.325
925   1219.2 45720.    0.
1057  3657.6 45720. 2376.650
1090  3657.6 45720. 1188.325
1123  3657.6 45720.    0.
NGENERATION TIMES=6 NSTEP=1 YSTEP=-1900.
562 595 628 760 793 826 859 892 925 1057 1090 1123
NGENERATION TIMES=6 NSTEP=1 YSTEP=-1200.
568 601 634 766 799 832 865 898 931 1063 1096 1129
NGENERATION TIMES=6 NSTEP=1 YSTEP=-1100.
574 607 640 772 805 838 871 904 937 1069 1102 1135
NGENERATION TIMES=4 NSTEP=1 YSTEP=-1050.
580 613 646 778 811 844 877 910 943 1075 1108 1141
NGENERATION TIMES=10 NSTEP=1 YSTEP=-1632.
584 617 650 782 815 848 881 914 947 1079 1112 1145
ENODES
ENTRIES EL N1 N8 N4 N5 N13 N7 N2 N6 N3
  1  562  563  564  595  596  597  628  629  630
 33  760  761  762  793  794  795  826  827  828
```

```
49  859  860  861  892  893  894  925  926  927
81 1057 1058 1059 1090 1091 1092 1123 1124 1125
EGENERATION TIMES=15 ESTEP=1 NSTEP1=2
1 33 49 81
THICKNESS 2 25.4
THICKNESS 3 12.7
*STRESSTABLE 2 1 2 3 4 5 6 7 8 9
EDATA
ENTRIES EL NTH TABLE
1 3 1
TO
16 3 1
17 2 1
TO
32 2 1
33 3 1
TO
64 3 1
65 2 1
TO
80 2 1
81 3 1
TO
96 3 1
*LIST ENODES 1 96
BOUNDARIES IDOF=111001
693 STEP 33 TO 759/660 858
990 STEP 33 TO 1056/957 1155
BOUNDARIES IDOF=101001
661 STEP 33 TO 727/628 826
958 STEP 33 TO 1024/925 1123
LIST BOUNDARIES
CONSTRAINT
562  1  67 1/TO/594  1  99 1
562  2  67 2/TO/594  2  99 2
562  3  67 3/TO/594  3  99 3
562  5  67 5/TO/594  5  99 5
760  1 199 1/TO/792  1 231 1
760  2 199 2/TO/792  2 231 2
760  3 199 3/TO/792  3 231 3
760  5 199 5/TO/792  5 231 5
859  1 331 1/TO/891  1 363 1
859  2 331 2/TO/891  2 363 2
859  3 331 3/TO/891  3 363 3
859  5 331 5/TO/891  5 363 5
1057 1 463 1/TO/1089 1 495 1
1057 2 463 2/TO/1089 2 495 2
1057 3 463 3/TO/1089 3 495 3
1057 5 463 5/TO/1089 5 495 5
629  1 662 1/TO/659  1 692 1
```

```
629  2 662 2/TO/659  2 692 2
629  3 662 3/TO/659  3 692 3
629  5 662 5/TO/659  5 692 5
628  2 661 2
628  5 661 5
660  5 693 5
827  1 728 1/TO/857 1 758 1
827  2 728 2/TO/857 2 758 2
827  3 728 3/TO/857 3 758 3
827  5 728 5/TO/857 5 758 5
826  2 727 2
826  5 727 5
858  5 759 5
926  1 939 1/TO/956 1 989 1
926  2 959 2/TO/956 2 989 2
926  3 959 3/TO/956 3 989 3
926  5 959 5/TO/956 5 989 5
925  2 958 2
925  5 958 5
957  5 990 5
1124 1 1025 1/TO/1154 1 1055 1
1124 2 1025 2/TO/1154 2 1055 2
1124 3 1025 3/TO/1154 3 1055 3
1124 5 1025 5/TO/1154 5 1055 5
1123 2 1024 2
1123 5 1024 5
1155 5 1056 5
LOADS CONCENTRATED
*73  3  70060. 1
*79  3  87570. 1
*85  3 122600. 1
*89  3  26270. 1
*205 3  89940. 1
*211 3 112430. 1
*217 3 157400. 1
*221 3  33730. 1
*337 3  89940. 1
*343 3 112430. 1
*349 3 157400. 1
*353 3  33730. 1
*469 3  70060. 1
*475 3  87570. 1
*481 3 122600. 1
*485 3  26270. 1
73   3  68300. 1
79   3  85380. 1
85   3 119530. 1
89   3  25610. 1
205  3 100480. 1
211  3 125600. 1
```

```
217 3 175840. 1
221 3  37680. 1
337 3 -10540. 1
343 3 -13180. 1
349 3 -18440. 1
353 3  -3950. 1
469 3   1760. 1
475 3   2200. 1
481 3   3070. 1
485 3    660. 1
FRAME
MESH
ADINA OPTIM=YES
*LIST COOR 1 1155
END
```

```
'PLOTSIZE' 30.00 27.50
DATABASE CREATE
HEAD 'Continuous Box Girder Bridge (CBGB-3N) '
MASTER IDOF=000001 NSTEP=1
ITERATION METHOD=BFGS
TOLERANCES TYPE=E ETOL=0.001 ITEMAX=30
STIFFNESS-STEPS
EQUILIBRIUM-STEPS
TIMEFUNCTION 1
0 0.
1 -1.0
PRINTOUT MINIMUM
PRINTNODES 1 1110 1
COORDINATES
ENTRIES NODE X Y Z
*CONCRETE DECK SLAB
1   -6700.0 54000. 1687.
7   -6700.0 42000. 1687.
13  -6700.0 34800. 1687.
19  -6700.0 28800. 1687.
21  -6700.0 27600. 1687.
25  -6700.0 20400. 1687.
37  -6700.0     0. 1687.
75  -5700.0 54000. 1687.
111 -5700.0     0. 1687.
445  5700.0 54000. 1687.
481  5700.0     0. 1687.
519  6700.0 54000. 1687.
525  6700.0 42000. 1687.
531  6700.0 34800. 1687.
537  6700.0 28800. 1687.
539  6700.0 27600. 1687.
543  6700.0 20400. 1687.
555  6700.0     0. 1687.
*STEEL FLANGES
556  -5700.0 54000. 0.
562  -5700.0 42000. 0.
568  -5700.0 34800. 0.
574  -5700.0 28800. 0.
576  -5700.0 27600. 0.
580  -5700.0 20400. 0.
592  -5700.0     0. 0.
630  -3420.0 54000. 0.
636  -3420.0 42000. 0.
642  -3420.0 34800. 0.
648  -3420.0 28800. 0.
650  -3420.0 27600. 0.
654  -3420.0 20400. 0.
666  -3420.0     0. 0.
667  -1140.0 54000. 0.
```

```
673  -1140.0 42000. 0.
679  -1140.0 34800. 0.
685  -1140.0 28800. 0.
687  -1140.0 27600. 0.
691  -1140.0 20400. 0.
703  -1140.0     0. 0.
741   1140.0 54000. 0.
747   1140.0 42000. 0.
753   1140.0 34800. 0.
759   1140.0 28800. 0.
761   1140.0 27600. 0.
765   1140.0 20400. 0.
777   1140.0     0. 0.
778   3420.0 54000. 0.
784   3420.0 42000. 0.
790   3420.0 34800. 0.
796   3420.0 28800. 0.
798   3420.0 27600. 0.
802   3420.0 20400. 0.
814   3420.0     0. 0.
852   5700.0 54000. 0.
858   5700.0 42000. 0.
864   5700.0 34800. 0.
870   5700.0 28800. 0.
872   5700.0 27600. 0.
876   5700.0 20400. 0.
888   5700.0     0. 0.
SHELLNODES DIRECTOR=-2 SYSTEM=DEFAULT=L DIRTOL=20
  75 -2 G TO 111 -2 G
149 -2 G TO 185 -2 G
223 -2 G TO 259 -2 G
297 -2 G TO 333 -2 G
371 -2 G TO 407 -2 G
445 -2 G TO 481 -2 G
556 -2 G TO 592 -2 G
630 -2 G TO 666 -2 G
667 -2 G TO 703 -2 G
741 -2 G TO 777 -2 G
778 -2 G TO 814 -2 G
852 -2 G TO 888 -2 G
LINE STRAIGHT    1    7    EL=3 MID=1 NF=2
LINE STRAIGHT    7   13    EL=3 MID=1 NF=8
LINE STRAIGHT   13   19    EL=3 MID=1 NF=14
LINE STRAIGHT   19   21    EL=1 MID=1 NF=20
LINE STRAIGHT   21   25    EL=2 MID=1 NF=22
LINE STRAIGHT   25   37    EL=6 MID=1 NF=26
LINE STRAIGHT   37  111    EL=1 MID=1 NF=74   NS=37
LINE STRAIGHT  111  481    EL=5 MID=1 NF=148  NS=37
LINE STRAIGHT  481  555    EL=1 MID=1 NF=518  NS=37
LINE STRAIGHT    1   75    EL=1 MID=1 NF=38   NS=37
```

```
LINE STRAIGHT   75  445    EL=5 MID=1 NF=112  NS=37
LINE STRAIGHT  445  519    EL=1 MID=1 NF=482  NS=37
LINE STRAIGHT  519  525    EL=3 MID=1 NF=520
LINE STRAIGHT  525  531    EL=3 MID=1 NF=526
LINE STRAIGHT  531  537    EL=3 MID=1 NF=532
LINE STRAIGHT  537  539    EL=1 MID=1 NF=538
LINE STRAIGHT  539  543    EL=2 MID=1 NF=540
LINE STRAIGHT  543  555    EL=6 MID=1 NF=544
LINE COMBINE     1   37    7   13   19   21   25
LINE COMBINE    37  555  111  481
LINE COMBINE     1  519   75  445
LINE COMBINE   519  555  525  531  537  539  543
LINE STRAIGHT  556  562    EL=3 MID=1 NF=557
LINE STRAIGHT  562  568    EL=3 MID=1 NF=563
LINE STRAIGHT  568  574    EL=3 MID=1 NF=569
LINE STRAIGHT  574  576    EL=1 MID=1 NF=575
LINE STRAIGHT  576  580    EL=2 MID=1 NF=577
LINE STRAIGHT  580  592    EL=6 MID=1 NF=581
LINE STRAIGHT  592  666    EL=1 MID=1 NF=629  NS=37
LINE STRAIGHT  556  630    EL=1 MID=1 NF=593  NS=37
LINE STRAIGHT  630  636    EL=3 MID=1 NF=631
LINE STRAIGHT  636  642    EL=3 MID=1 NF=637
LINE STRAIGHT  642  648    EL=3 MID=1 NF=643
LINE STRAIGHT  648  650    EL=1 MID=1 NF=649
LINE STRAIGHT  650  654    EL=2 MID=1 NF=651
LINE STRAIGHT  654  666    EL=6 MID=1 NF=655
LINE COMBINE   556  592  562  568  574  576  580
LINE COMBINE   630  666  636  642  648  650  654
LINE STRAIGHT  667  673    EL=3 MID=1 NF=668
LINE STRAIGHT  673  679    EL=3 MID=1 NF=674
LINE STRAIGHT  679  685    EL=3 MID=1 NF=680
LINE STRAIGHT  685  687    EL=1 MID=1 NF=686
LINE STRAIGHT  687  691    EL=2 MID=1 NF=688
LINE STRAIGHT  691  703    EL=6 MID=1 NF=692
LINE STRAIGHT  703  777    EL=1 MID=1 NF=740  NS=37
LINE STRAIGHT  667  741    EL=1 MID=1 NF=704  NS=37
LINE STRAIGHT  741  747    EL=3 MID=1 NF=742
LINE STRAIGHT  747  753    EL=3 MID=1 NF=748
LINE STRAIGHT  753  759    EL=3 MID=1 NF=754
LINE STRAIGHT  759  761    EL=1 MID=1 NF=760
LINE STRAIGHT  761  765    EL=2 MID=1 NF=762
LINE STRAIGHT  765  777    EL=6 MID=1 NF=766
LINE COMBINE   667  703  673  679  685  687  691
LINE COMBINE   741  777  747  753  759  761  765
LINE STRAIGHT  778  784    EL=3 MID=1 NF=779
LINE STRAIGHT  784  790    EL=3 MID=1 NF=785
LINE STRAIGHT  790  796    EL=3 MID=1 NF=791
LINE STRAIGHT  796  798    EL=1 MID=1 NF=797
LINE STRAIGHT  798  802    EL=2 MID=1 NF=799
LINE STRAIGHT  802  814    EL=6 MID=1 NF=803
```

```
LINE STRAIGHT  814  888    EL=1 MID=1 NF=851  NS=37
LINE STRAIGHT  778  852    EL=1 MID=1 NF=815  NS=37
LINE STRAIGHT  852  858    EL=3 MID=1 NF=853
LINE STRAIGHT  858  864    EL=3 MID=1 NF=859
LINE STRAIGHT  864  870    EL=3 MID=1 NF=865
LINE STRAIGHT  870  872    EL=1 MID=1 NF=871
LINE STRAIGHT  872  876    EL=2 MID=1 NF=873
LINE STRAIGHT  876  888    EL=6 MID=1 NF=877
LINE COMBINE   778  814  784  790  796  798  802
LINE COMBINE   852  888  858  864  870  872  876
*CONCRETE DECK AND STEEL BOXES
MATERIAL 1 ELASTIC E=28000. NU=.15 D=0. K=.833
MATERIAL 2 PLASTIC H=I E=2.E5 NU=.3 Y=350. ET=0. D=0.
EGROUP 1 SHELL M=1 RINT=3 SINT=3 TINT=2
GSURFACE 1 37 555 519 EL1=18 EL2=7 NODES=9 NF=2 EF=1
THICKNESS 1 230.
STRESSTABLE 1 1 2 3 4 5 6 7 8
EDATA
ENTRIES EL NTH TABLE
1 1 1
TO
126 1 1
*LIST ENODES 1 126
EGROUP 2 SHELL M=2 RINT=5 SINT=3 TINT=-3
GSURFACE 556 592 666 630 EL1=18 EL2=1 NODES=9 NF=557 EF=19
GSURFACE 667 703 777 741 EL1=18 EL2=1 NODES=9 NF=668 EF=73
GSURFACE 778 814 888 852 EL1=18 EL2=1 NODES=9 NF=779 EF=127
COORDINATES
ENTRIES NODE X Y Z
*STEEL WEBS
889  -5700.0 54000.  843.5
926  -3420.0 54000.  843.5
963  -1140.0 54000.  843.5
1000  1140.0 54000.  843.5
1037  3420.0 54000.  843.5
1074  5700.0 54000.  843.5
NGENERATION TIMES=6 NSTEP=1 YSTEP=-2000.
889 926 963 1000 1037 1074
NGENERATION TIMES=6 NSTEP=1 YSTEP=-1200.
895 932 969 1006 1043 1080
NGENERATION TIMES=6 NSTEP=1 YSTEP=-1000.
901 938 975 1012 1049 1086
NGENERATION TIMES=2 NSTEP=1 YSTEP=-600.
907 944 981 1018 1055 1092
NGENERATION TIMES=4 NSTEP=1 YSTEP=-1800.
909 946 983 1020 1057 1094
NGENERATION TIMES=12 NSTEP=1 YSTEP=-1700.
913 950 987 1024 1061 1098
ENODES
ENTRIES EL N1 N8 N4 N5 N13 N7 N2 N6 N3
```

```
  1   75   76   77  889  890  891  556  557  558
 37  149  150  151  926  927  928  630  631  632
 55  223  224  225  963  964  965  667  668  669
 91  297  298  299 1000 1001 1002  741  742  743
109  371  372  373 1037 1038 1039  778  779  780
145  445  446  447 1074 1075 1076  852  853  854
EGENERATION TIMES=17 ESTEP=1 NSTEP1=2
1 37 55 91 109 145
THICKNESS 2 16.0
THICKNESS 3 10.0
*STRESSTABLE 2 1 2 3 4 5 6 7 8 9
EDATA
ENTRIES EL NTH TABLE
1 3 1
TO
18 3 1
19 2 1
TO
36 2 1
37 3 1
TO
72 3 1
73 2 1
TO
90 2 1
91 3 1
TO
126 3 1
127 2 1
TO
144 2 1
145 3 1
TO
162 3 1
*LIST ENODES 1 162
BOUNDARIES IDOF=111101
592 STEP 37 TO 666
703 STEP 37 TO 777
814 STEP 37 TO 888
BOUNDARIES IDOF=101001
556 STEP 37 TO 630
667 STEP 37 TO 741
778 STEP 37 TO 852
BOUNDARIES IDOF=010101
37 STEP 37 TO 555
925 962 999 1036 1073 1110
LIST BOUNDARIES
LOADS CONCENTRATED
   81  3  61920. 1
   87  3  77400. 1
```

```
  93  3  54180. 1
  95  3  54180. 1
  97  3  23220. 1
 155  3  97580. 1
 161  3 121970. 1
 167  3  85380. 1
 169  3  85380. 1
 171  3  36590. 1
 229  3  80500. 1
 235  3 100630. 1
 241  3  70440. 1
 243  3  70440. 1
 245  3  30190. 1
 303  3  80500. 1
 309  3 100630. 1
 315  3  70440. 1
 317  3  70440. 1
 319  3  30190. 1
 377  3  97580. 1
 383  3 121970. 1
 389  3  85380. 1
 391  3  85380. 1
 393  3  36590. 1
 451  3  61920. 1
 457  3  77400. 1
 463  3  54180. 1
 465  3  54180. 1
 467  3  23220. 1
FRAME
MESH
ADINA OPTIM=YES
*LIST COOR 1 1110
END
```

```
'PLOTSIZE' 30.00 27.50
DATABASE CREATE
HEAD 'Continuous Box Girder Bridge (CBGB-3P)'
MASTER IDOF=000001 NSTEP=1
ITERATION METHOD=BFGS
TOLERANCES TYPE=E ETOL=0.001 ITEMAX=30
STIFFNESS-STEPS
EQUILIBRIUM-STEPS
TIMEFUNCTION 1
0 0.
1 -1.0
PRINTOUT MINIMUM
PRINTNODES 1 1098 1
COORDINATES
ENTRIES NODE X Y Z
*CONCRETE DECK SLAB
1    -6700.0 108000. 1687.
9    -6700.0  93000. 1687.
15   -6700.0  87600. 1687.
17   -6700.0  86400. 1687.
23   -6700.0  80400. 1687.
29   -6700.0  69600. 1687.
37   -6700.0  54000. 1687.
61   -6700.0      0.  1687.
123  -5700.0 108000. 1687.
183  -5700.0      0. 1687.
367  -1140.0 108000. 1687.
427  -1140.0      0. 1687.
489      0.0 108000. 1687.
497      0.0  93000. 1687.
503      0.0  87600. 1687.
505      0.0  86400. 1687.
511      0.0  80400. 1687.
517      0.0  69600. 1687.
525      0.0  54000. 1687.
549      0.0      0. 1687.
*STEEL FLANGES
550  -5700.0 108000. 0.
558  -5700.0  93000. 0.
564  -5700.0  87600. 0.
566  -3700.0  86400. 0.
572  -5700.0  80400. 0.
578  -5700.0  69600. 0.
586  -5700.0  54000. 0.
610  -5700.0      0. 0.
672  -3420.0 108000. 0.
680  -3420.0  93000. 0.
686  -3420.0  87600. 0.
688  -3420.0  86400. 0.
694  -3420.0  80400. 0.
```

```
700  -3420.0  69600. 0.
708  -3420.0  54000. 0.
732  -3420.0      0. 0.
733  -1140.0 108000. 0.
741  -1140.0  93000. 0.
747  -1140.0  87600. 0.
749  -1140.0  86400. 0.
755  -1140.0  80400. 0.
761  -1140.0  69600. 0.
769  -1140.0  54000. 0.
793  -1140.0      0. 0.
855      0.0 108000. 0.
863      0.0  93000. 0.
869      0.0  87600. 0.
871      0.0  86400. 0.
877      0.0  80400. 0.
883      0.0  69600. 0.
891      0.0  54000. 0.
915      0.0      0. 0.
SHELLNODES DIRECTOR=-2 SYSTEM=DEFAULT=L DIRTOL=20
123 -2 G TO 183 -2 G
245 -2 G TO 305 -2 G
367 -2 G TO 427 -2 G
550 -2 G TO 610 -2 G
672 -2 G TO 732 -2 G
733 -2 G TO 793 -2 G
LINE STRAIGHT    1    9    EL=4  MID=1 NF=2
LINE STRAIGHT    9   15    EL=3  MID=1 NF=10
LINE STRAIGHT   15   17    EL=1  MID=1 NF=16
LINE STRAIGHT   17   23    EL=3  MID=1 NF=18
LINE STRAIGHT   23   29    EL=3  MID=1 NF=24
LINE STRAIGHT   29   37    EL=4  MID=1 NF=30
LINE STRAIGHT   37   61    EL=12 MID=1 NF=38
LINE STRAIGHT   61  183    EL=1  MID=1 NF=122  NS=61
LINE STRAIGHT  183  427    EL=2  MID=1 NF=244  NS=61
LINE STRAIGHT  427  549    EL=1  MID=1 NF=488  NS=61
LINE STRAIGHT    1  123    EL=1  MID=1 NF=62   NS=61
LINE STRAIGHT  123  367    EL=2  MID=1 NF=184  NS=61
LINE STRAIGHT  367  489    EL=1  MID=1 NF=428  NS=61
LINE STRAIGHT  489  497    EL=4  MID=1 NF=490
LINE STRAIGHT  497  503    EL=3  MID=1 NF=498
LINE STRAIGHT  503  505    EL=1  MID=1 NF=504
LINE STRAIGHT  505  511    EL=3  MID=1 NF=506
LINE STRAIGHT  511  517    EL=3  MID=1 NF=512
LINE STRAIGHT  517  525    EL=4  MID=1 NF=518
LINE STRAIGHT  525  549    EL=12 MID=1 NF=526
LINE COMBINE     1   61     9   15   17   23   29   37
LINE COMBINE    61  549   183  427
LINE COMBINE     1  489   123  367
LINE COMBINE   489  549   497  503  505  511  517  525
```

```
LINE STRAIGHT  550  558    EL=4  MID=1 NF=551
LINE STRAIGHT  558  564    EL=3  MID=1 NF=559
LINE STRAIGHT  564  566    EL=1  MID=1 NF=565
LINE STRAIGHT  566  572    EL=3  MID=1 NF=567
LINE STRAIGHT  572  578    EL=3  MID=1 NF=573
LINE STRAIGHT  578  586    EL=4  MID=1 NF=579
LINE STRAIGHT  586  610    EL=12 MID=1 NF=587
LINE STRAIGHT  610  732    EL=1  MID=1 NF=671  NS=61
LINE STRAIGHT  550  672    EL=1  MID=1 NF=611  NS=61
LINE STRAIGHT  672  680    EL=4  MID=1 NF=673
LINE STRAIGHT  680  686    EL=3  MID=1 NF=681
LINE STRAIGHT  686  688    EL=1  MID=1 NF=687
LINE STRAIGHT  688  694    EL=3  MID=1 NF=689
LINE STRAIGHT  694  700    EL=3  MID=1 NF=695
LINE STRAIGHT  700  708    EL=4  MID=1 NF=701
LINE STRAIGHT  708  732    EL=12 MID=1 NF=709
LINE COMBINE   550  610  558  564  566  572  578  586
LINE COMBINE   672  732  680  686  688  694  700  708
LINE STRAIGHT  733  741    EL=4  MID=1 NF=734
LINE STRAIGHT  741  747    EL=3  MID=1 NF=742
LINE STRAIGHT  747  749    EL=1  MID=1 NF=748
LINE STRAIGHT  749  755    EL=3  MID=1 NF=750
LINE STRAIGHT  755  761    EL=3  MID=1 NF=756
LINE STRAIGHT  761  769    EL=4  MID=1 NF=762
LINE STRAIGHT  769  793    EL=12 MID=1 NF=770
LINE STRAIGHT  793  915    EL=1  MID=1 NF=854  NS=61
LINE STRAIGHT  733  855    EL=1  MID=1 NF=794  NS=61
LINE STRAIGHT  855  863    EL=4  MID=1 NF=856
LINE STRAIGHT  863  869    EL=3  MID=1 NF=864
LINE STRAIGHT  869  871    EL=1  MID=1 NF=870
LINE STRAIGHT  871  877    EL=3  MID=1 NF=872
LINE STRAIGHT  877  883    EL=3  MID=1 NF=878
LINE STRAIGHT  883  891    EL=4  MID=1 NF=884
LINE STRAIGHT  891  915    EL=12 MID=1 NF=892
LINE COMBINE   733  793  741  747  749  755  761  769
LINE COMBINE   855  915  863  869  871  877  883  891
*CONCRETE DECK AND STEEL BOXES
MATERIAL 1 ELASTIC E=28000. NU=.15 D=0. K=.833
MATERIAL 2 PLASTIC H=I E=2.E5 NU=.3 Y=350. ET=0. D=0.
EGROUP 1 SHELL M=1 RINT=3 SINT=3 TINT=2
GSURFACE 1 61 549 489 EL1=30 EL2=4 NODES=9 NF=2 EF=1
THICKNESS 1 230.
STRESSTABLE 1 1 2 3 4 5 6 7 8
EDATA
ENTRIES EL NTH TABLE
1 1 1
TO
120 1 1
*LIST ENODES 1 120
EGROUP 2 SHELL M=2 RINT=5 SINT=3 TINT=-3
```

```
GSURFACE 550 610 732 672 EL1=30 EL2=1 NODES=9 NF=551 EF=31
GSURFACE 733 793 915 855 EL1=30 EL2=1 NODES=9 NF=734 EF=121
COORDINATES
ENTRIES NODE X Y Z
*STEEL WEBS
916  -5700.0 108000. 843.5
977  -3420.0 108000. 843.5
1038 -1140.0 108000. 843.5
NGENERATION TIMES=8 NSTEP=1 YSTEP=-1875.
916 977 1038
NGENERATION TIMES=6 NSTEP=1 YSTEP=-900.
924 985 1046
NGENERATION TIMES=2 NSTEP=1 YSTEP=-600.
930 991 1052
NGENERATION TIMES=6 NSTEP=1 YSTEP=-1000.
932 993 1054
NGENERATION TIMES=6 NSTEP=1 YSTEP=-1800.
938 999 1060
NGENERATION TIMES=8 NSTEP=1 YSTEP=-1950.
944 1005 1066
NGENERATION TIMES=24 NSTEP=1 YSTEP=-2250.
952 1013 1074
ENODES
ENTRIES EL N1 N8 N4 N5 N13 N7 N2 N6 N3
  1  123  124  125  916  917  918  550  551  552
61  245  246  247  977  978  979  672  673  674
91  367  368  369 1038 1039 1040  733  734  735
EGENERATION TIMES=29 ESTEP=1 NSTEP1=2
1 61 91
THICKNESS 2 16.0
THICKNESS 3 10.0
*STRESSTABLE 2 1 2 3 4 5 6 7 8 9
EDATA
ENTRIES EL NTH TABLE
1 3 1
TO
30 3 1
31 2 1
TO
60 2 1
61 3 1
TO
120 3 1
121 2 1
TO
150 2 1
*LIST ENODES 1 150
BOUNDARIES IDOF=111001
586 STEP 61 TO 708
769 STEP 61 TO 891
```

```
BOUNDARIES IDOF=101001
550 STEP 61 TO 672
733 STEP 61 TO 855
610 STEP 61 TO 732
793 STEP 61 TO 915
BOUNDARIES IDOF=100011
855 TO 915
489 TO 549
LIST BOUNDARIES
LOADS CONCENTRATED
133  3  23220. 1
137  3  54180. 1
139  3  54180. 1
145  3  77400. 1
149  3  61920. 1
255  3  36590. 1
259  3  85380. 1
261  3  85380. 1
267  3 121970. 1
271  3  97580. 1
377  3  30190. 1
381  3  70440. 1
383  3  70440. 1
389  3 100630. 1
393  3  80500. 1
FRAME
MESH
ADINA OPTIM=YES
*LIST COOR 1 1098
END
```